

# Biomedical Applications of Functionalized ZnO Nanomaterials: from Biosensors to Bioimaging

Ping Zhu, Zhengyang Weng, Xia Li, Xiangmei Liu, Shuilin Wu,\* K. W. K. Yeung, Xianbao Wang, Zhenduo Cui, Xianjin Yang, and Paul. K. Chu

The richness of the structures and properties of members of the ZnO-based nanostructure family endows these materials with diverse functionalities. In the last decade, the great potential of ZnO-based nanostructures for biomedical applications due to their unique electronic, optical, catalytic, and antimicrobial properties, as well as their excellent biocompatibility, has been recognized. The ever-deteriorating environment and the rapidly aging population have given rise to an increase in diseases, healthcare concerns and medical costs, particularly in developing countries, which has led to a high demand for better and lower-cost biomedical devices with novel bio-functionalities. Here, we review the recent advances in research on nano-structured ZnO-based biomaterials that have been developed for biomedical applications, such as in biosensing, tissue regeneration, bioimaging and drug delivery.

## 1. Introduction

In nature, ZnO exists in two forms, namely, wurtzite (B4) and zinc-blende (B3) structures.<sup>[1]</sup> At ambient temperature and pressure, ZnO is a thermodynamically stable wurtzite structure. The zinc-blende ZnO structure is stable only when growing on cubic substrates. Because of its low cost, large band gap (3.37 eV) and large exciton-binding energy (60 meV) at ambient temperature,<sup>[2]</sup> ZnO is becoming one of the most important basic materials, particularly in semiconductors. The exciton-binding energy of ZnO is not only much higher than its thermal energy at room temperature (26 meV) but also much higher than that of other prospective materials, such as ZnSe (22 meV) and

GaN (25 meV), which makes it an outstanding semiconducting material.<sup>[2]</sup> Moreover, this material can be obtained through wet chemical processing, which makes it more effective in resisting radiation damage. The unique structures and basic properties of ZnO-containing materials endow them with excellent piezoelectricity, conductivity, photoemission, sensitivity, catalytic activity, biocompatibility and antibacterial activity.<sup>[3]</sup> In view of their great potential for use in photoelectric devices and biomedicine, one-dimensional ZnO nanostructures have been extensively investigated since a nanobelt composed of semiconducting oxides was discovered in 2001.<sup>[4]</sup> To our knowledge, to date, the ZnO nanostructure family is one of such families that is rich in structural variation, the typical morphologies of which are shown in **Figure 1**,<sup>[5]</sup> including highly ordered nanowire arrays, nanorods, nanobelts, tower-like structures, nanorings, nanocombs, and even nanosprings. Numerous methods, such as microemulsion techniques,<sup>[6]</sup> capping-agent/surfactant-assisted synthesis,<sup>[7]</sup> electrochemical deposition,<sup>[8]</sup> hydrothermal/solvothermal processes,<sup>[9]</sup> vapor deposition,<sup>[10]</sup> and pulsed laser deposition,<sup>[11]</sup> have been developed for the production of these nanostructures.

It is accepted that the performance of ZnO-based devices depends upon the microstructure of the ZnO nanostructures. Hence, the size, orientation, morphology, aspect ratio and density of the crystals are critical factors in determining the potential applications of nanostructured ZnO materials in photoemitters, transducers, sensors and catalysts. Therefore, strategies for controlling these factors has been a focus of research on ZnO-based materials. For example, oriented ZnO nanorods, tubes

P. Zhu, Z. Y. Weng, X. Li, Dr. X. M. Liu,  
Prof. S. L. Wu, Prof. X. B. Wang  
Hubei Collaborative Innovation Center for Advanced  
Organic Chemical Materials  
Ministry-of-Education Key Laboratory for the Green  
Preparation and Application of Functional Materials  
Hubei Province Key Laboratory of  
Industrial Biotechnology  
School of Materials Science and Engineering  
Hubei University  
Wuhan 430062, China  
E-mail: shuilin.wu@hubu.edu.cn; sxwsl1976@163.com



Prof. K. W. K. Yeung  
Division of Spine Surgery  
Department of Orthopedics and Traumatology  
Li Ka Shing Faculty of Medicine  
The University of Hong Kong  
Pokfulam, Hong Kong 518053, China  
Prof. K. W. K. Yeung  
Shenzhen Key Laboratory for Innovative Technology  
in Orthopedic Trauma  
The University of Hong Kong Shenzhen Hospital  
1 Haiyuan 1<sup>st</sup> Road, Futian Distract, Shenzhen 518053, China  
Prof. Z. D. Cui, Prof. X. J. Yang  
School of Materials Science and Engineering  
Tianjin University  
Tianjin 300072, China  
Prof. P. K. Chu  
Department of Physics and Materials Science  
City University of Hong Kong  
Tat Chee Avenue, Kowloon, Hong Kong, China

DOI: 10.1002/admi.201500494

and porous membranes have been produced using high-temperature vacuum-deposition techniques,<sup>[12–14]</sup> hydrothermal solution synthesis,<sup>[15]</sup> and electrochemical deposition,<sup>[16]</sup> respectively.

Recently, nanostructured ZnO-based materials have attracted the attention of biomaterial scientists and surgeons because their unique characteristics endow these materials with novel biological functionalities. For instance, the excellent electronic properties of ZnO nanostructures make them suitable for the fabrication of biosensors, and their unique photoluminescent properties, such as a tunable emission wavelength, together with their high aqueous stability and high quantum yield (QY) make ZnO-based quantum dots (QDs) promising candidates as bioprobes for cell and tissue imaging. In addition, the combination of their excellent catalytic and antimicrobial properties together with their biocompatibility makes ZnO nanostructures promising materials for tissue regeneration, bacterial resistance, and wound dressing. For example, the Zn<sup>2+</sup> ions released from ZnO nanostructures not only have the ability to stimulate bone formation *in vitro*<sup>[17]</sup> but can also enhance keratinocyte migration toward a wound site and promote healing.<sup>[18]</sup> The formation of reaction oxygen species (ROS) and the release of Zn<sup>2+</sup> ions from ZnO nanoparticles (NPs) can lead to fatal damage of the bacterial cell membrane.<sup>[19,20]</sup> Furthermore, as a type of pH-responsive ZnO, it could be used as a drug carrier in pH-responsive systems. However, to our knowledge, there is controversy concerning the nanotoxicity of ZnO nanostructures toward healthy tissue.<sup>[21–23]</sup>

Due to the ever-deteriorating environment, the rapidly aging population, and the abuse of antibiotics, there has been an increase in diseases such as osteoporotic nonunion, diabetes mellitus, diabetic foot ulcers, and various skin lesions as well as the occurrence of antibiotic-resistant bacteria, which has caused a great demand for biomaterials with novel and better performance. Nanostructured ZnO-based material is one of the most promising biomaterials for improving the diagnosis and therapy of these diseases. The objective of this study is to review recent advances in the application of nanostructured ZnO-based materials in biomedicine, with an emphasis on biosensing, tissue regeneration, bioimaging and drug delivery.

## 2. ZnO-Based Biosensors

A biosensor system allows for the quantitative detection of the values of certain parameters during the occurrence of complex biochemical reactions through a transducer coupled with a biologically derived recognition entity.<sup>[24]</sup> The development of biosensors has involved three generations. In the case of first-generation biosensors, normal reaction products diffused to the transducer, leading to an electrical response.<sup>[25]</sup> The sensing process of second-generation biosensors includes an initial redox reaction performed by a mediator between the enzyme and its substrate and the eventual oxidation of the mediator by the electrode.<sup>[25]</sup> In third-generation biosensors, the biosensing process is accompanied by co-immobilization of the enzyme and mediator at an electrode surface, which makes the biorecognition component an integral part of the electrode transducer, i.e., there is direct electrical contact between the enzyme and the electrode.<sup>[26,27]</sup> Because the addition of neither



**Shuilin Wu** received his MS in Materials Science & Engineering from Tianjin University in 2003 and PhD in Biomaterials Engineering from City University of Hong Kong in 2007. After graduation, he joined the Plasma Laboratory at the City University of Hong Kong as a postdoctoral researcher from August 2007 to October 2012.

Currently, he is a Professor of Biomaterials and Surface Engineering at Hubei University. His current research focuses on the design and synthesis of novel advanced materials for biomedical applications.



**Kelvin W. Yeung** received his Ph.D. in Tissue Engineering from the University of Hong Kong in 2004. He is presently an assistant Professor at the Department of Orthopaedics and Traumatology, Faculty of Medicine, University of Hong Kong. The research areas of expertise of Dr. Yeung include biomaterials development, biomechanical characteriza-

tion, minimal invasive surgery using shape memory alloys, bone tissue engineering, and *in vitro* and *in vivo* responses to biomaterials.



**Paul K. Chu** received his PhD in chemistry from Cornell University and is Chair Professor of Materials Engineering at City University of Hong Kong. He is fellow of the APS, AVS, IEEE, and MRS. He has been active in the design of biomaterials and related biomedical fields. His current research interests include biomaterials, surface

engineering, optoelectronic materials, functional thin films as well as nanostructured materials.

a mediator nor an enzyme is necessary, this design facilitates repeated measurements. Therefore, for the direct and precise detection of chemical/biological molecules, it is important to design mediator-free third-generation enzyme-based electrodes that allow direct electron transfer between the enzymes and the conjoint electrodes.<sup>[28–31]</sup> However, direct electron communication between the immobilized enzymes and the electrode is often shielded by an insulating outer protein shell.<sup>[32]</sup> Therefore,

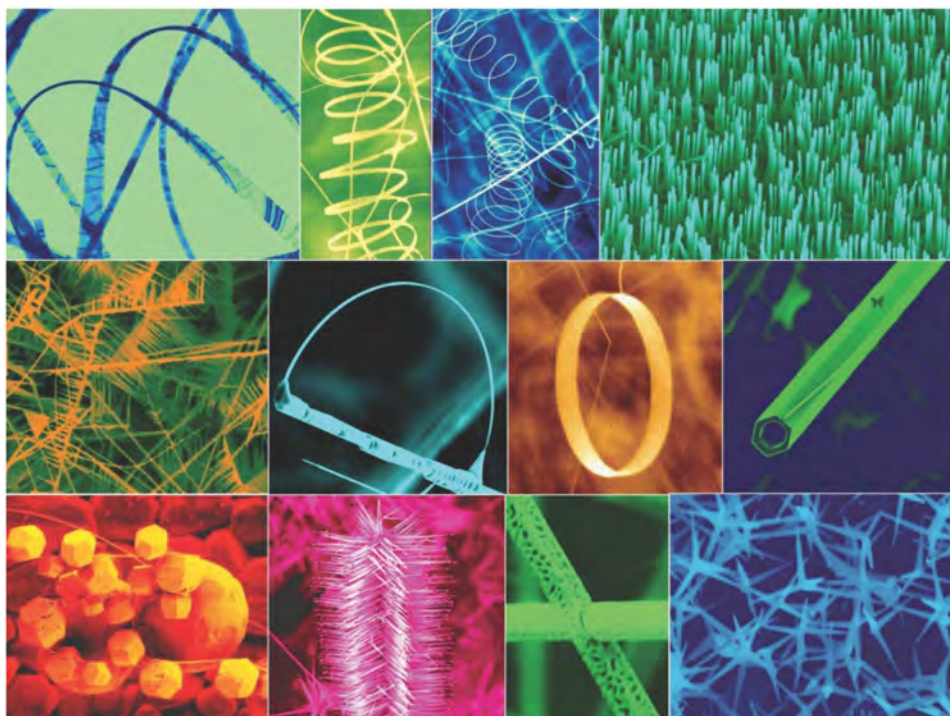


**Figure 1.** A collection of nanostructures of ZnO synthesized under controlled conditions by thermal evaporation of solid powders. Most of the structures presented can be produced with 100% purity. Reproduced with permission.<sup>[5]</sup> Copyright 2004, Elsevier.

it is necessary to connect the active center of the redox enzymes with the electrode surface by developing a specific conducting material or developing a special electrode that can directly contact the active center of enzymes.

Until very recently, an electrode architecture was proposed, consisting of a single-crystalline (such as ZnO, TiO<sub>2</sub>, and Si) nanorod/nanowire/nanotube array grown directly on a metallic substrate.<sup>[33–35]</sup> The aligned one-dimensional (1D) ZnO nanostructures provide not only large-area scaffolds for enzyme immobilization but also direct channels for electron transport from the redox enzymes to the current collector. In addition, the high isoelectric point (IEP) of  $\approx 9.5$  makes ZnO nanostructures suitable for the absorption of proteins with low IEPs through electrostatic interaction.<sup>[36]</sup> In addition to their strong protein-absorption ability, the large surface-to-volume ratio, nontoxicity, chemical stability, high catalytic activity, electrochemical activity, and excellent electron-communication features make ZnO nanostructures the best candidates for biosensor applications.<sup>[37]</sup> To date, ZnO-based NPs, porous films, nanocombs, and nanorods have been developed into biosensors to detect cytochrome C,<sup>[38]</sup> uric acid,<sup>[39–41]</sup> protein,<sup>[42,43]</sup> glucose,<sup>[44–46]</sup> hydrogen peroxide,<sup>[47,48]</sup> and phenolic compounds,<sup>[49]</sup> respectively. Glucose and hydrogen are critical signaling molecules for living organisms. In the next sections, we will focus on ZnO-based nanostructure hydrogen peroxide biosensors and glucose biosensors.

## 2.1. Hydrogen Peroxide Biosensors

In recent years, hydrogen peroxide has been reported to be not only an essential mediator in biological, medical, food

industrial, pharmaceutical, clinical and environmental analyses but also an important intermediate product of several highly selective oxidases.<sup>[50–52]</sup> Furthermore, this chemical is also involved in regulating some biological processes of immune-cell activation and vascular remodeling in mammals,<sup>[53,54]</sup> and can be generated in response to a variety of stimuli, cytokines and growth factors. However, considering its cytotoxicity, such as the oxidative stress and cellular damage caused by high levels of hydrogen peroxide in cells, for hydrogen peroxide to operate as a signaling molecule, its concentration is generally precisely regulated. Hence, depending on the level of hydrogen peroxide and the cell type, hydrogen peroxide can have both positive and negative effects on the cells. In recent decades, numerous investigations of techniques for the detection of hydrogen peroxide have been conducted and many methods, such as titrimetry, chromatography, photometry, fluorescence and electrochemical techniques, have been proposed for the precise determination of the level of hydrogen peroxide. Of these, the electrochemical tracking of biological targets is particularly promising because of its simplicity, selectivity, high sensitivity and accurate determination of the level of hydrogen peroxide.<sup>[55,56]</sup> Among the peroxidases, horseradish peroxidase (HRP), which is available in high purity and at low cost with long-term stability, has been one of the most widely studied enzymes for the development of enzyme-based amperometric biosensors. In the case of enzymatic biosensors, to achieve a higher level of biosensor performance, it is very important to fabricate novel electrode materials for both effective immobilization of the enzyme and rapid electron transport from the enzyme to the metallic electrode.<sup>[57–59]</sup> Most of the hydrogen peroxide sensors reported in the literature are based on enzymes, and many of them possess

**Table 1.** Nano-ZnO and nano-ZnO based materials available for hydrogen peroxide biosensors and related properties.

Electrode matrix	Enzymatic/ nonenzymatic	Analytical range ( $\mu\text{M}$ )	Sensitivity ( $\mu\text{A cm}^{-2}\text{mM}^{-1}$ )/ detection limit ( $\mu\text{M}$ )	Response time(s)/applied potential (V)	Reference
ZnO/Au	horseradish peroxidase (HRP)	0.015–1.1	—/0.009	<5/–0.3	[61]
C-ZnO nanowires/Ti	horseradish peroxidase (HRP)	—	237.8/0.2	4/–0.4	[62]
ZnO NPs	microperoxidase (MP)	0.01–0.4	11/0.003	1.5/—	[63]
forklike nano-ZnO	horseradish peroxidase (HRP)	0.05–0.7	201.12 /0.3	3/–0.2	[64]
ZnO nanosheet	Hemoglobin (Hb)	1–410	137/—	—/–0.675	[65]
ZnO NPs	Hemoglobin (Hb)	0.1–36.6	3660/0.02	>2/–0.34	[66]
Ag nanoparticles/ZnO nanorods	nonenzymatic	8–983	152.1/0.9	30–40/–0.55	[67]
ZnO nanorod	nonenzymatic	$5.0 \times 10^{-7}$ – $1.4 \times 10^{-4}$	—/ $1.0 \times 10^{-7}$	—	[68]
Ag NPs/ZnO	nonenzymatic	2–550	115.6/0.42	<10/–0.25	[69]
reduced graphene/ZnO	nonenzymatic	1.0–22.48	13490/—	<5/–0.38	[70]

good selectivity and sensitivity. However, enzymatic sensors are environmentally unstable and very costly.<sup>[60]</sup> Those nonenzymatic biosensors based on inorganic ZnO have been developed. In Table 1, we present the nano-structured ZnO materials that have been used to produce hydrogen peroxide sensors to date and provide brief descriptions of detection methods, the use of enzymatic or nonenzymatic operations, the sensitivity, the detection limit, the response time, and the applied potential.<sup>[61–70]</sup>

### 2.1.1. Enzymatic Biosensors

Many researchers have focused a great deal of attention on the quantitative detection of hydrogen peroxide because  $\text{H}_2\text{O}_2$  is widely used as an oxidizing agent in the chemical and food industries.<sup>[71]</sup> Most third-generation hydrogen peroxide sensors reported in the literature are based on enzymes, such as HRP<sup>[72,73]</sup> and microperoxidase (MP),<sup>[74]</sup> or on hemoglobin (Hb)<sup>[75,76]</sup> whereby the direct electrochemical reaction is observed through a ZnO nanoparticle-modified electrode. Recent reports showed that the shape and structure of ZnO nanostructures significantly affect the sensitivity of enzymatic  $\text{H}_2\text{O}_2$  biosensors. Yang et al. fabricated a new complex multiple forklike ZnO nanostructure which is composed of nanorods that grow from a thin platelet base.<sup>[64]</sup> They constructed a novel third-generation enzymatic biosensor based on glassy carbon electrodes (GCE) modified using this complex multiple forklike ZnO nanostructure, the process of which is schematically illustrated in Figure 2a<sub>1</sub>.<sup>[64]</sup> As  $\text{H}_2\text{O}_2$  was injected into the stirred phosphate buffer, the biosensor reached 95% of the steady-state current in less than 3 s (Figure 2a<sub>2</sub>). This indicated that the uniform complex ZnO multiple forklike nanostructure yields a very low mass transport barrier for a rapid diffusion between the solution and enzyme and the novel ZnO nanostructure could effectively retain the bioactivity of the HRP. As shown in Figure 2a<sub>3</sub>, the complex multiple forklike ZnO nanostructure-based  $\text{H}_2\text{O}_2$  biosensor exhibited a low detection limit of 0.3  $\mu\text{M}$ , and the sensitivity of this biosensor, which was found to be as high as 201.12  $\mu\text{A mM}^{-1}$ , is better than many previous reports.<sup>[63,65]</sup> It indicated the enzyme electrode had good

bioelectrocatalytic activity for  $\text{H}_2\text{O}_2$ . The waxberry-like ZnO microstructures, which are composed of 8–10 nm nanorods, had hundreds of pinholes on their surface.<sup>[77]</sup>

It can be clearly observed from Figure 2b<sub>2</sub> that the reduction peak current increased as the concentration of  $\text{H}_2\text{O}_2$  increased, suggesting that hydrogen peroxide was being reduced. The inserted graph in Figure 2b<sub>2</sub> demonstrates that the linear detection ability of this biosensor ranged from  $1.5 \times 10^{-4}$  to 15 mM, with a correlation coefficient of 0.9952 and a detection limit of  $1.15 \times 10^{-4}$  mM, which was lower than that of previously reported counterparts.<sup>[78,79]</sup> It was found that the waxberry-like ZnO balls, with their characteristic alveolate structure, high-defect density, large surface area, and good biocompatibility, acted as excellent materials for the immobilization of HRP and as rapid electron-transfer agents for the fabrication of efficient biosensors.<sup>[77]</sup> It can be speculated that enzymes should be entrapped in the matrix of the multiple forklike ZnO or waxberry-like ZnO nanostructure much more effectively. Lu and colleagues synthesized porous nanosheet-based ZnO microspheres for the construction of direct electrochemical biosensors.<sup>[65]</sup> There are numerous nanoscaled cavities on the surface of the ZnO microspheres, which are composed of interconnected nanosheets. The thickness of these nanosheets is approximately 20 nm, and the size of the cavities is approximately several hundred nanometers. Proteins can readily access the cavities and sequester in them or bind to the surface of these microspheres, which favors the precise detection of  $\text{H}_2\text{O}_2$ . Liu et al. synthesized flower-like ZnO nanostructures for application as a matrix for electro-biosensing with a rapid response of less than 5 s, and this biosensor, which was based on an organic-inorganic hybrid matrix, exhibited satisfactory reproducibility and stability.<sup>[80]</sup>

The various nanostructured ZnO materials provide efficient matrices for accelerating electron transfer from proteins and consequently, a ZnO inorganic–organic composite film can facilitate electron transfer between protein molecules and the electrode. The high sensitivity of this type of  $\text{H}_2\text{O}_2$  biosensor can be ascribed to several factors. First, the good biocompatibility of the nanostructured ZnO composite prevents protein denaturation and preserves the essential secondary structure of the entrapped protein. More importantly, due to its high surface

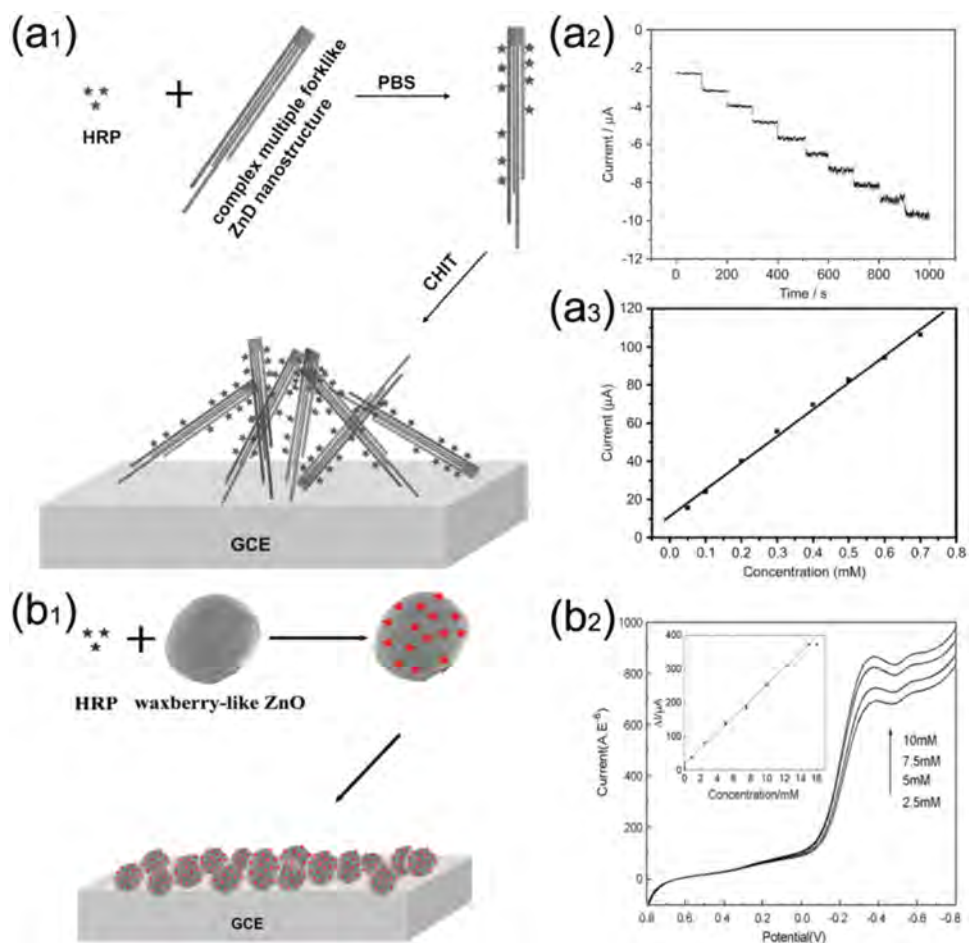


**Figure 2.** a<sub>1</sub>) Schematic illustration of the preparation process of the multiple forklike ZnO-based enzyme electrode. a<sub>2</sub>) The typical current-time response of the biosensor on successive step changes of 0.5 mM H<sub>2</sub>O<sub>2</sub> in 0.067 M PBS buffer (pH = 7.0) at an applied potential of -0.2 V under stirring. a<sub>3</sub>) The corresponding calibration curve of the biosensor. All panels in (a) reproduced with permission.<sup>[64]</sup> Copyright 2010, Elsevier. b<sub>1</sub>) Schematic illustration of the preparation process of the waxberry-like ZnO-based enzyme electrode. b<sub>2</sub>) Cyclic voltammograms of nano-ZnO/HRP/GCE electrode in 0.01 mol L<sup>-1</sup> pH 6.0 phosphate buffer solution (PBS) at a scan rate: 0.1 V s<sup>-1</sup>. Curves were obtained using different concentrations of H<sub>2</sub>O<sub>2</sub> (2.5, 5, 7.5, 10 mM). Inset: the linear fitting program of the reduction peak currents with the H<sub>2</sub>O<sub>2</sub> concentrations. Reproduced with permission.<sup>[77]</sup> Copyright 2008, Elsevier.

area, such as multiple forklike ZnO, waxberry-like ZnO, and porous nanosheet-based ZnO microspheres, these nanostructured ZnO largely enhance the active surface area of the electrode available for protein binding. Moreover, the ZnO nanostructure can also act as a scaffold that favors the conformation of the entrapped proteins, resulting in the rapid transmission of electrons ( $e^-$ ) between the redox protein and the underlying electrode. Thirdly, the ZnO nanostructures allow the use of a mild immobilization process for the enzyme that is responsible for the reduction of H<sub>2</sub>O<sub>2</sub> because these nanostructures can not only retain the bioactivity of HRP effectively but also favor electron transfer between the active site of the enzyme and the electrode.

### 2.1.2. Nonenzymatic Biosensors

Compared with enzyme-based assays, inorganic metal oxides and their composites are more cost effective, very easily

prepared and more stable, even at high temperatures. In view of these aspects, many efforts have been made to measure H<sub>2</sub>O<sub>2</sub> electrochemically without using enzymes.<sup>[81–83]</sup> Palanisamy et al. developed a hydrogen peroxide sensor based on a reduced graphene oxide (RGO)/ZnO composite prepared through the simultaneous electrodeposition of ZnO and the electrochemical reduction of graphene oxide (GO).<sup>[70]</sup> The flower-like ZnO microstructures, which were 0.5–1 μm in size, anchored near the surface of the RGO sheets and the branched networks of the thin RGO sheets interconnected these micro flowers, demonstrating that the original morphology of the nano-ZnO material and the wrinkled structure of the RGO structures could be well retained using this eco-friendly approach, and furthermore, even after 80 °C heat treatment, this composite exhibited no cracks, indicating its thermal stability.<sup>[70]</sup> Due to the large surface area and the edge-plane-like defective sites on the RGO structures that offered more catalytic sites for the efficient diffusion of the analyte, this composite exhibited high electrocatalytic activity, which was confirmed by

the extremely rapid response time of the RGO/ZnO composite film toward  $\text{H}_2\text{O}_2$  (Figure 3). This suggested the occurrence of a rapid catalytic reduction process at the surface of the composite film and consequently, the RGO/ZnO sensor displayed high sensitivity of  $13.49 \mu\text{A} \mu\text{M}^{-1} \text{cm}^{-2}$ , with a broad linear detection range of 1.0 to  $22.48 \mu\text{M}$  as well as a stable response to  $\text{H}_2\text{O}_2$ , with 89.3% of the response current retained even after 13 h.<sup>[70]</sup>

Wang et al. synthesized ZnO nanorod arrays on an indium-tin oxide (ITO) substrate using an electrochemical deposition method to produce a highly sensitive sensor for the determination of  $\text{H}_2\text{O}_2$  levels.<sup>[68]</sup> It was found that there was an optimal sintering temperature within a certain range that greatly enhanced the crystalline quality and the carrier mobility of the ZnO nanorods. In their studies,  $400^\circ\text{C}$  was the optimal sintering temperature, and it was found that high-temperature sintering improved the intensity and stability of the photocurrent

of the ZnO nanorod array-modified electrode. Consequently, the ZnO nanorod array-modified electrode was highly sensitive and showed a linear response to  $\text{H}_2\text{O}_2$ . Wang and Zheng fabricated a nonenzymatic hydrogen peroxide sensor by electrodepositing silver nanoparticles on a zinc oxide (ZnO) film.<sup>[69]</sup> The Ag NPs/ZnO/GCE sensor showed a sensitivity of  $0.1156 \text{ A M}^{-1}$ , which was much higher than that of the Ag NPs/GCE sensor ( $0.0416 \text{ A M}^{-1}$ ),<sup>[84]</sup> and a low detection limit. After the 50th cycle, the peak currents dropped by 2% and 30% for Ag NPs/ZnO/GCE and Ag NPs/GCE sensors, respectively. The ZnO film clearly improved the stability of  $\text{H}_2\text{O}_2$  detection by the Ag NPs/ZnO/GCE sensor.<sup>[69]</sup>

In summary, in addition to possessing good storage and operational stability, the nanostructured ZnO mixed with high surface area materials such as RGO or Ag NPs exhibited much higher electrocatalytic activity toward  $\text{H}_2\text{O}_2$ , which is ascribed to the large surface area and the high rate of electron communication of the anchored ZnO systems, as well as their synergistic effects.

## 2.2. Glucose Biosensors

Glucose is a critical metabolite for living organisms, particularly for patients who are suffering from diabetes. According to the reports of the World Health Organization, there are approximately 346 million diabetic patients worldwide,<sup>[85]</sup> and recent reports showed that approximately 29.1 million Americans had diabetes in 2012, whereas there were 25.8 million diabetic Americans in 2010. Diabetes was the 7th leading cause of death in the United States in 2010, with 69 071 death cases caused by diabetes directly and 234 051 death certificates listing diabetes as an underlying or indirect cause of death.<sup>[86]</sup> Generally, a disorder of glucose metabolism results from insulin deficiency and hyperglycemia and is reflected in the blood glucose level being higher or lower than the normal clinical range of  $80\text{--}120 \text{ mg dL}^{-1}$  ( $4.4\text{--}6.6 \text{ mM}$ ).<sup>[28]</sup> Therefore, precise real-time monitoring of the level of blood glucose in diabetic patients is quite important. Numerous techniques have been developed for the determination of glucose levels, such as liquid chromatography,<sup>[87]</sup> spectroscopic techniques,<sup>[88]</sup> and other methods.<sup>[89]</sup> Among the available glucose monitors, a glucose biosensor has overwhelming advantages, such as a rapid response, high sensitivity, good stability and a facile fabrication process, which prompted a considerable amount of fascinating research on detection strategies for novel glucose biosensors.<sup>[90]</sup>

Since 1962, when Clark and Lyons proposed the initial concept of glucose enzyme-coupled electrodes,<sup>[91]</sup> many efforts have been made to optimize the performance of glucose biosensors. At present, three generations of glucose oxidase-based biosensors have been developed, including the following: 1) first-generation biosensors based on natural oxygen as the cofactor and the detection of hydrogen peroxide, 2) second-generation biosensors using a synthetic electron acceptor as the redox mediator, and 3) third-generation biosensors in which there is direct electron transfer between glucose oxidase and the electrode (Figure 4).<sup>[28]</sup> However, it is challenging to convert the biological signal to an easily processed electronic signal because connecting an electronic device directly to a biological

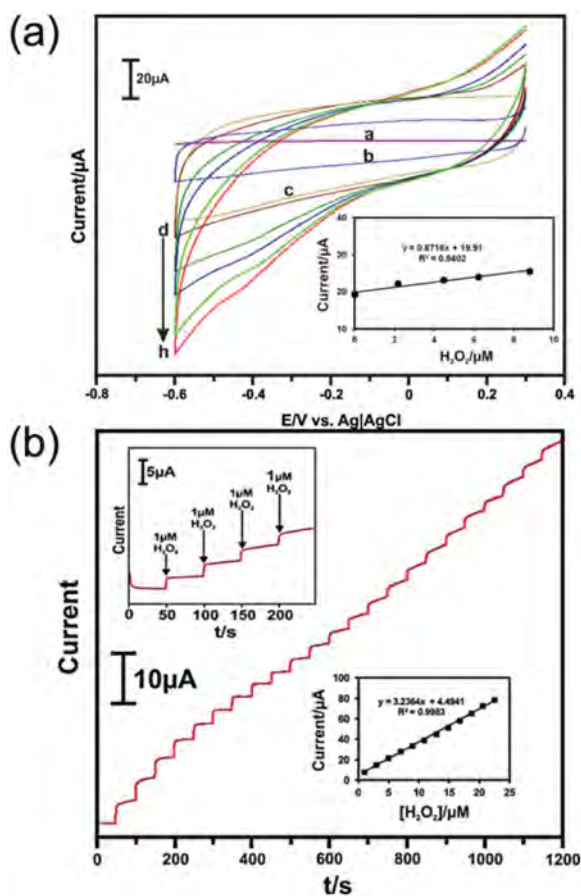


**Figure 3.** a) Cyclic voltammograms obtained at bare/GCE (a) and RGO/ZnO/GCE (b) in the presence of  $8.8 \mu\text{M}$   $\text{H}_2\text{O}_2$  at the scan rate of  $50 \text{ mV s}^{-1}$ . Cyclic voltammograms obtained at RGO/ZnO/GCE in the absence (c) and presence of  $0.02$  (d),  $2.19$  (e),  $4.48$  (f),  $6.24$  (g) and  $8.8 \mu\text{M}$   $\text{H}_2\text{O}_2$  (h) under similar conditions. Supporting electrolyte:  $\text{N}_2$  saturated  $0.05 \text{ M}$  PBS ( $\text{pH} = 7$ ). Inset is the plot of cathodic peak current vs.  $[\text{H}_2\text{O}_2]$ . b) Amperometric  $i-t$  response at a RGO/ZnO film modified rotating disc GCE upon successive additions of  $1\text{--}22.24 \mu\text{M}$   $\text{H}_2\text{O}_2$  into continuously stirred  $\text{N}_2$  saturated  $0.05 \text{ M}$  PBS ( $\text{pH} = 7$ ). Applied potential:  $-0.38\text{V}$ ; Rotation rate:  $1200 \text{ rpm}$ . Inset (above) is the enlarged view of the amperometric  $i-t$  response for  $1\text{--}4 \mu\text{M}$   $\text{H}_2\text{O}_2$ . Inset (below) is the plot of response current vs.  $[\text{H}_2\text{O}_2]$ . Reproduced with permission.<sup>[70]</sup> Copyright 2012, Elsevier.

environment is highly complex. In addition, the management of diabetes requires personalized medicine and stable and reliable continuous glycemic monitoring in vivo. The intrinsic advantages of electrochemical biosensors are their robustness, easy miniaturization, and excellent detection limits, as well as their use of small sample volumes and their ability to be used in turbid biofluids. Consequently, different varieties of materials possessing good specificity, selectivity, and rapid response,<sup>[92–94]</sup> were investigated for the preparation of glucose biosensors. Among them, nanostructured ZnO is one of the most promising materials for glucose biosensors because of its unique advantages, including a facile fabrication process, excellent biocompatibility, and low cost. The properties of nanostructured ZnO-based glucose biosensors of various shapes are summarized in Table 2.<sup>[95–106]</sup> It is evident that the shape

and structure play important roles in determining the performance of ZnO-based glucose biosensors. Moreover, using modified ZnO, such as doped or mixed ZnO, can also affect the sensitivity and detection limit of glucose biosensors as well as the response time. These inorganic electrodes exhibit advantages because glucose detection is based on direct electron transfer, whereas the electronic transmission process of mediator-based biosensors is possibly mediated by an organic film.<sup>[107–111]</sup> Zhao et al. developed a novel third-generation amperometric glucose biosensor based on an assembled thin film of ZnO:Co nanoclusters on which glucose oxidase was immobilized using a Nanofion-assisted cross-linking technique.<sup>[101]</sup> This novel glucose biosensor displayed a high sensitivity level of  $13.3 \mu\text{A mM}^{-1} \text{cm}^{-2}$  and low detection limit of  $20 \mu\text{M}$ , which was ascribed to the following factors. The small nanocrystallites of approximately 5 nm in diameter and the nanoporous network structure endowed the electrode with highly specific active sites and an excellent ability to absorb the enzyme, which

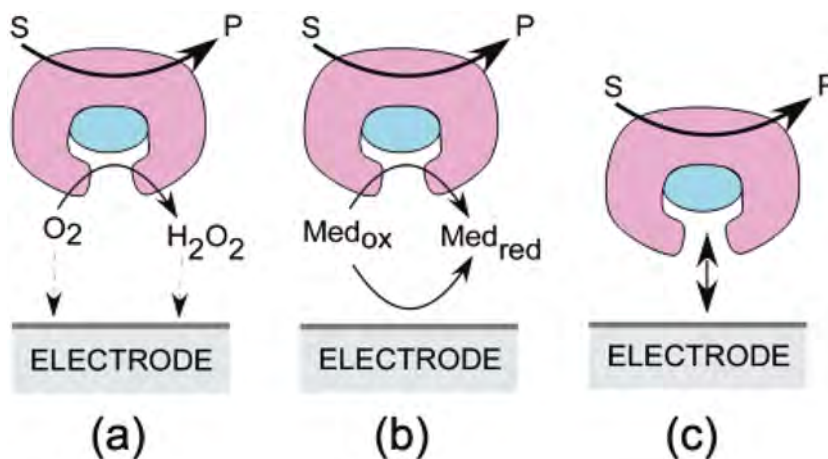


**Figure 4.** Three generations of amperometric enzyme electrodes for glucose based on the use of a) natural oxygen cofactor, b) artificial redox mediators, or c) direct electron transfer between GOx and the electrode. Reproduced with permission.<sup>[28]</sup> Copyright 2008, American Chemical Society.

was confirmed by its lower Michaelis–Menten constant ( $K_M^{\text{app}}$ ) of 21 mM than that of the GOx–DMFc–CPE system (33 mM) and the GOx–polypyrrole system (25.3 mM).<sup>[112,113]</sup> The smaller  $K_M^{\text{app}}$  indicated that the enzyme electrode possessed a higher glucose-oxidation enzymatic activity and a higher affinity for glucose. In addition, co-doping enhanced the electrocatalytic activity of the ZnO nanoclusters.

In the case of nanostructured ZnO-based biosensors, the immobilization of glucose oxidase was predominantly determined by physical adsorption. In addition to the intrinsic high isoelectric point of this material offering a friendly microenvironment for the negatively charged GOx, the shape and morphologies of the ZnO-based electrodes also affect their adsorptive ability. Recently, a tetragonal pyramid-shaped porous ZnO (TPSP-ZnO) nanostructure was developed by Dai et al. using a simple polyglycol-assisted wet chemical method; the GOx immobilized on the TPSP-ZnO-modified GCE exhibited a rapid direct electrochemical reaction corresponding to its

**Table 2.** ZnO nanostructure based glucose sensors and their functional properties.

Working electrode	Enzyme	Linear range (mM)	Sensitivity ( $\mu\text{A mM}^{-1} \text{cm}^{-2}$ ) / detection limit ( $\mu\text{M}$ )	$K_M^{\text{app}}$ (mM)	Response time (s)	Reference
tetragonal pyramid-shaped porous ZnO	GOx	0.05–8.2	—/10	—	—	[95]
ZnO nanorod	GOx	0.01–3.45	23.1/10	2.9	<5	[96]
ZnO nanocomb	GOx	0.02–4.5	15.33/20	2.19	<10	[97]
ZnO nanotube	GOx	0.01–4.2	30.85/10	2.59	<6	[98]
ZnO nanofiber	GOx	0.25–19.0	70.2/1.0	2.19	<4	[99]
ZnO hollow nano-spheres	GOx	$5.0 \times 10^{-3}$ –13.15	65.82/1.0	—	<5	[100]
ZnO:Co nanoclusters	GOx	0–4	13.3/20	21	8	[101]
ZnO nanorods/Au	GOx	$1.0 \times 10^{-4}$ – $3.3 \times 10^{-2}$	1492/0.01	0.41	<5	[102]
ZnO/multiwalled carbon nanotubes (MWCNTs)	GOx	0.1–16	0.052/0.25	8.9	8	[103]
ZnO nanowires/Au	GOx	0.2–2.0	19.5/<50	1.57	<5	[104]
ZnO/Cu nanocomposite	GOx	1–15	0.097/40	1.47	<6	[105]
Mn-doped ZnO multilayer structure	GOx	2–16	—/0.42	—	—	[106]

redox-couple content, and its reduction products electrocatalyzed the reduction of dissolved oxygen, which was determined by the properties of the TPSP-ZnO GCE.<sup>[47,95]</sup> The biosensor that was developed displayed a linear response to the glucose concentration in the range of 0.05 to 8.2 mM, which was a much wider range than that of the GOx/spherical ZnO/Nafion-modified GCE. At a given potential of  $-0.50$  V, the detection limit was 0.01 mM, which was much lower than that of the aforementioned ZnO nanocluster-based biosensor (0.02 mM) and the GOx/spherical ZnO/Nafion-modified biosensor (0.07 mM), ascribed to the relatively larger specific surface area of TPSP-ZnO resulting in more GOx loading and better catalytic activity triggered by the greater number of surface atoms on the edges and corners.<sup>[95,101]</sup> Furthermore, the response was not hampered by cooxidizable substances, such as ascorbic acid, uric acid and *p*-acetaminophen, possibly because these smaller substances were oxidized after diffusing through the porous film to the electrode surface.<sup>[95]</sup> This TPSP-ZnO nanostructure therefore provided a good matrix for protein immobilization and biosensor preparation.

It is accepted that the degree of enzyme immobilization on mediators is crucial for the development of a high-performance glucose sensor. In addition to the shape and morphology of the nanostructured ZnO, the aspect-ratio (AR) of ZnO also affects the performance of related glucose biosensors. Ahmad et al. fabricated amperometric glucose biosensors using Si/Ag that was modified using AR-controlled ZnO nanorods as electrodes and found that the glucose biosensor with an AR = 60 demonstrated better performance than lower-AR ZnO nanorod-modified electrodes.<sup>[114]</sup> The calculated  $K_M^{\text{app}}$  of the glucose biosensors were 0.229, 0.176 and 0.137 mM for AR = 5, 15 and 60, respectively. These results showed that the affinity of GOx for glucose increased with an increasing AR, which enhanced the direct electron transfer through the ZnO nanorods to the Ag electrode. It was believed that well-aligned ZnO nanorod arrays could induce more immobilization of the enzyme and favor the direct electron transmission between the nanorods and the Si/Ag electrode. So, the nanostructured ZnO with the higher-AR or larger surface area would be more beneficial to be a glucose biosensor.

As the development of a novel portable electrochemical biosensors is necessary and such a device would be well suited to personal glucose testing. Personal blood-glucose monitors should be mainly based on the use of disposable screen-printed enzyme-electrode test strips.<sup>[115]</sup> The diabetic patients prick their fingers, place a small blood droplet on the sensor strip, and obtain the blood-glucose level within 5–30 s. Although this portable biosensor has some remarkable technological advances, the low and irregular frequency of home testing frequency is often due to the inconvenience and discomfort associated with its use. Thus, more integrated and functionalized glucose biosensors based on nanostructured ZnO materials should be developed to provide a non-invasive, painless, low-cost and convenient testing method for diabetic patients.

All in all, in comparison with the traditional biosensors, functionalized ZnO-based biosensors present superior performance, including enhanced absorption of biological components and increased surface active sites, a good reaction microenvironment, accelerated electron transfer, shortened response time, and heightened sensitivity. The current sensitivity of

nano-biosensors can be obtained only under highly optimized conditions in a laboratory. However, even under optimal conditions, the reported results disclosed a certain discrepancy of current sensitivity, which is possibly due to the heterogeneous structures or compositions of ZnO-based biosensors. Hence, it is necessary to control the uniformity of ZnO precisely to guarantee the measurement of current sensitivity by developing novel synthesis methods. In addition, the integration of ZnO nanostructures with commercial detection systems will be beneficial for their real sensing applications.

## 3. ZnO Nanostructures for Tissue Regeneration

### 3.1. ZnO as an Antibacterial Agent

Currently, infection is the major reason for the failure of guided tissue regeneration in clinical applications, constituting a significant healthcare burden.<sup>[116,117]</sup> Antibacterial biomaterials exhibit the greatest potential in the war against implant-related infections and represent the broadest group of anti-infective biomaterials.<sup>[118]</sup> Antibacterial agents can be broadly classified into two types, organic and inorganic. Compared with inorganic antimicrobial materials, organic antimicrobial agents are fast acting, but the abuse of antibiotics has induced drug resistance in an increasing number of bacteria.<sup>[119]</sup> Furthermore, organic antimicrobial agents are often less stable, particularly at high temperatures or pressures. In contrast, inorganic antibacterial materials, such as metal oxides, can achieve appropriate disinfection without introducing harmful byproducts and are robust and durable, therefore having the unique advantages of enhanced stability and safety compared to those of organic agents.<sup>[120]</sup> Consequently, research on inorganic antimicrobial materials such as metal and metal oxides has intensified in the past decade.<sup>[121–124]</sup> Due to their good thermostability, marked antimicrobial activity and low cost, ZnO nanostructures are becoming one of the most promising inorganic antimicrobial materials, particularly for tissue regeneration.<sup>[125,126]</sup> Their antibacterial activity is generally determined using pathogenic and nonpathogenic bacteria, such as *Staphylococcus aureus* and *Escherichia coli*.<sup>[127]</sup>

#### 3.1.1. Antibacterial Mechanism

To date, myriad studies have explored the antibacterial mechanisms of ZnO NPs, which involve the generation of ROS,<sup>[128,129]</sup> the release of zinc ions from ZnO and the penetration and disorganization of the bacterial membrane upon contact with specific ZnO nanostructures, such as nanoneedles and nanorod arrays,<sup>[130,131]</sup> as will be described below.

1) Photocatalytic antibacterial mechanism. ROS that are generated by the photocatalytic reaction of ZnO<sup>[132,133]</sup> typically include hydroxyl radicals, singlet oxygen and superoxide radicals that are toxic to the cells because they damage cellular constituents such as DNA, lipids, and proteins.<sup>[134,135]</sup> Consequently, the generation of ROS has been recognized as the predominant antimicrobial mechanism underlying

the effects of photoexcited ZnO on mammalian and bacterial cells.<sup>[136,137]</sup> The general principle is that when illuminated by light with a photoenergy equal to or greater than its band-gap energy,  $e^-$  of ZnO NPs are promoted across the band gap to the conduction band, which creates a hole ( $h^+$ ) in the valence band.<sup>[138]</sup> The  $e^-$  in the conduction band and the  $h^+$  in the valence band exhibit strong reducing and oxidizing power, respectively.<sup>[107]</sup> Superoxide anion radicals ( $O_2^{\cdot-}$ ) are generated when the electron reacts with molecular oxygen through a reductive process.<sup>[139]</sup> The  $h^+$  can capture the  $e^-$  from water and/or hydroxyl ions to generate hydroxyl radicals ( $OH^{\cdot}$ ) through an oxidative process.<sup>[140]</sup> Singlet oxygen ( $^1O_2$ ) is mostly produced indirectly from aqueous reactions of  $O_2^{\cdot-}$ .<sup>[138]</sup>  $OH^{\cdot}$  is the most reactive oxygen radical known because it reacts very quickly with almost every type of organic biomolecule, including nucleic acids, lipids, carbohydrates, proteins, DNA, and amino acids.<sup>[141]</sup> Such reactions generally produce hydrogen peroxide ( $H_2O_2$ ) due to the dominating recombination of two  $OH^{\cdot}$  radicals. Some researchers have proposed that the chemical interactions between bacteria and the  $H_2O_2$  generated from ZnO powder slurry were the predominant mechanism underlying the antibacterial activity of ZnO.<sup>[142,143]</sup>  $O_2$  is another main mediator of photocytotoxicity and can damage treated tissues irreversibly,<sup>[144]</sup> causing biomembrane oxidation and degradation.<sup>[145]</sup> Although  $O_2^{\cdot-}$  is not a strong oxidant as a precursor for  $OH^{\cdot}$  and  $^1O_2$ ,  $O_2^{\cdot-}$  also has significant biological repercussions.<sup>[146]</sup> Consequently, these three types of ROS ( $O_2^{\cdot-}$ ,  $OH^{\cdot}$ , and  $^1O_2$ ) contribute to the majority of oxidative stress in biological systems.

2) Antibacterial mechanism of  $Zn^{2+}$  ions. Some of the  $Zn^{2+}$  ions released from ZnO nanostructures can adsorb to the surface of bacteria with a high degree of negative charge through electrostatic force. The interaction between  $Zn^{2+}$  ions and bacteria can destroy the charge balance, leading to severe deformation of the cells until the bacteria die due to bacteriolysis.<sup>[147–149]</sup> Furthermore,  $Zn^{2+}$  ions that enter bacteria via the cell membrane interact with some of the functional groups on bioactive proteases, such as sulfhydryl groups (ASH), amino groups ( $ANH_2$ ), hydroxyl groups (AOH), to change the structure and performance of proteins, which induces the death of the bacteria due to unbalanced metabolism.<sup>[150]</sup> A recent study revealed that a solution containing low concentrations of  $Zn^{2+}$  ions exhibited better antibacterial activity for specific strains than did a solution with a high concentration of zinc ions. Moreover, zinc (Zn) complexes exhibited a much higher level of antimicrobial activity. However, there is still some debate regarding the antibacterial mechanism of  $Zn^{2+}$  ions. Li et al. evaluated the effect of zinc ion release on antibacterial activity by monitoring the release of  $Zn^{2+}$  ions from suspensions of different ZnO NPs during 2 h of UV irradiation.<sup>[151]</sup> In their study, the antibacterial effect of the  $Zn^{2+}$  released from solutions containing various concentrations of  $ZnSO_4$  was evaluated using an antibacterial assay. The results showed that no significant inhibitory effect toward *E. coli* cells was observed even when the concentration of  $Zn^{2+}$  was as high as  $1\text{ mg L}^{-1}$ . This finding indicated that the released  $Zn^{2+}$  had a minor antibacterial effect.<sup>[151]</sup> However, another study found that the

growth of *S. mutans* was severely inhibited by an initially high level of ion release from zinc-containing cements and that the antibacterial activity decreased over time due to the significantly decreased levels of ion release.<sup>[152]</sup> In this investigation, treatment using 1-h aged cements detectably inhibited the growth of *S. mutans* and no inhibition was detectable when materials that had been aged for 15 days were applied, although materials that had been aged for intermediate periods were not tested.<sup>[153]</sup>

3) Nano-antibiotic mechanism. The penetration and disorganization of the bacterial membrane upon contact with ZnO particles may also play a role in their antibacterial mechanism because it is accepted that disorganization of the membrane by unfavorable or foreign substances can cause the loss of membrane integrity, which leads to the malfunction of the permeability barrier.<sup>[154–158]</sup> Due to the larger specific surface area and higher surface energy of nanostructured ZnO, bacteria adsorb to the nanostructured ZnO, preventing the exchange of matter and energy with the environment so that the bacteria die due to lack of normal metabolism. Brayner et al. reported that ZnO NPs hindered *E. coli* growth due to disorganization of their membranes, which increased the membrane permeability, leading to the accumulation of NPs in the bacterial membrane and cytoplasm.<sup>[158]</sup> Huang et al. observed that the ZnO NPs successfully penetrated *S. agalactiae* cells grown in a liquid medium by damaging their membranes, and in this case, the new cells presented considerable damage, with a very disorganized cell wall and an abnormal morphology.<sup>[156]</sup> Moreover, Stoimenov et al. reported that the binding of ZnO NPs to the bacterial surface through electrostatic forces directly killed bacteria.<sup>[154]</sup> It was assumed that the surface abrasiveness of ZnO NPs was responsible for the high antibacterial performance of ZnO NPs through initiating disorganization of the cell membrane.<sup>[159]</sup>

Although the above mentioned factors such as concentration, particle size and shape have been reported to affect the antimicrobial activity of ZnO NPs,<sup>[160,161]</sup> their main antibacterial mechanisms may be different in different media because their physicochemical properties and the species of dissolved Zn can be altered by the medium components. The detailed mechanism underlying the antimicrobial activity of ZnO is still under debate and requires further investigation.

### 3.1.2. ZnO Nanostructures Modified with Inorganic Antimicrobial Agents

Although the ROS generated by the photocatalytic reactions of ZnO nanostructures endow these materials with excellent antibacterial activity, the photoexcited  $e^-$  and  $h^+$  can also recombine to reduce their photocatalytic activity, consequently reducing their antimicrobial activity. It has been reported that modification of ZnO nanostructures can minimize this effect.<sup>[162]</sup> Metals, such as silver, gold and copper, are excellent inorganic broad-spectrum antimicrobial agents and have attracted considerable interest for this reason.<sup>[163–165]</sup> Therefore, modifying ZnO nanostructures with Ag, Au and Cu can not only maximize the

antibacterial efficacy of ZnO but also adds the antimicrobial activity of these metals. Recent studies showed that regardless of the shape and morphology of the ZnO nanostructures, incorporating Ag NPs resulted in a significantly enhanced antibacterial efficacy compared with that of the pure ZnO nanostructures and that the photocatalytic activity related to the antimicrobial efficacy was determined mainly by the concentration of Ag.<sup>[166–174]</sup> Ren et al. prepared a silver-modified ZnO nanorod array using a wet-chemical route and subsequently, a photo-deposition method, and their results showed that the photocatalytic activity of these samples varied in the following order: pure ZnO < ZnO/Ag (0.02 M) < ZnO/Ag (0.05 M) > ZnO/Ag (0.1 M) > ZnO/Ag (0.2 M), i.e., neither the composite with the highest Ag content nor that with the lowest Ag content had the best photocatalytic activity.<sup>[167]</sup> A similar trend was also observed by other researchers.<sup>[170–172]</sup> In the study of Lin et al., heterostructural Ag-ZnO nanofibers containing 7.5 at.% Ag exhibited the best photocatalytic activity among the samples containing 0, 1.0, 3.0, 5.0, 7.5, and 10.0 at.% Ag, which was 25 times higher than that of pure ZnO nanofibers.<sup>[170]</sup> In the case of dendrite-like ZnO@Ag heterostructural nanocrystals, i.e., nanocrystals with oriented ZnO nanorods as the branches on trunks of single-crystal Ag nanowires (NWs), samples containing 8 at.% Ag possessed the highest photocatalytic activity among the samples, including pure Ag NWs, pure ZnO, and composites containing 3 or 11 at.% Ag.<sup>[171]</sup> When a core-shell heterostructure composed of a core of single-crystal Ag NWs and an outer shell of ZnO particles was used, the concentration of Ag that provided the best photocatalytic performance was 2.8 at.%.<sup>[172]</sup> Similarly, other types of nanostructures, such as three-dimensional hollow Ag/ZnO microspheres also displayed this tendency.<sup>[173]</sup> This phenomenon is schematically illustrated in Figure 5.<sup>[167,173,175]</sup> As shown in Figure 5a, because the Fermi energy level of Ag ( $E_{fm}$ ) is higher than that of ZnO ( $E_f$ ),  $e^-$  will be transferred from Ag to ZnO until the two systems attain equilibrium and a new Fermi energy level ( $E_f$ ) exists.<sup>[167]</sup> Therefore, by acting as electron sinks, Ag NPs minimize the recombination of photoinduced  $e^-$  and  $h^+$  and enhance the photocatalytic activity of ZnO. In contrast, as shown in Figure 5b,<sup>[167]</sup> the lower energy level of the conduction band of ZnO is higher than the new equilibrium Fermi

energy level ( $E_f$ ) of Ag/ZnO, inducing the transmission of the photoexcited  $e^-$  on the conduction band from ZnO to the Ag NPs; consequently, when a higher density of Ag particles cover the surface, silver NPs with a high silver concentration can also act as recombination centers, thus decreasing the photocatalytic activity of the ZnO NPs.<sup>[167,170–173]</sup> Accordingly, the antibacterial activity of ZnO/Ag can be enhanced, depending on the extent of Ag modification.

Au doping has also been proven to be effective in strengthening the photocatalytic activity of ZnO nanostructures and consequently enhancing their antimicrobial performance.<sup>[176–179]</sup> Li et al.<sup>[176]</sup> prepared Au-ZnO hybrid NPs with a hexagonal pyramid-like structure by regulating the heterogeneous nucleation and selective growth of ZnO on presynthesized Au seeds, and these Au-ZnO hybrid NPs showed much higher photocatalytic efficacy than that of pure ZnO NPs.<sup>[176]</sup> It was suggested that under UV irradiation, changes in the band gap and the enhanced efficacy of electron transfer in the Au-ZnO hybrid NPs were both responsible for the observed enhancement of photocatalytic activity and ROS generation, which is schematically shown in Figure 6.<sup>[165]</sup> Consequently, the antibacterial performance was significantly improved, as was proven through antibacterial testing. In their studies, under simulated sunlight, the antibacterial efficacy of ZnO/Au hybrid nanostructures at a concentration of 0.05 mg mL<sup>-1</sup> was approximately 2 times and 3 times, respectively, that of the pure ZnO NPs in killing *S. aureus* and *E. coli*, and the corresponding values were increased approximately 3.5 and 4.5 times, respectively, when the particle concentration was increased to 0.1 mg mL<sup>-1</sup>.<sup>[165]</sup>

Among the various metallic doping elements, Cu is important because it has an electronic shell structure and physical and chemical properties similar to those of Zn and it can change the microstructure and the optical properties of ZnO systems.<sup>[180,181]</sup> It has been found that Cu doping a ZnO system using a soft chemical metathesis route remarkably improved its solar spectrum absorbance from 0.4 to 34% and that one containing 1.5 mol% Cu:ZnO was the most efficient photocatalyst under both visible and UV illumination.<sup>[166]</sup> Careful Cu doping evidently improved the performance of ZnO photocatalysts, which merited further theoretical and experimental investigation of their antibacterial activity. Bai et al. successfully synthesized a novel

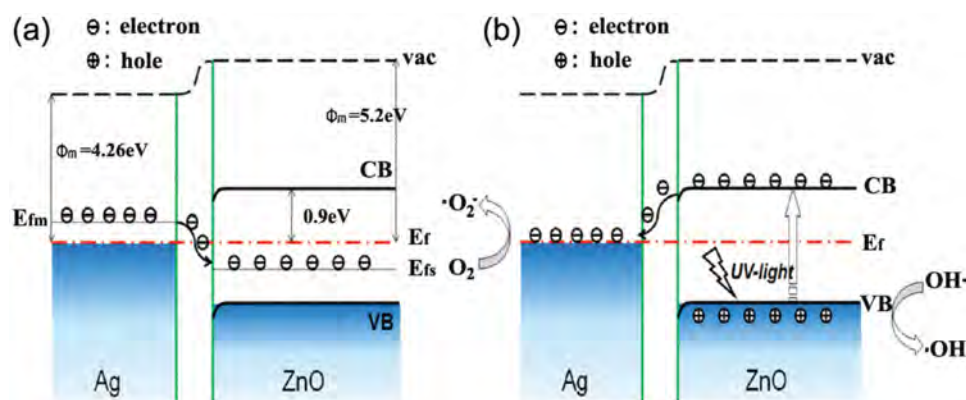


**Figure 5.** a) The band structures of Ag and ZnO junctions and the Fermi energy level equilibrium without UV irradiation. b) The proposed charge separation process and the photocatalytic mechanism of as-prepared Ag/ZnO samples under UV irradiation. The electrons in the Ag sinks can be trapped by the chemisorbed  $O_2$  and the hole can be captured by the surface hydroxyl. Reproduced with permission.<sup>[167]</sup> Copyright 2010, Elsevier.

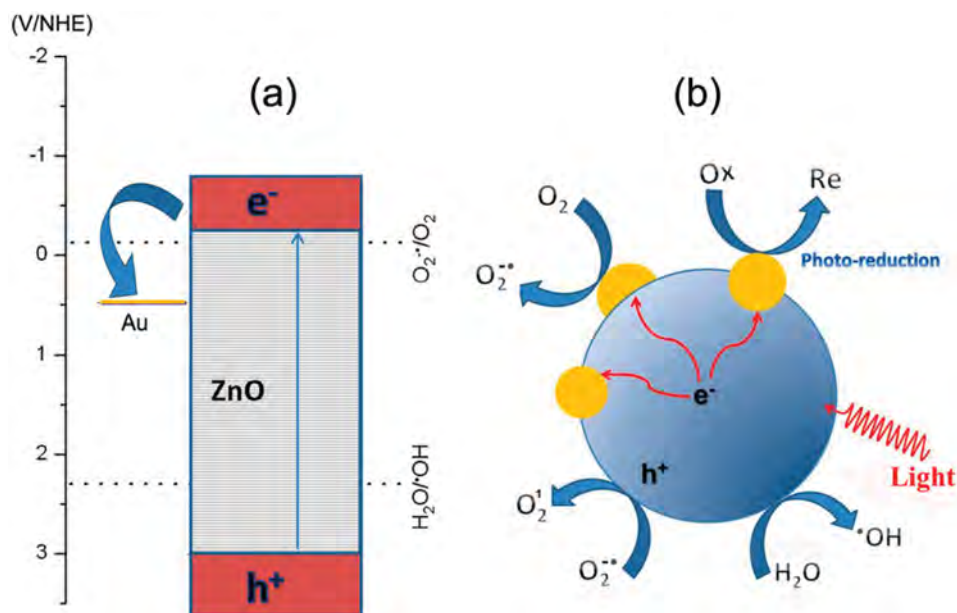


**Figure 6.** a) Position of the Fermi level of Au and energy bands of ZnO compared with the redox potential of  $O_2^-/O_2$  and  $H_2O/OH$ , b) The expected reaction mechanism for an enhancement effect on the generation of ROS and photocatalytic activity. Deposition of Au onto ZnO increases the charge carrier separation and transport efficiency in photoexcited ZnO NPs. Reproduced with permission.<sup>[165]</sup> Copyright 2014, American Chemical Society.

hierarchical ZnO/Cu “corn-like” material via facile low-temperature hydrothermal and photo-deposition methods.<sup>[182]</sup> In their study, the Cu NPs were uniformly deposited on the surface of the ZnO nanorods and the novel hierarchical material combined the advantages of both ZnO and Cu, maximizing its photocatalytic activity.<sup>[182]</sup> Both ZnO nanorods and the ZnO/Cu “corn-like” materials promoted the photocatalytic degradation, whereas the ZnO/Cu “corn-like” material displayed a higher rate of methyl-blue photodegradation under the visible-light irradiation. The survival rate of *E. coli* treated using pristine Cu or ZnO nanorods in the dark was approximately 76.12% and 58.02%, respectively, which was much higher than the 3.12% survival rate of *E. coli* treated using ZnO/Cu material.<sup>[182]</sup> These results suggested that the enhanced antimicrobial performance of the ZnO/Cu “corn-like” material was due to a synergistic effect. Moreover, the enlarged specific surface area and mesoporous property of this material was beneficial for the attachment and killing of *E. coli*.<sup>[183,184]</sup> It was clear that the ZnO/Cu “corn-like” materials had a greatly improved photocatalytic antibacterial activity through enhancing the rate of visible-light utilization and providing more reaction sites and a larger specific area for electron transfer. In the case of the ZnO/Cu “corn-like” materials, only approximately 50% of the *E. coli* were killed in the absence of visible-light irradiation at a dosage of  $0.1 \text{ g L}^{-1}$ , whereas with the visible-light irradiation, these ZnO/Cu materials killed all of the *E. coli* within 20 min.<sup>[182]</sup> Liang et al. prepared polyaniline/Cu<sub>0.05</sub>Zn<sub>0.95</sub>O (PANI/CZO) nanocomposites using an in situ inverse microemulsion method and determined the antibacterial activities of ZnO, CZO, PANI and PANI/CZO composites.<sup>[185]</sup> Their results showed that both ZnO and CZO composites had a broad spectrum of antibacterial activities against *S. aureus*, *E. coli*, and *Candida albicans* and that the CZO composite had better antibacterial activities than did the pure ZnO composites. It was also discovered that the

Cu<sup>2+</sup> ions embedded in the ZnO lattice and ZnO particles cooperatively hindered bacterial growth.<sup>[166,185]</sup> Consequently, both the CZO and PANI/CZO composites exhibited excellent bacteriostatic and bactericidal activities that were much greater than those of the PANI and ZnO composites. The overall photocatalytic activity of the PANI/CZO nanocomposites was governed mainly by the synergistic effect of the mentioned antibacterial mechanisms which promotes their antibacterial efficacy. Similarly, Mn doping achieved similar antibacterial enhancement for ZnO NPs.<sup>[186]</sup>

Hence, nanostructured ZnO doped with inorganic metal could restrain the combination of the photoexcited  $e^-$  and  $h^+$  to enhance their antimicrobial activity, which provide a new route to develop novel ZnO-based antibacterial agents with improved antimicrobial activity.

### 3.1.3. ZnO-Doped Organic Antimicrobial Agents

In addition to metals and the associated metal oxides, hybrids composed of organic antimicrobial agents and ZnO nanostructures have been reported to exhibit better antibacterial activity than did pure ZnO nanomaterials. In this case, the former is generally immobilized or embedded in the latter. Chitosan (CS) is partially N-deacetylated chitin, which is a linear homopolymer of 1,4 $\beta$ -linked N-acetyl-D-glucosamine that exhibits bacteriostatic and fungistatic activities and has been widely used for bone healing and in biological dressings.<sup>[187,188]</sup> The cooperative antimicrobial properties of CS/nano-ZnO hybrids have been reported.<sup>[189–191]</sup> A possible mechanism for the co-antimicrobial effect of CS and nano-ZnO in a nanofibrous membrane has been proposed (Figure 7).<sup>[189]</sup> Through electrostatic attraction, CS, ZnO NPs, and released Zn ions accumulated and adhered to the surface of the microbial cell membrane, consequently

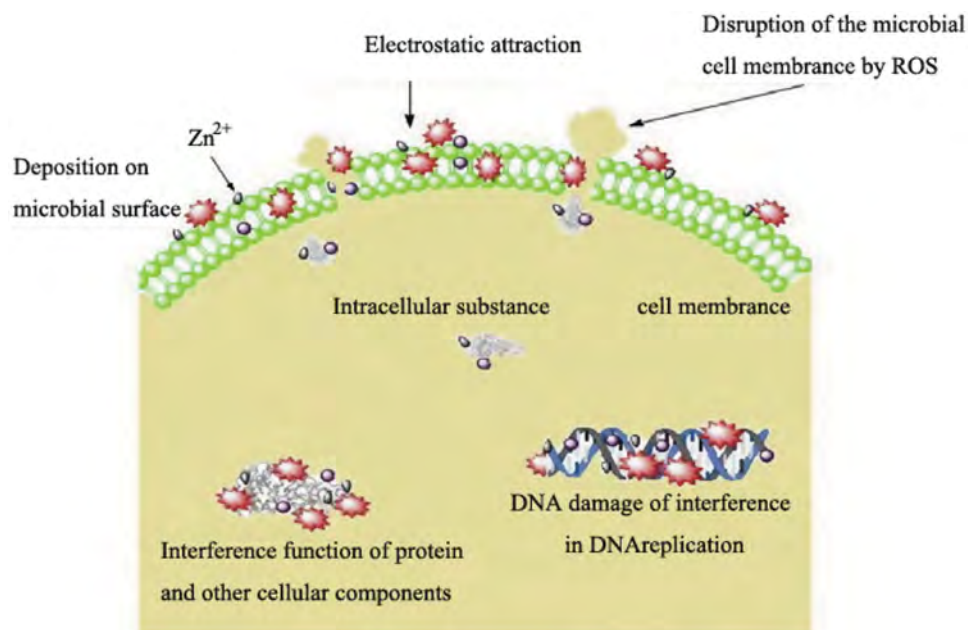


**Figure 7.** Schematic illustration of the antimicrobial mechanism of composite CS/nano-ZnO. Reproduced with permission.<sup>[189]</sup> Copyright 2012, Elsevier.

resulting in the denaturation of membrane proteins and a change in membrane permeability, which finally destroyed the membrane structure.<sup>[189]</sup> Petkova et al. observed that a hybrid ZnO/CS coating led to a 98% reduction in the growth of *S. aureus* at 60 min of incubation, whereas nanostructured ZnO and CS alone reduced bacterial growth by 61 and 31%, respectively, and that the viability of *E. coli* treated with this hybrid coating was reduced by no less than 96% after only 15 min.<sup>[191]</sup> Furthermore, the presence of CS improved the durability of the antimicrobial activity of this hybrid coating, which was ascribed to the high viscosity and low solubility of CS.<sup>[191]</sup> In addition to CS, ZnO NPs can also be carried on the surface of a biodegradable hydrogel and subsequently immobilized on the surface of biomedical devices, which mitigated bacterial infection and inflammation. Recently, a hybrid film composed of ZnO NPs and biocompatible poly (*N*-isopropylacrylamide) (PNIPAAm) exhibited efficient antimicrobial activity against *E. coli* at a very low ZnO concentration,<sup>[192]</sup> whereas most studies found that only ZnO NPs at much higher concentrations exhibited a comparable performance. Compared with nano-silver/organic hybrids, ZnO NPs/organic hybrids appear to be more promising for antibacterial applications because the bioactive organics in these hybrids such as CS and PNIPAAm, are biocompatible, biodegradable and non-toxic, and thus can be used as protective layers for tissue engineering,<sup>[192–195]</sup> whereas Ag/ZnO hybrids that leached Ag at high concentrations will induce the death of normal cells and tissues.<sup>[196]</sup>

Interaction between positively charged CS molecules and negatively charged microbial cell membranes leads to the leakage of proteinaceous and other intracellular constituents.<sup>[197–199]</sup> CS penetration toward the nuclei of the microorganisms and interference with the synthesis of mRNA and proteins by the combination of CS and DNA and inhibition of mRNA synthesis.<sup>[200,201]</sup> Therefore, the synergistic effect of composited nanostructured ZnO with CS could exhibit better antibacterial activity. Thus,

developing hybrids composed of nano ZnO and some nature polymers will be one of the best choices for antimicrobial agents.

### 3.1.4. Factor Affecting the Antibacterial Activity of ZnO Nanoparticles

**Concentration:** The antibacterial activity of nano ZnO reported in the literature varied, with the inhibitory concentration ranging from several to hundreds of mg L<sup>-1</sup>.<sup>[156,202–204]</sup> The differential results observed in many published nanotoxicological studies may be largely due to the fundamental dissimilarity of the testing media and the cell types employed. One Gram-positive bacteria, *Bacillus subtilis*, and two Gram-negative bacteria, *Pseudomonas putida* and *e. coli* were selected by Li et al. for a comparison of the toxic responses of different types of bacterial cells.<sup>[203]</sup> Although the viability rate of all of these cells decreased with the increasing dose of ZnO NPs, three bacterial species behaved differently upon exposure to the same level of nanoparticle suspension (**Figure 8**). In general, the two Gram-negative bacteria (*P. putida* and *E. coli*) were more resistant to the antibacterial activity of the ZnO NPs than the Gram-positive bacteria (*B. subtilis*). Increasing the ZnO concentration gradually reduced the percentage of viable *P. putida* cells exposed to 500 mg L<sup>-1</sup> of NPs from 85% to 58%. In contrast, exposure to 1 mg L<sup>-1</sup> of ZnO NPs resulted in the complete inactivation of *B. subtilis*. Moreover, *E. coli* showed an intermediate susceptibility to inactivation by ZnO NPs.<sup>[203]</sup> Brayner et al.<sup>[158]</sup> studied the toxicological impact of ultrafine ZnO NPs in a colloidal medium on *e. coli* bacteria. The presence of these NPs at concentrations between 10<sup>-2</sup> and 3.4 × 10<sup>-3</sup> M caused nearly 100% inhibition of bacterial growth. At concentrations of between 2.6 × 10<sup>-3</sup> and 1.7 × 10<sup>-3</sup> M, these NPs inhibited bacterial growth by approximately 85%. When these NPs were applied at concentrations of between 1.3 × 10<sup>-3</sup> and 10<sup>-3</sup> M, an increase in the number of *E. coli* colonies was observed. One might predict from these results that this increase in colony number was

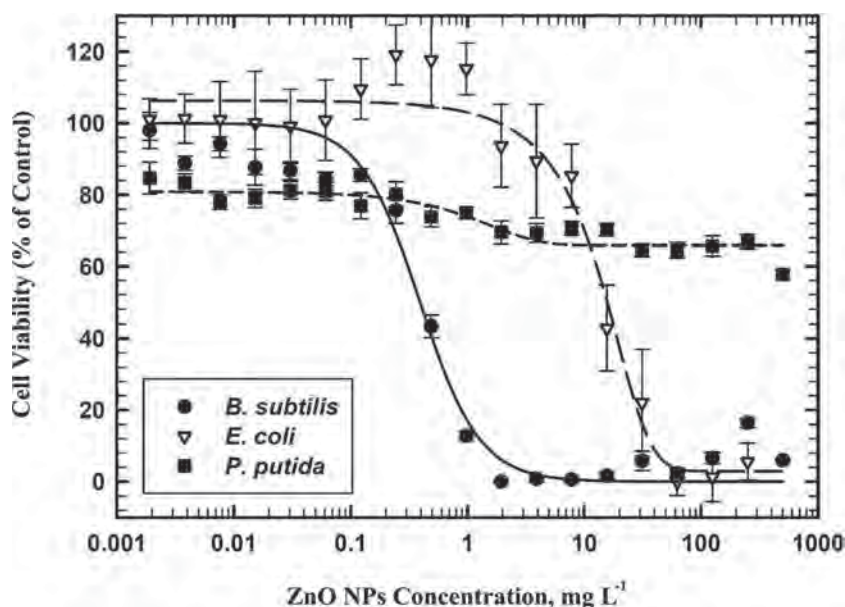


**Figure 8.** Typical dose–response curves of ZnO nanoparticles for three types of bacteria cells in fresh water. Reproduced with permission.<sup>[203]</sup> Copyright 2011, American Chemical Society.

metabolism-dependent because bacteria metabolize  $Zn^{2+}$  as an oligoelement, demonstrating that ZnO NPs are not toxic for *E. coli* at these concentrations.<sup>[158]</sup> It was demonstrated by Roselli et al. that ZnO NPs at concentrations of 0.01 to 1 mmol  $L^{-1}$  did not affect cell permeability, whereas the cell permeability slightly increased when the ZnO NPs were applied at 5 mmol  $L^{-1}$  compared with that of untreated cells.<sup>[205]</sup> Moreover, Brayner and colleagues obtained preliminary results showing the cellular internalization of ZnO NPs and cell-wall disorganization of treated *E. coli*, i.e., the cell membrane of all of the *E. coli* was extensively damaged and, most likely, the intracellular contents had leaked out when the cells contacted ZnO NPs applied at concentrations greater than 1.3 mmol  $L^{-1}$ .<sup>[158]</sup> Yan et al. also evaluated the colony formation of *S. aureus*, *Streptococcus agalactiae*, and *E. coli* cultured in the presence of ZnO NPs at different concentrations.<sup>[202]</sup> The results showed that ZnO NPs had a 50% inhibitory effect on *S. agalactiae* at concentrations of >100 mM, whereas ZnO NPs applied at the same concentrations only slightly inhibited the growth of *S. aureus* and *e. coli*. When applied at a concentration of 50 mM, the ZnO NPs induced a remarkable proliferation of *S. aureus* and *E. coli* but slightly inhibited the growth of *S. agalactiae*. Applying  $\leq 25$  mM of ZnO NPs significantly promoted bacterial growths of all of groups. These observations suggested that the mineralized ZnO NPs possessed favorable cytocompatibility. The relatively low toxicity of ZnO NPs to *S. aureus* and *E. coli* was most likely due to their relatively high tolerance of Zn ions.<sup>[202]</sup>

**Particle Size:** Several studies suggested that the unique properties (i.e., the small size and corresponding large specific surface area) of the small nanometer-scaled ZnO particles impose several qualities that govern their antibacterial activity, with smaller NPs having a more effective antibacterial activity.<sup>[21,125,157,206,207]</sup> Yamamoto et al. studied the antibacterial activity of ZnO powders of various particle sizes, in the range of 0.1–0.8  $\mu m$ .<sup>[207]</sup> The activity of the ZnO powder slurries was

monitored by measuring the change in electrical conductivity with bacterial growth, and it was found that the antibacterial activity increased with the decreasing size of the ZnO-powder particle. Apperlot performed a study of the effects of particle size on the antibacterial activity using two bacterial species: *E. coli* and *S. aureus*.<sup>[125]</sup> The viability rate of each bacterial strain after incubation with ZnO suspensions indicated that the antibacterial activity of the ZnO NPs was size-dependent, with the smallest NPs presenting the highest antibacterial efficacy of 71% inactivation of *S. aureus* and 98% inactivation of *E. coli* when an equivalent ZnO mass content was used. Increasing the size of the ZnO NPs led to a less effective antibacterial activity with respect to *S. aureus*, whereas the effect of particle size on their antibacterial activity toward *E. coli* was less obvious. To exclude the possibility that the zinc ions in the aqueous suspension of ZnO NPs were responsible for the antibacterial activity, specific control experiments were conducted. It

was demonstrated that the concentration of  $Zn^{2+}$  ions resulting from dissolving  $Zn(Ac)_2 \cdot 2H_2O$  in water at more than 5 times the aqueous solubility of ZnO did not have any effect on the viability rate of *E. coli* or *S. aureus*. Based on the mechanism underlying the antibacterial activity of the ZnO NPs, their size-related biocidal behavior was revealed by the following results: 1) more cellular internalization was observed when smaller NPs were applied, and 2) the smaller NPs generated a larger amount of hydroxyl radicals in the aqueous suspensions.<sup>[125]</sup> Raghupathi et al. synthesized high-quality ZnO NPs of varying sizes using simple room temperature or solvothermal methods and tested their antibacterial activity using either turbidity or plate assays to understand their antibacterial activities.<sup>[21]</sup> They synthesized seven ZnO NPs of various sizes, using a combination of room temperature and solvothermal synthetic methods. As shown in **Figure 9a**, it was clearly shown that the ZnO NPs exerted size-dependent inhibition of *S. aureus* growth at a concentration of 6 mM. It was demonstrated that the viability of *S. aureus* cells decreased significantly with the decrease in the size of ZnO NPs applied at 6 mM (Figure 9b). To verify these results, they provided evidence that the rate of release of free  $Zn^{2+}$  ions from the ZnO colloidal solution was minimal under the experimental conditions and that the antibacterial activity of the ZnO NPs was dependent on the size of the NPs, which was mainly ascribed to the activity of the ZnO NPs rather than that of the free  $Zn^{2+}$  ions.<sup>[21]</sup>

Taken together, except for the testing medium and cell types employed, it could be concluded that the antibacterial activity of ZnO NPs was strongly dependent upon their concentrations and particle size.

### 3.2. ZnO-Based Bone Implants

A bone implant should act as a scaffold to support the formation of new bone, blood vessels and soft tissues, and consequently

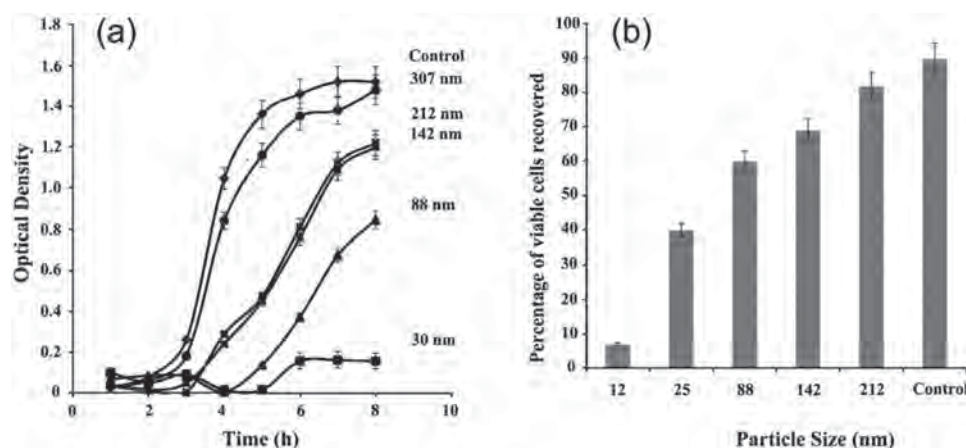


**Figure 9.** Effect of different sizes of ZnO nanoparticles on the growth of methicillin sensitive *S. aureus* strain. a) Growth analysis curves measured by monitoring the optical density (OD) at 600 nm, and b) the viable *S. aureus* 6390 recovered from TSA plates after 24 h of incubation at 37 °C. Cultures were grown in the presence of 6 mM of various sizes ZnO nanoparticles and after 6 h cultures were diluted to  $10^{-6}$  and placed on TSA plates in triplicates. Colonies were counted and the percentage of growth inhibition was calculated and plotted against particle sizes. The experiments were repeated at least three independent times and the average data was presented in the figures. Reproduced with permission.<sup>[21]</sup> Copyright 2011, American Chemical Society.

form a bridge between the existing bone and the graft material to favor the reconstruction of damaged bone tissues. Due to the bacterial colonization of the surface of implanted materials, a well-known problem of bone implants is bacterial infection and the subsequent complications for orthopedic surgery, which often leads to implant failure, prolonging the period and raising the costs of hospitalization, and sometimes even resulting in the patient's death.<sup>[208]</sup> Therefore, the perfect bone implant should not only be biocompatible, easy to manipulate, mechanocompatible with bone tissues and readily available as well as resorbable or biodegradable in the long term, but should also inhibit the growth of pathogens.<sup>[209]</sup> Because natural bone tissues or organs are nanoscale in size and cells directly interact with nanostructured extra-cellular matrices (ECM), the ECM complex plays a key role in promoting new bone formation and guiding tissue regeneration. Due to their ability to mimic the dimensions of the constituents of natural bone, such as proteins and hydroxyapatite, researchers have fabricated cyto-compatible biomimetic nanomaterial scaffolds encapsulating cells (such as osteoblasts and stem cells) for tissue engineering applications. Importantly, the nanoscale biocomposites possess the hardness and the compressive, bending, and tensile strengths comparable to conventional materials and are more similar to physiological bone. Apart from the dimensional similarity to bone tissue, nanomaterials exhibit several unique surface properties (such as their surface topography, surface wettability and surface energy) due to their larger surface area and greater roughness. Hybrid scaffolds composed of polymers and nanoceramics possess great advantages over those made of traditional biomaterials, such as pure ceramics and biopolymers, in satisfying these demands. ZnO is one of the most promising candidates for inclusion in these novel hybrid scaffolds due to its intrinsic characteristics.

Firstly, Zn has been widely recognized as an essential trace element for the proper maintenance of bone growth, with over 85% of the total body Zn residing in bone.<sup>[210]</sup> Zn has a positive effect on bone metabolic factors, such as growth hormone (GH)

or insulin-like growth factor 1 (IGF-1).<sup>[211,212]</sup> Furthermore, Zn stimulates bone formation in vivo by activating protein synthesis in osteoblast cells and increasing ATPase activity in bone. Moreover, Zn deficiency has been associated with the retardation and failure of bone growth in animals.<sup>[213–215]</sup> Ito et al. showed that the presence of Zn in bioceramics, such as those containing tricalcium phosphate and hydroxyapatite, stimulated osteoblastic differentiation and increased the ALP activity of stromal cells.<sup>[216]</sup> It was also found that Zn-substituted HAP modulated osteogenic activity.<sup>[217,218]</sup> Moreover, Zn showed a potent inhibitory effect on bone resorption by inhibiting the formation of osteoclasts in mouse marrow cultures.<sup>[158]</sup> These results indicated that Zn affects the activity of bone cell. More recently, Zn was identified as a regulator of the transcription of osteoblastic differentiation genes, such as the collagen I, ALP, osteopontin and osteocalcin genes.<sup>[219]</sup> It was suggested that Zn could be a Runx2-stimulatory agent through directly stimulating bone formation by increasing the transcription rate of Runx2-targeted osteoblastic differentiation genes.<sup>[219]</sup> Yamaguchi et al. studied the role of Zn both in vitro and in vivo in rats, and they found that treatment with  $Zn^{2+}$  at a concentration of  $6.5 \text{ mg L}^{-1}$  increased the calcium content, bone protein content and alkaline phosphatase activity of rat calvariae.<sup>[213,220]</sup> Administering a low dose of Zn to rats was shown to lead to an increase in the alkaline phosphatase activity and DNA content of bone tissue.<sup>[221]</sup>

CS and poly( $\epsilon$ -caprolactone) (PCL) have been blended with zinc-doped hydroxyapatite NPs (nZnHA) using a mixed formic acid/acetic acid solvent system to electrospin nanofibrous scaffolds.<sup>[222]</sup> These PCL/CS/nZnHA scaffolds had an elastic modulus (approximately 3-fold higher) and tensile strength (nearly 1.5-fold higher) that were higher than those of the corresponding PCL/CS scaffold. In contrast to the smooth surface of PCL/CS nanofibers, the nZnHA that was dispersed on the surface of the PCL/CS fibers led to rougher surfaces. Hydrophilicity, roughness, porosity and pore size have a significant impact on the protein adsorptive capacity of

polymer/bioceramic composite scaffolds. Their studies clearly demonstrated that the PCL/CS(10)/nZnHA composite had the highest level of protein adsorptivity among the samples tested due to its higher levels of hydrophilicity and roughness. The order of the proliferation rates of adipose tissue-derived mesenchymal stem cells (hAD-MSCs) grown on various types of scaffolds at five days of culture was as follows: PCL/CS (10)/nZnHA > PCL/CS (10)/nHA > PCL/CS (10) > PCL, and the PCL/CS (10)/nZnHA nanofibrous scaffold had a significantly larger number of cells adhering to its surface, as shown using a cell-adhesion assay.<sup>[222]</sup> Amna et al. fabricated one-dimensional ZnO doped TiO<sub>2</sub> nanofibers through electrospinning and evaluated these hybrid nanofibers as an extracellular scaffold the support of myoblasts.<sup>[223]</sup> In this study, the number of C2C12 cells attached to the surface of the nanostructured ZnO/TiO<sub>2</sub> hybrid nanofibers was greater than that on the titanium-containing and control samples at 180 and 240 min of culturing. Cell counting using a Kit-8 assay and phase-contrast microscopy at regular intervals revealed that the C2C12 cells proliferated well on ZnO/TiO<sub>2</sub> nanofibers applied at between 1 and 10  $\mu\text{g m}^{-1}$ . Additionally, the cells displayed extensive spreading on the surface of the hybrid sample.<sup>[223]</sup> This group also fabricated a ZnO-doped poly(urethane) (PU) nanofibrous scaffold with unique spider nets via the cost-effective one-step electrospinning method, and analyzed the morphology of the resulting spider nanonets attached to the main fibers and morphological features of the fibroblast cells attached to the nanofibers.<sup>[224]</sup> These nanofibrous structures had a large surface area and provided multiple binding points for the strong physical adhesion and interaction of cells. As shown in **Figure 10a**, it was clear

that the pristine PU electrospun fibers that were obtained had a smooth surface and uniform diameters. After ZnO doping, an interconnected spider net-like structure formed (**Figure 10b**). This result suggested that the presence of ZnO during the ionization of the polymer solution during electrospinning led to the formation of the spider net-like structure. Additionally, it was also found that the proportion of living cells was maximal on the composite nanofibers (**Figure 10c,d**).<sup>[224]</sup> Taken together, the results indicated that nano-ZnO doping increased the surface area of the nanocomposite and modified its surface properties to promote the adhesion, growth, proliferation and differentiation of cells and that it might be successfully exploited for various tissue-engineering applications. Park et al. demonstrated that ZnO nanoflowers were tightly osseointegrated with the regenerated bones in the calvarial bone defects of SD rats, which was ascribed to the more significant formation of lamellipodia, filopodia, and F-actin filaments on the surface of these nanostructures.<sup>[225]</sup> These results supported the hypothesis that ZnO nanostructures would promote the adhesion, proliferation, growth, and osseointegration of cells and could be successfully applied as orthopedic implantation materials.

### 3.3. ZnO-Based Wound Dressings

#### 3.3.1. Fundamentals of Wound Dressings

The concept of a wound dressing was introduced by Winter,<sup>[226]</sup> who was the pioneer of research to establish and maintain an optimal environment for wound healing. Awareness of this work led to the development of functionally active wound dressings that interacted with the wounds they covered to create and maintain a moist and healing environment. Currently, various types of wound dressing materials are available commercially, e.g., those made of synthetic polymers such as polyurethane, poly(vinyl alcohol), poly(lactic acid), and those using natural polymers, such as alginate, chitin, CS and collagen.<sup>[227–229]</sup>

An ideal dressing should maintain a moist environment at the wound interface, allow an adequate gaseous exchange, act as a barrier to microorganisms, remove the excess exudates to avoid maceration, and minimize scar formation. Such a wound dressing should also be non-toxic, non-allergenic, nonadherent, easily removed without trauma, biodegradable, exert a hemostatic potential, and biocompatible.<sup>[230]</sup> In addition, this wound dressing should be composed using an available biomaterial that requires minimal processing, possesses antimicrobial properties and promotes wound healing.

#### 3.3.2. ZnO-Based Wound-Dressing Materials

Wound infection is the major concern in the field of wound care management because

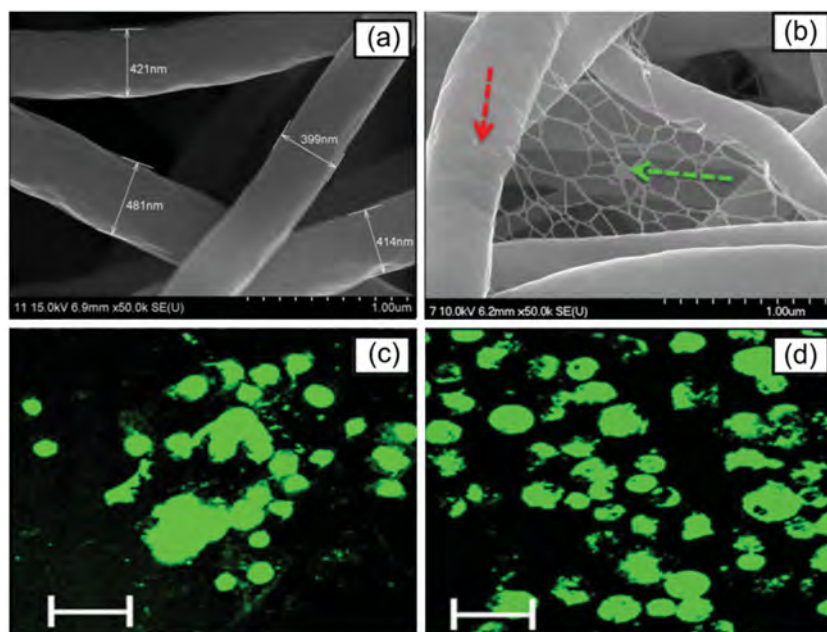


**Figure 10.** FE-SEM micrographs of a) pristine PU and b) ZnO-doped PU composite nanofibers; the red arrow indicates the main fibers, whereas the green arrow demonstrates the harbored ultrafine nets. Representative confocal images of cells cultured on c) a pristine PU, and d) on a composite matrix for 5 days. The cells were stained by DiOC18(3)/PI. Dead cells are labeled by PI and have red nuclei. Live cells are labeled by DiOC18(3) and have green nuclei. The scale bars represent 100  $\mu\text{m}$ . Reproduced with permission.<sup>[224]</sup> Copyright 2013, Springer.

wound infections can cause exudate formation, facilitate improper collagen deposition and prolong the healing process.<sup>[231]</sup> Both microbes and the dressing material–wound surface interaction can initiate infection. Microbes are the major cause of wound infection, and the major infection-causing bacteria are *S. aureus* and *E. coli*.<sup>[232,233]</sup> Microbes can enter the body through the wounds and reach the deeper portions of tissues, leading to internal infections.<sup>[232]</sup> At times, even the wound dressing itself can cause an infection due to the nature of the wound dressing–exudate interface or the nonsterility of the wound dressing.<sup>[234]</sup> For these reasons, the treatment of severe wounds requires inhibiting bacterial growth.

The main antibacterial strategy is to combine different antibacterial agents to overcome the resistance of the microorganisms and obtain synergic antibacterial activity.<sup>[235]</sup> Recently, the use of inorganic antimicrobial agents for the control of microbes has attracted interest because inorganic antimicrobial agents have a broader spectrum of antibacterial activity and bacteria might not evolve resistance to them as they have to organic antibiotics.<sup>[236,237]</sup> At present, most of the antibacterial inorganic materials are metallic NPs<sup>[238–240]</sup> and metal oxide NPs, such as ZnO.<sup>[241–244]</sup> At a neutral pH, the common dressing materials, such as chitin and CS, do not show any antibacterial activity due to their lack of free  $-\text{NH}_2$  groups;<sup>[231]</sup> therefore, antibacterial agents must be incorporated into them to achieve it.<sup>[245]</sup> ZnO NPs not only possess potent antibacterial activity but also have no adverse effect on normal cells at the appropriate concentration.<sup>[206]</sup>

Kumar et al. have developed flexible and microporous CS hydrogel/nano ZnO composite bandages (CZBs) via the incorporation of ZnO NPs into a CS hydrogel.<sup>[246]</sup> The swelling, degradation, blood-clotting activity, antibacterial activity, and cytocompatibility of the composite bandages, as well as the cellular attachment to the material and the cellular infiltration into the composite bandages were evaluated, and the results showed that the CZBs exhibited controlled degradation, enhanced blood clotting, excellent platelet-activation ability, and good cytocompatibility.<sup>[246]</sup> Furthermore, the *in vivo* evaluations in Sprague–Dawley rats revealed that these nanocomposite bandages enhanced wound healing and hastened re-epithelialization and collagen deposition. *In vitro* and *in vivo* antibacterial activity studies demonstrated the antibacterial potential of the prepared CZBs.<sup>[246]</sup> Together, these results indicated that these advanced CZBs could be used to treat burns, chronic lesions, and diabetic wound infections. In another study, ZnO NPs were prepared from polyester using the Pechini method by reacting citric acid with ethylene glycol in which metal ions were dissolved and incorporated into blendfilms of CS and PVA with polyoxyethylene sorbitan monooleate and Tween 80 at different concentrations; these ZnO NP-containing dressing films showed excellent antibacterial activity toward *S. aureus*.<sup>[247]</sup> The observed antibacterial activity of the composite films suggested that they could be used as hydrophilic wound and burn dressings.

In addition to their antibacterial activity, the Zn ions released from ZnO nanomaterial enhanced keratinocyte migration toward the wound site and promoted wound healing.<sup>[18]</sup> The effect of ZnO on wound re-epithelialization and its bacteriostatic properties endorsed it as an effective ingredient for

topical wound dressings. ZnO in paste bandages protects and soothes inflamed peri-ulcer skin. A ZnO-medicated occlusive dressing was significantly more effective in the debridement of diabetic foot ulcers than autodebridement using a standard hydrocolloid occlusive dressing.<sup>[248]</sup> A study in which the wounding process of mouse skin was monitored showed that Zn accumulated in proliferating epithelial cells at the wound margin within 12 h.<sup>[249]</sup> In addition, the wound healing process was also controlled by the up-regulation of the Zn-dependent metalloproteinases that are responsible for the degradation of the extracellular matrix.<sup>[250]</sup> The level of injury-related catabolism was found to affect the amount of Zn lost through excretion.<sup>[251–254]</sup> The greater the injury and rate of catabolism, the greater the Zn excretion. Chesters and Boyne found that serum-fed 3T3 fibroblasts had a critical Zn-dependent phase from 8 to 13 h after feeding.<sup>[255]</sup> The synergistic interaction of epidermal growth factor and Zn in promoting re-epithelialization and enhancing collagen deposition at the site of full-thickness skin wounds in mice has also been reported.<sup>[256]</sup>

In summary, ZnO doped with different micro/nano structured materials may influence the behaviors of the bone cells and the keratinocyte migration as well as bacterial behaviors. Past research mainly depended on the biological behavior of bone cells and keratinocyte on different ZnO-based nano-hybrids. In the case of tissue regeneration, the best way is to develop a new generation of biomaterials that can not only modulates the cell behavior but also possesses self-antibacterial activity, thus accelerating the tissue reconstruction. Functionalized ZnO-based hybrids may be one of the best candidates.

## 4. Bioimaging

In addition to the intrinsic advantages of ZnO QDs over conventional organic dyes, such as better photoluminescent (PL) properties, including broad-band absorption, a narrow and symmetrical emission band, a tunable emission wavelength, high stability against photo-bleaching,<sup>[257–260]</sup> and being one of the most important semiconductor materials, ZnO QDs are also much better than the commonly used QDs that are based on CdSe and CdTe species for biomedical imaging applications due to their excellent biocompatibility,<sup>[261]</sup> good biodegradability,<sup>[262]</sup> low cost and eco-friendliness,<sup>[263]</sup> whereas the latter exhibit biotoxicity.<sup>[264,265]</sup> The typical bioimaging applications of ZnO QDs include tracing live cells and real-time monitoring of target tissues.<sup>[266–268]</sup>

### 4.1. Live-Cell Imaging

ZnO QDs derived using traditional sol-gel approaches have several drawbacks, including low quantum yield, generally less than 10%, an unstable emission peak, and a broad photoluminescence (PL) band, which result from the insufficient protection from various physiological environments and the surface vacancy-driven ZnO luminescent mechanism.<sup>[269]</sup> In addition, conventional ZnO QDs are unstable in aqueous solutions because water exchanges with the organic protective groups on their surface, destroying the luminescent centers

and causing aggregation of the ZnO QDs, which consequently quenches their fluorescence.<sup>[270,271]</sup> This problem can be solved through surface modification using certain ligands, such as polyethylene glycol methyl ether (PEGME),<sup>[272]</sup> PEG(COOH)<sub>2</sub>,<sup>[273]</sup> polyvinylpyrrolidone (PVP),<sup>[274]</sup> oleic acid (OA) together with diethanolamine (DEA),<sup>[275]</sup> and hyperbranched polymers.<sup>[276]</sup> However, some new problems occur after hybridization with these ligands, such as unstable long-wavelength emission,<sup>[277]</sup> reduced luminescent efficacy or hypochromic shifted emission, which can be difficult to quantify due to the autofluorescence of the targeting cells.<sup>[278]</sup> For example, Fu et al. showed that ZnO QDs could be stabilized in aqueous solutions by coating them with DEA and OA, and the hybrids exhibited blue emission in the visible range only at 430 nm, meaning that they could not be used for bioimaging because most cells and tissues also appear blue under UV light.<sup>[275]</sup> Structural and particle-size designing of hybrids has been widely employed to solve these problems. Using a two-step polymerization process, Xiong et al. fabricated two types of highly stable luminescent nano ZnO@poly(MAA-co-PEGMEMA) hybrids of different sizes but with the same core-shell structure, i.e., ZnO QD cores with a binary polymeric ligand shell composed of an internal layer of hydrophobic MAA (methyl acrylic acid) and an external layer of hydrophilic PEGMEMA, which exhibited tunable PL for cell imaging, and hydrophobic-hydrophilic copolymer shells that made the NPs miscible with water yet protected the ZnO cores from water.<sup>[279]</sup> As shown in **Figure 11**, within human hepatoma cells, ZnO-1 QDs with an average size of 3 nm emitted green light, whereas 4-nm ZnO-2 ODs emitted yellow light, at 520 nm and 550 nm (typical ZnO-vacancy luminescence), respectively.<sup>[279]</sup> Cytotoxicity tests revealed that more than 90% of human hepatoma cells survived when the concentrations of ZnO-1 and ZnO-2 QDs were less than 0.2 mg mL<sup>-1</sup>.<sup>[279]</sup> Furthermore, these ZnO QDs were located in the cytoplasm, whereas the nuclei were not luminescent, and under continuous UV-light irradiation, the luminescence was very stable during cell culturing and the cells were alive at 45 min of exposure.<sup>[279]</sup>

It has been reported that the luminescence of ZnO-QDs is not very stable in circulating blood due to their possible decomposition or site-quenching by organs.<sup>[280]</sup> Therefore, recent research has focused on the development of core-shell hybrids composed of ZnO QDs modified with a silica shell or silane groups to strengthen their stability within complex biological environments.<sup>[281–286]</sup> Silica was selected as the shell material because of its biocompatibility, aqueous stability, and rich surface chemistry.<sup>[284,285]</sup> Using a facile ethanol-based precipitation method, Tang et al. encapsulated the precipitated ZnO NPs with silica to form ZnO@silica core-shell nanostructures (**Figure 12a**), which exhibited emission colors of blue, green, yellow, and orange under 365-nm excitation via the adjustment of the pH of the precipitation solutions (as shown in

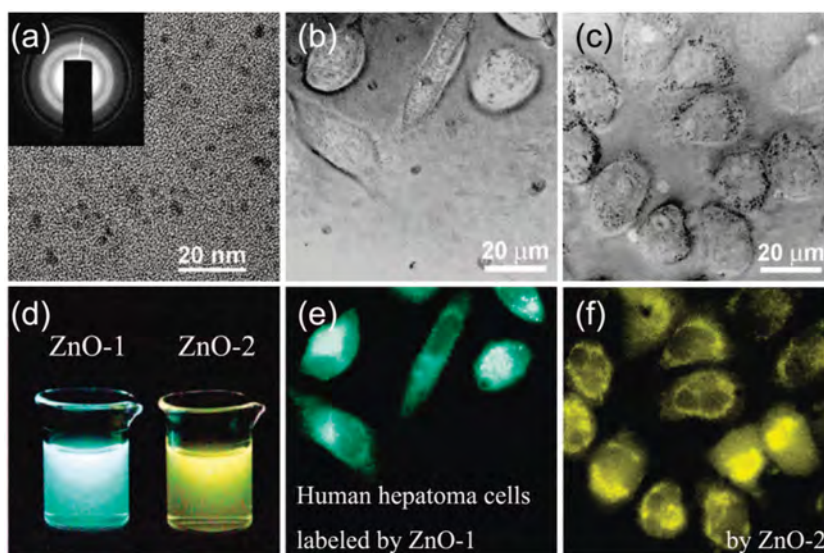


**Figure 11.** a) HRTEM image of ZnO-1 with the electron diffraction pattern in the inset. d) Aqueous solutions of ZnO-1 and ZnO-2 under a UV light. b) DIC and e) fluorescent images of the cells labeled by ZnO-1. shows c) DIC and f) fluorescent image of the cells labeled by ZnO-2. Reproduced with permission.<sup>[279]</sup> Copyright 2008, American Chemical Society.

Figure 12b), and these core-shell NPs exhibited excellent stability not only in water but also in PBS at up to one week.<sup>[281]</sup> In vitro culture studies revealed that NIH/3T3 cells could easily uptake the three types of ZnO@silica hybrids with green, yellow and orange light emission resulting from the different surface charges of the oxides formed during their precipitation in solutions with different pH values (Figure 12c).<sup>[281]</sup> As shown in Figure 12d, more than 85% of the cells survived when the concentration of ZnO NPs in the medium was less than 30 μg mL<sup>-1</sup>, suggesting that these ZnO NPs were quite safe for living cells and consequently suitable for cell labeling.<sup>[281]</sup> Subsequent research confirmed that these types of silica-coated ZnO NPs were promising candidates for live-cell labeling after suitable surface modification.<sup>[286]</sup> After amino groups of MAA were grafted to them, the ZnO@silica NPs were very stable in water, PBS and Roswell Park Memorial Institute (RPMI) medium. This was attributed to the tight and dense shell surrounding the ZnO NPs that was produced during the three-step silanization process, which favored the subsequent polymerization of vinyltriethoxysilane (VTES) and 3-aminopropyltriethoxysilane (APS), so that the emission wavelength could be easily modulated by controlling the particle size via changing the reactant ratio and the reaction time.<sup>[286]</sup> Cellular labels were largely found in the cytoplasm rather than the nucleus, and the fluorescence intensity of the targeting cells rose gradually with increased exposure to the medium containing the hybrids, indicating the progressive uptake of the ZnO@silica particles by the cells.<sup>[286]</sup> In addition, 4.4-nm ZnO@silica NPs caused a much higher ROS level in cells exposed to UV irradiation, which could possibly be used for killing cancer cells.<sup>[281]</sup>

In addition to the aforementioned issue of their chemical stability, another critical issue for the bioimaging applications of ZnO QDs is their photoluminescent quantum yield (PLQY). It has been reported that QYs of ZnO QDs produced using chemical sol-gel processes could reach as high as 26%.<sup>[281]</sup>

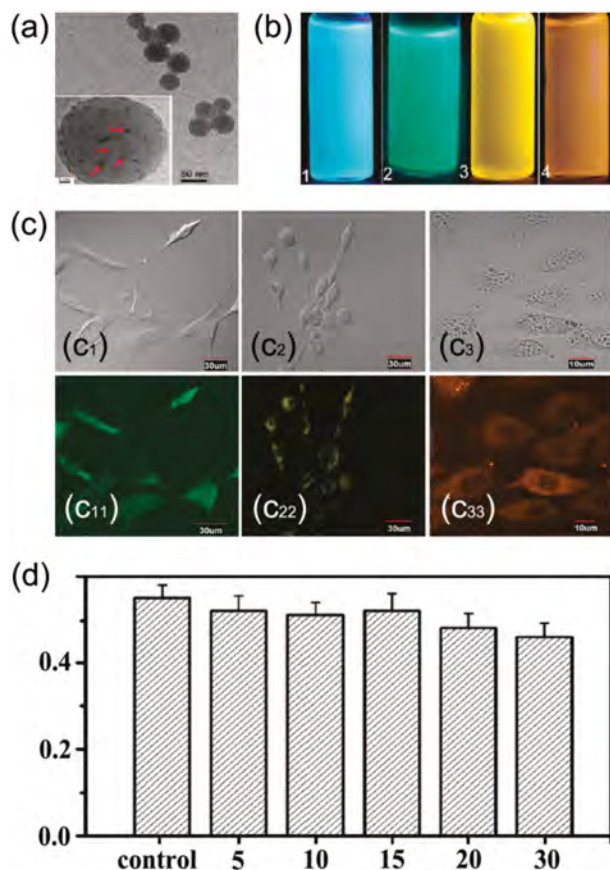


**Figure 12.** a) TEM image of ZnO@silica core shell nanospheres. ZnO was prepared at pH 10. The inset is the high-magnification image of a single nanosphere. b) Corresponding photographs of ZnO nanoparticles prepared at pH 1) 12, 2) 10, 3) 8, and 4) 6 under 365 nm excitation. c) DIC photograph (c<sub>1</sub>) and fluorescent image (c<sub>11</sub>) of the cells labeled with ZnO@silica nanoparticles with green emission. DIC photograph (c<sub>2</sub>) and fluorescent image (c<sub>22</sub>) of the cells labeled with ZnO@silica nanoparticles with yellow emission. DIC photograph (c<sub>3</sub>) and fluorescent image (c<sub>33</sub>) of the cells labeled with ZnO@silica nanoparticles with orange emission. d) Cell viability of incubated NIH/3T3 cells with increasing concentrations of ZnO nanoparticles for 24 h. Cell viability was measured using the 3-(4,5)-dimethylthiazolazo(-z-y1)-3,5-di-phenyltetrazoliumromide (MTT) assay. Reproduced with permission.<sup>[281]</sup> Copyright 2010, American Chemical Society.

Through designing a special core-shell structure, Xiong prepared blue fluorescent ZnO QDs with a high PLQY of up to 80%.<sup>[276,287]</sup> More recently, Felbier et al. produced ZnO QDs in a radiofrequency capacitively coupled plasma, which exhibited a size-dependent PLQY of up to 60% in the visible part of the spectrum after exposure to air.<sup>[288]</sup> After exposure to ambient air for one day, a peak PLQY of 12% and 60% was achieved by 3.4-nm and 2.1 nm-ZnO QDs, respectively, whereas the value after one hour of air exposure was 9% and 42%, respectively, indicating the importance of the QD diameter for the PLQY, which was contrary to the results obtained for

Si and CdSe QDs, i.e., the PLQY of the latter increased with the increasing QD size.<sup>[288]</sup> It was believed that the surface states of the ZnO QDs were quite different from those of the others.<sup>[288]</sup>

In addition to ZnO@polymer and ZnO@silica QDs, some ZnO-based compounds have also been developed as cellular probes. Aboulaich et al. adopted a two-step procedure to prepare biocompatible ZnSe:Mn/ZnO core/shell QDs using 1-thioglycerol as the stabilizer in an aqueous solution.<sup>[289]</sup> Compared with the QY of ZnSe:Mn QDs, the PLQY of these compound QDs was found to be enhanced by 12%, which was attributed to the presence of ZnO.<sup>[290–292]</sup> Moreover, under ambient conditions, these compound QDs were found to be stable for months. This finding indicated that these nanocrystals could be used as building blocks to produce bioprobes for cell and tissue imaging.

#### 4.2. In Vivo Animal Imaging

Studies have revealed that the aforementioned ZnO-based QDs could be injected into the body through intradermal and intravenous injections to facilitate clinical diagnosis and the treatment of the targeted tissues.<sup>[280,293]</sup> At only 5 minutes post-intradermal injection of ZnO@poly(MAA-co-PEGMEMA) QDs, their fluorescence could be clearly observed under UV light (Figure 13a) and it was still observed at 60 minutes post-injection (Figure 13b). Furthermore, the fluorescence of the ZnO QDs could be observed in the aortas, livers and kidneys of intravenously injected mice that had been sacrificed after 5 minutes of exposure to UV light (Figure 13c).<sup>[280]</sup> The latest research showed that after the consecutive intravenous injection of ZnO QDs and ZnO@PEG QDs, these two types of QDs did not affect the liver coefficient or the levels of serum aminotransferases and that although the levels of antioxidant enzymes and lipid peroxidation significant changed by 24 h after the injection of 5 mg kg<sup>-1</sup> of ZnO QDs, all of these parameters returned to the control levels by 28 days (Figure 14).<sup>[293]</sup> These results suggested that this type of ZnO QD might be a good bioprobe for labeling specific tissues such as the skin, aorta, liver and of kidneys, to potentially assist in their treatment.

However, the risk of injuries to live organs under long-term UV irradiation and the limited depth of UV-light penetration restrict the application of ZnO QDs in vivo because UV light

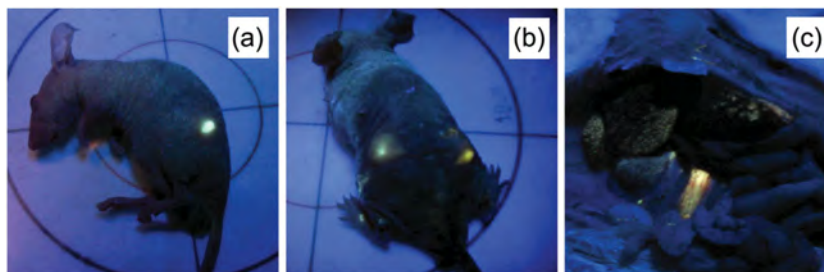


**Figure 13.** A mouse under UV light after intradermal injection. a) 5 min after intradermal injection of ZnO-1; b) 60 min after intradermal injection of ZnO-1 (left side) and ZnO-2 (right side); c) An intravenously injected mouse was sacrificed after 5 min and imaged under UV light. Note that ZnO-2 nanoparticles locate mainly in the aorta, liver and kidney. Reproduced with permission.<sup>[280]</sup> Copyright 2011, Wiley-VCH.

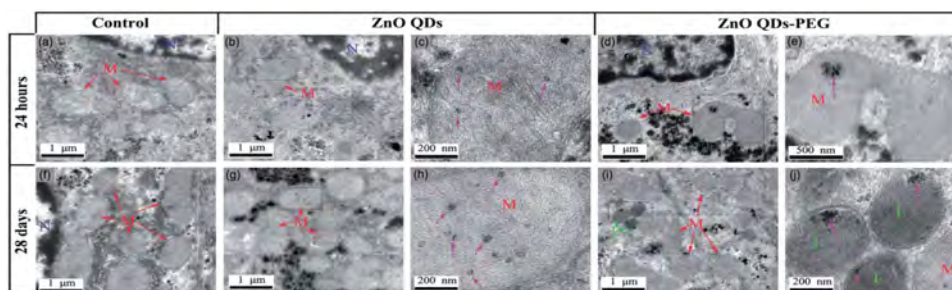


**Figure 14.** Ultrastructure of hepatocyte after treatment at a-e) 24 h and f-j) 28 days with a control (a,f), 5 mg kg<sup>-1</sup> of ZnO QDs (b,c,g,h), and ZnO QDs-PEG (d,e,i,j). Red arrows indicate mitochondria, green arrows indicate lysosome, and pink arrows indicate ZnO QDs. Abbreviations: (N) nucleus, (M) mitochondria, (L) lysosome. Reproduced with permission.<sup>[293]</sup> Copyright 2014, Royal Society of Chemistry.

is necessary to excite ZnO fluorescence due to its bandgap being in the UV region.<sup>[287,294]</sup> In contrast, magnetic resonance imaging (MRI) can penetrate deep into tissue to provide anatomical details and high-quality three-dimensional images of soft tissue in a non-invasive monitoring manner.<sup>[295]</sup> Unfortunately, this technique generally shows lower spatial resolution than fluorescence endoscopy.<sup>[296,297]</sup> Therefore, various multimodal imaging probes that allow the combination of different imaging modalities have been developed for more accurate imaging and diagnosis, and studies have been focused on the investigation of magnetic-fluorescent NPs that could serve as magnetic-resonance contrast agents for MRI and optical probes for intravital fluorescence imaging (FI).<sup>[298–302]</sup> It has been reported that ZnO QDs doped with magnetic elements such as magnesium (II),<sup>[303]</sup> and rare earth elements, such as europium (III) and lanthanum,<sup>[304,305]</sup> possessed fluorescent and magnetic properties making them suitable as MRI molecular imaging probes within the body.<sup>[306–309]</sup> For instance, fluorescent and magnetic bifunctional ZnO:Er,Yb,Gd QDs were synthesized via a simple homogeneous precipitation method and were found to successfully label human hepatocellular carcinoma (HepG2) cells and to present low toxicity even at the high concentration of 2 mg mL<sup>-1</sup>.<sup>[307]</sup> In that study, the longitudinal relaxivity rate ( $r_1$ ) of these QDs was tunable in a range of 23.03 mM<sup>-1</sup> s<sup>-1</sup> to 36.84 mM<sup>-1</sup> s<sup>-1</sup>, which was a much larger range than that of previously reported Gd-based NPs, suggesting that they would be good candidates for MRI applications.<sup>[307]</sup> Liu and colleagues demonstrated that Gd-doped ZnO QDs that showed contrast enhancement in MRI and exhibited significantly enhanced down-conversion of the yellow emission resulting from the Gd doping, successfully labeled HeLa cells within a short period and did not present any toxicity or adverse effect on cellular growth at a concentration of up to 1 mM.<sup>[308]</sup> As shown in **Figure 15b,c**, the yellow emission by the cells intensified as the incubation period increased, but no emission from cells incubated in the absence of the QDs was observed (**Figure 15a**); moreover, Gd-doped ZnO QDs adhered to the surface of the cells and exhibited a strong yellow emission within

30 min of exposure.<sup>[308]</sup> As shown in **Figure 16a**,  $T_1$ -weighted MRI revealed an enhancement of the MR signal as the concentration of Gd<sup>3+</sup> ions was increased within the range of 0 to 0.05 mM, and the Gd-doped ZnO QDs appeared to be effective  $T_1$ -MRI contrast agents because the  $T_1$ -weighted MR images of HeLa cells treated with Gd-doped ZnO QDs were brighter than those of untreated HeLa cells (**Figure 16c**). Similar results were found in a subsequent study. Based on the paramagnetic property of Gd<sup>3+</sup> and the high X-ray absorptive property of Yb<sup>3+</sup>, Yin et al. developed a ZnO:Gd,Yb probe functionalized with folate (FA).<sup>[309]</sup> Upon intravenous injection, the uptake and deposition of the FA-modified nanoprobe was observed to occur primarily in the spleen, lung and liver, but these NPs were completely excreted from the body of mice without causing obvious toxicity, which was verified by histological analysis (**Figure 17**), i.e., no obvious injury or other noticeable abnormality was observed in the major organs of these mice, including the heart, liver, spleen, lungs, and kidneys, and their morphological features were normal. These nanoprobe not only exhibited a relatively higher longitudinal relaxivity ( $r_1$ ) of 6.29 mM<sup>-1</sup> s<sup>-1</sup> than that of commercial Gd(III)-diethylenetriamine pentaacetic acid

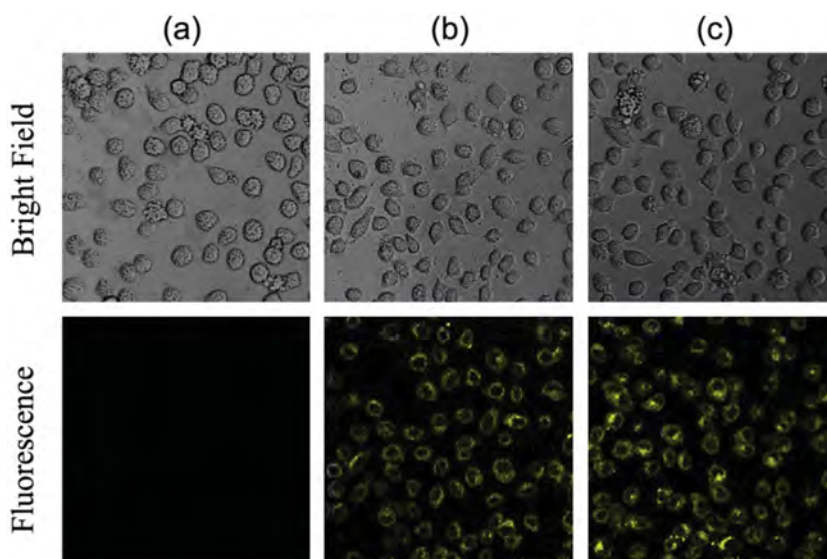


**Figure 15.** a) Confocal laser scanning microscopic images of HeLa cells incubated without Gd-doped ZnO QDs ( $\chi = 0.08$ ). b,c) HeLa cells incubated with Gd-doped ZnO QDs ( $\chi = 0.08$ ) for 30 min and 2 h at the same concentration (0.625 mM). Reproduced with permission.<sup>[308]</sup> Copyright 2011, Elsevier.

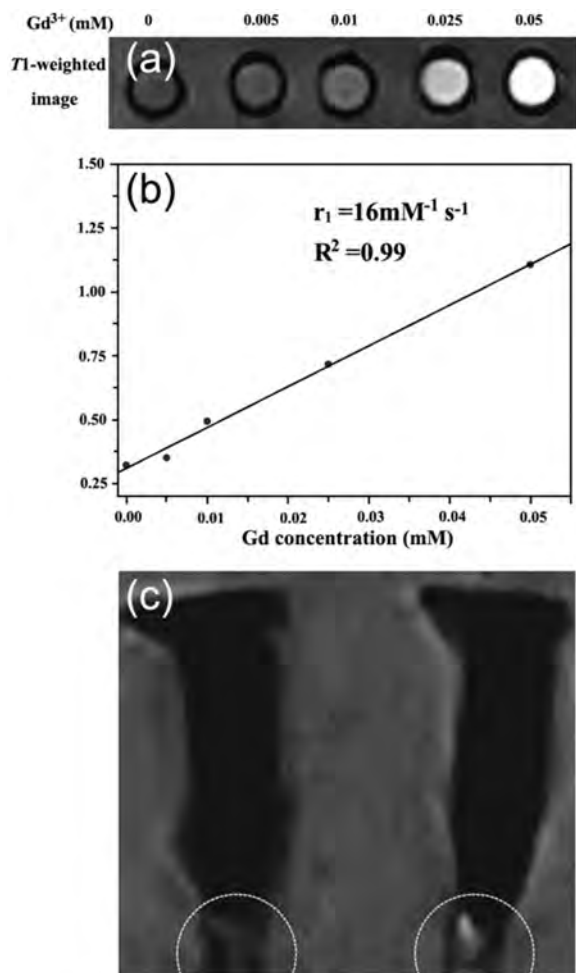


**Figure 16.** a)  $T_1$ -weighted magnetic resonance image for various  $Gd^{3+}$  concentrations of Gd-doped ZnO QDs ( $\chi = 0.08$ ) in water from a 1.5 T clinical MRI system. b) The linear relationship between  $T_1$  relaxation rates ( $1/T_1$ ) and  $Gd^{3+}$  ion concentrations for Gd-doped ZnO QDs ( $\chi = 0.08$ ). c)  $T_1$ -weighted image of blank HeLa cells pellet (left) and HeLa cells incubated with Gd-doped ZnO QDs at 0.01 M  $Gd^{3+}$  ions for 2 h. Reproduced with permission.<sup>[308]</sup> Copyright 2011, Elsevier.

complexes but also maintained a strong X-ray-attenuation capability. In  $T_1$ -weighted magnetic-resonance imaging (MRI) and X-ray computed-tomography (CT) studies, these QDs efficiently

induced positive-contrast enhancement.<sup>[309]</sup> Consequently, these properties allowed the Gd-doped ZnO QDs to function as effective dual modal imaging nanoprobe. However, extensive investigation of the possible chronic toxicity of these ZnO-based hybrid QDs are required before their clinical application.

Compared with the relatively low penetration in tissue of luminescent bioimaging and the low sensitivity of MRI, positron emission tomography (PET) possesses high quantitative capacity, has no tissue penetration limitation, and is widely used for bioimaging in vivo to monitor and quantify changes.<sup>[310–314]</sup> Radionuclide-based imaging is different from other molecular imaging modalities, because radionuclide-based imaging detects the radiolabel while others detect NPs itself. Lee et al. used PET imaging to detect the behavior and accumulation of nano-scaled ZnO (20 nm) and submicro-scaled ZnO (100 nm) particles in organic tissues after oral administration.<sup>[315]</sup> The surface area of nano-scaled NPs (20nm) is larger than that of submicro-scaled NPs (100 nm), resulting in stronger bioadhesive interactions of the former with the gastrointestinal (GI) mucosa than the latter, so it can be clearly observed that the flow rate of  $^{18}F$ -labeled 20 nm ZnO NPs along the GI tract is slower than  $^{18}F$ -labeled nano-scaled 100 nm ZnO NPs.<sup>[316]</sup> But, the former showed weaker radioactivity in the liver and kidney than the latter. In conclusion, PET imaging using radionuclides has become an established clinical tool for whole-body imaging. Since the dual-modality of FI and PET can collect synergistic information on molecular events,<sup>[317]</sup> Hong et al. synthesized green fluorescent ZnO NWs and demonstrated that the ZnO NWs can be adopted for targeted imaging of cancer cells.<sup>[318]</sup> The labeled ZnO NWs with  $^{64}Cu$  ( $t_{1/2}$ , 12.7h) were evaluated the biodistribution with PET in normal mice, and results disclosed that nontargeted ZnO NWs mostly accumulated in the liver. In addition, fluorescent ZnO NWs could be used for cancer-targeted optical imaging through the surface functionalization to improve water solubility, biocompatibility, and low cellular toxicity. Furthermore, they also developed red fluorescent ZnO NPs by conjugation of  $^{64}Cu$  ( $t_{1/2} = 12.7$  h) and TRC105 to ZnO NPs via well-developed surface engineering procedures for tumor-targeted.<sup>[319]</sup> It should be sufficient for in vivo tumor targeting, because the blood pool radioactivity of  $^{64}Cu$ -NOTA-ZnO-PEG-TRC105 was similar to that of  $^{64}Cu$ -NOTA-ZnO-PEG-NH<sub>2</sub> in the few-hour circulation  $t_{1/2}$  (shown in the coronal PET slices of **Figure 18a**). High radioactivity accumulation from  $^{64}Cu$ -NOTA-ZnO-PEG-TRC105 could be observed in the liver, tumor, and

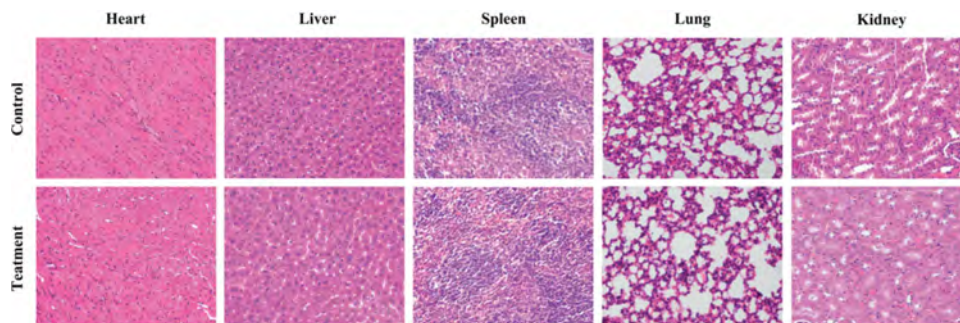


**Figure 17.** H&E-stained organ sections harvested from mice before and 7 days after injection of ZnO: Gd, Yb-FA NPs. No noticeable abnormality was observed in major organs including heart, liver, spleen, lung, and kidney. Reproduced with permission.<sup>[309]</sup> Copyright 2014, Royal Society of Chemistry.

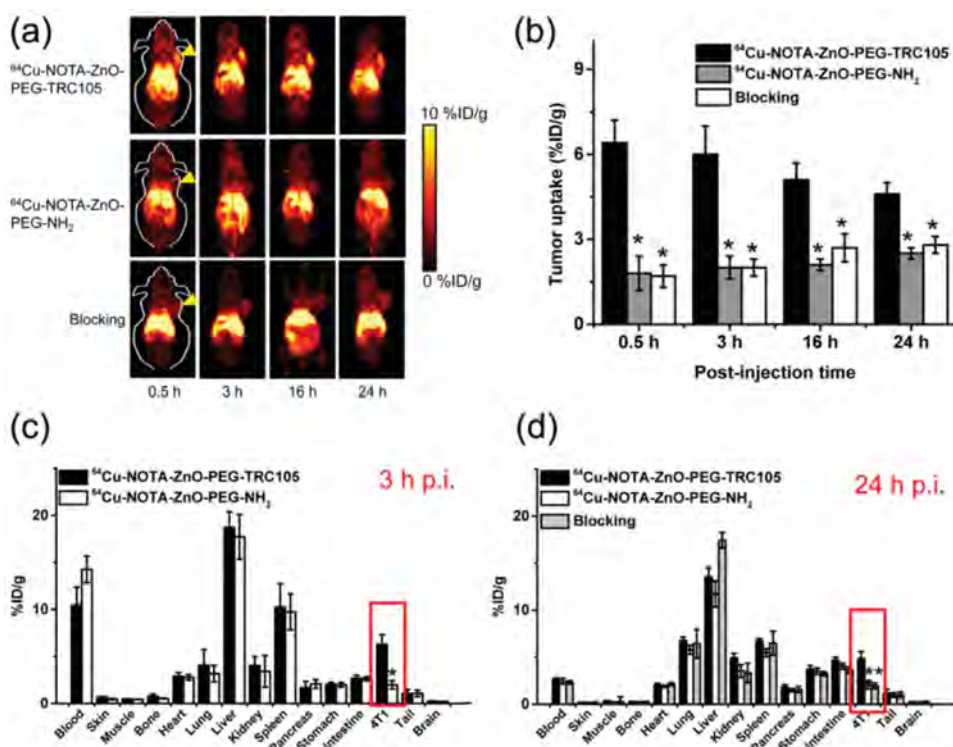


**Figure 18.** a) Serial coronal PET images of 4T1 tumor-bearing mice at chosen time points postinjection of  $^{64}\text{Cu}$ -NOTA-ZnO-PEG-TRC105,  $^{64}\text{Cu}$ -NOTA-ZnO-PEG-NH<sub>2</sub>, and blocking group. Yellow arrowheads show the tumor locations in the mice. b) The tumor uptakes for the ZnO nanoconjugates in part (a). c) Biodistribution of  $^{64}\text{Cu}$ -NOTA-ZnO-PEG-TRC105 and  $^{64}\text{Cu}$ -NOTA-ZnO-PEG-NH<sub>2</sub>, at 3 h postinjection. d) Biodistribution of  $^{64}\text{Cu}$ -NOTA-ZnO-PEG-TRC105,  $^{64}\text{Cu}$ -NOTA-ZnO-PEG-NH<sub>2</sub>, and blocking group (50 mg kg<sup>-1</sup> TRC105 injected 1 h prior to  $^{64}\text{Cu}$ -NOTA-ZnO-PEG-TRC105) at 24 h postinjection. Reproduced with permission.<sup>[319]</sup> Copyright 2015, American Chemical Society.

abdominal area besides blood. Nevertheless, there was no accumulation in most other tissues, this exhibits good tumor targeting and image contrast. From Figure 18b, the tumor uptake of  $^{64}\text{Cu}$ -NOTA-ZnO-PEG-TRC105 was much more than that of  $^{64}\text{Cu}$ -NOTA-ZnO-PEG-NH<sub>2</sub> within the whole time frame of PET imaging. This confirmed that the major factor for the elevated uptake of  $^{64}\text{Cu}$ -NOTA-ZnO-PEG-TRC105 in 4T1 tumor is the conjugation of TRC105. The uptake of  $^{64}\text{Cu}$ -NOTA-ZnO-PEG-TRC105 in the 4T1 tumor was higher than all the major organs/tissues except liver and spleen by biodistribution studies in accordance with PET studies (Figure 18c,d). Actually, the red-fluorescing ZnO NPs possess better tissue penetration of the optical signal compared with green fluorescent ZnO NWs they developed, but the requirement of UV light excitation for their fluorescence limited their applications in vivo. PET provided an alternative method and enabled the accurate quantification of ZnO NPs in vivo by conjugating  $^{64}\text{Cu}$  onto the surface of ZnO NPs. The PET imaging capacity of  $^{64}\text{Cu}$ -NOTA-ZnO-PEG-TRC105 makes it more clinically translatable<sup>[320,321]</sup> and applicable for quantitative and sensitive tumor detection.<sup>[322]</sup>

In summary, the drawback is the indispensable UV excitation for ZnO PL. UV light cannot penetrate the animal body, so ZnO fluorescent probes are confined to in vitro monitoring. Doping with rare-earth elements or radionuclide, a dual modal imaging ZnO-based nanoprobe could resolve the excitation problem. Potential applications in multimodal imaging techniques exist, including the combination of MRI (or PET) and FI.

## 5. Drug Delivery

Plenty of drug delivery systems based on NPs have been designed for the targeted delivery of anticancer drugs. It is required to develop a smart nanocarrier that precisely delivers antitumor drugs to target cancer cells as well as release the drugs in response to the pathophysiological states of diseased cells.<sup>[323–325]</sup> The majority of studies have used inorganic carriers, such as carbon nanotubes, mesoporous silica NPs (MSNs), and iron oxide in drug delivery because of their ability of enter cells by intracellular endocytic pathways and efficient release of drugs at target sites.<sup>[326–330]</sup> Different responding agents or conditions including pH,<sup>[331]</sup> temperature,<sup>[332]</sup> as well as the application of ultrasound<sup>[333]</sup> or magnetic fields have been employed for controllable release.<sup>[334]</sup> pH enables exploitation of the acidic environment of cancerous tissue, so changing the pH represents an effective strategy for cancer therapies. For example, many researches have shown that tumor and inflammatory tissues exhibit lower pH values than blood and normal tissue, and are more acidic with endosomes and lysosomes.<sup>[335–337]</sup> The pH-responsive systems usually use pH-sensitive linkers,<sup>[338]</sup> pH-responsive polymeric micelles,<sup>[339]</sup> and pH-responsive molecules<sup>[340]</sup> to connect hosts and guests, in order to encapsulate the drug and to cover the pores of the MSNs, respectively. Because of its sensitive dissolution in acidic conditions, and according to the phase diagram, ZnO should dissolve below a pH of 6.7 at physiological temperature.<sup>[341,342]</sup> Hence, in the

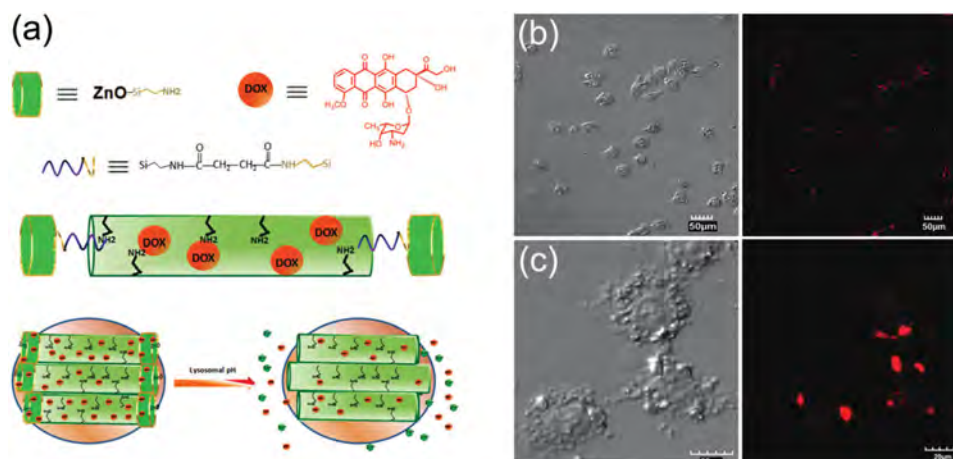


**Figure 19.** a) Schematic illustration of the synthesis of ZnO@MSNs-DOX and working protocol for pH-triggered release of the anticancer drug (DOX) from ZnO@MSNs-DOX to cytosol via selective dissolution of ZnO QDs in the acidic intracellular compartments of cancer cells. b) Low- and c) high-magnification CLSM images of HeLa cells after incubation with  $100 \mu\text{g mL}^{-1}$  ZnO@MSNs-DOX for 3 h: (left) transmission images; (right) fluorescence images. Reproduced with permission.<sup>[344]</sup> Copyright 2011, American Chemical Society.

past years, as a type of pH-responsive drug carrier, ZnO nanostructured materials have been rapidly developed.<sup>[343–349]</sup>

Muhammad et al. developed a pH-triggered controlled drug release system to release doxorubicin (DOX) to HeLa cells in vitro by employing ZnO QDs to seal the MSNs (Figure 19a).<sup>[344]</sup> ZnO QDs are stable at pH 7.4 but rapidly dissolve at pH <5.5, and as a result, DOX is released into cytosol from the MSNs. In fact, ZnO is recognized as safe, but after decomposition  $\text{Zn}^{2+}$  ions are cytotoxic. Consequently, ZnO QDs has a synergistic antitumor effect on cancer cells. Furthermore, the fluorescence of ZnO QDs can be used to monitor the drug delivery process. In order to assemble such a system, the inner channels of the MSNs were partially functionalized with amines to erase electrostatic interactions between the cationic anticancer drug DOX and the negatively charged MSNs. After the drug was loaded, the nanopores of the MSNs were sealed with  $\text{NH}_2$ -ZnO QDs. Upon internalization by cells, it demonstrated negligible DOX release from ZnO@MSNs-DOX at physiological pH (7.4), signifying efficient confinement of DOX in the pores of the MSNs for capping with ZnO QDs lids. In contrast, the fast release of DOX at pH 5.0 reached a plateau at 30% of the adsorbed DOX within 5 h. The MSNs were rapidly internalized into the cells and localized mainly in the cytoplasm and subcellular vesicles after incubation of HeLa cells for 3 h (Figure 19b,c). Hence, the intracellular release of DOX was attributed to the decomposition of ZnO nanolids in the acidic lysosomal compartments (pH  $\approx$  6.5–4.5) to kill the HeLa cells. MSNs possess remarkable biocompatibility and stability for drug delivery, whereas, the degradation in the animal body is an issue of much debate. In their study, the DOX loading was about  $40 \text{ mg g}^{-1}$ , and the DOX releasing efficiency was about 32% after 12 h of incubation in pH 5.0 buffer solutions. It indicated that the DOX loading capacity and releasing efficiency are not very good. As a consequence, the novel drug delivery system was defective for the undegradable MSNs and the residual DOX when applied in vivo. In a practical drug delivery system, the nanocarriers should not only be biodegradable or excretable, but also have a considerable loading capacity for the drugs.

Hence, Muhammad and their colleagues also designed ZnO QDs as a platform for targeted and pH responsive intracellular delivery of an anticancer drug by loading DOX to kill the HeLa cells.<sup>[345]</sup> This system was composed of DOX loaded onto ZnO QDs through a complexation strategy and folic acid (FA), which is a molecular targeting ligand because cancer cells overexpress folate binding proteins (FBPs) on their cell membranes (Figure 20a). In order to assemble such a system, FA was conjugated onto ZnO- $\text{NH}_2$  QDs via complexation with  $\text{Zn}^{2+}$  ions of ZnO-FA QDs. Finally, DOX is successfully loaded onto the FA functionalized ZnO QDs. Drug loaded ZnO-FA QDs remain stable at physiological pH but readily disintegrate in the mildly acidic intracellular environment of cancer cells (Figure 20b). Exposure to pH 7.0, the release of DOX revealed a negligible release, but it induced a considerable (60%) release of DOX in the extracellular tumor environment at pH 7.0. As the pH reduced to 5.0, burst drug release was observed within a few seconds. Because the acidic conditions broken the reaction between  $\text{Zn}^{2+}$  and DOX and the coordinate bond between  $\text{Zn}^{2+}$  and DOX was dissociated upon protonation of the phenolic group of DOX. The toxicity of DOX-loaded ZnO QDs was lower than that of free DOX, and ZnO-FA QDs efficiently inhibited the viability of HeLa cells (Figure 20g). It revealed that DOX-ZnO-FA QDs achieved a 70% reduction in cell viability at  $25 \text{ mg mL}^{-1}$ , while the corresponding concentration of only ZnO-FA QDs had no cytotoxic activity. Hence, the complexation of  $\text{Zn}^{2+}$  to DOX did not influence the inhibitory activity of the DOX and the drug remained potent after complexation. The weak green fluorescence in the cytoplasm was clear evidence that the ZnO-FA QDs permeated into the cells successfully via folate-receptor-mediated endocytosis, and the red fluorescence in HeLa cells demonstrated that the DOX released into cytosols upon the disintegration of ZnO QDs in intracellular acidic compartments (Figure 20c,d). In addition, the combination of DOX with ZnO QDs exerted synergistic cytotoxic activity against cancer cells, because ZnO-FA QDs not only served as a pH responsive nanocarrier but also exhibited a significant antitumor activity. These nanocarriers are speculated to be a

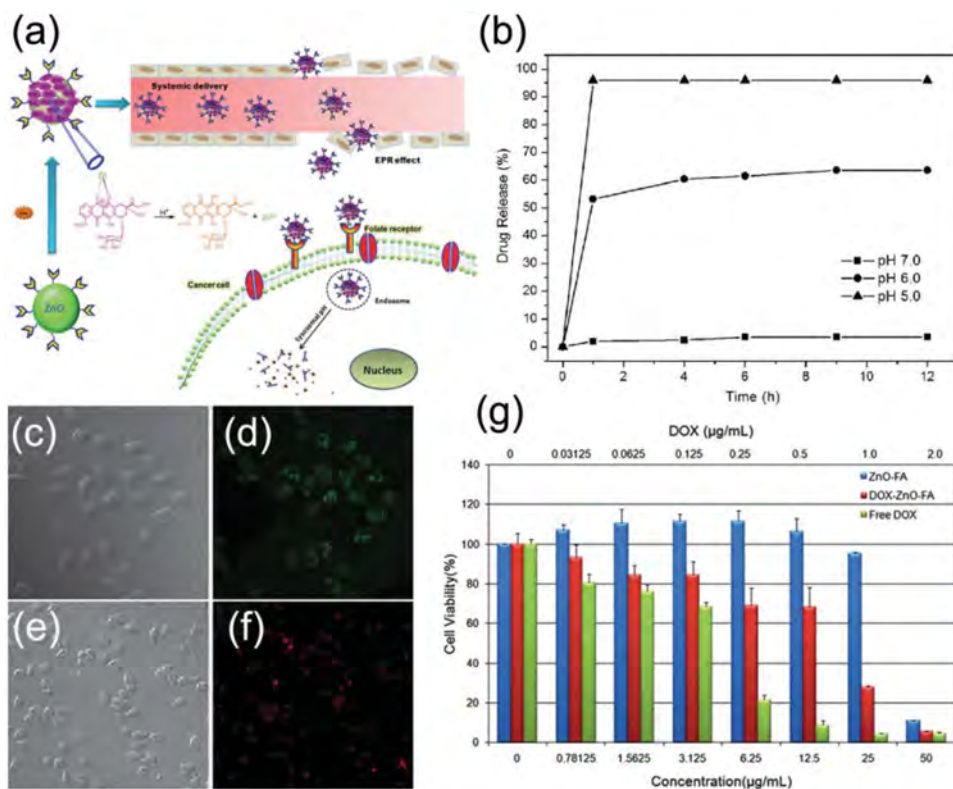


**Figure 20.** a) Schematic illustration of the synthetic and working protocol in which doxorubicin is anchored onto folic acid conjugated ZnO QDs via a complexation strategy. Upon folate receptor internalization, drug loaded ZnO QDs are instantly dissolved in the acidic environment of endosomes/lysosomes and in turn the loaded DOX is readily delivered to the cytoplasm. b) The drug release profile of the DOX-ZnO-FA in different pH environments. CLSM micrographs of HeLa cells after 3 h incubation with c) 50 mg mL<sup>-1</sup> ZnO-FA QDs, d) DOX-ZnO-FA QDs. e) Transmission and f) fluorescence images are presented alongside g) cell viability studies with MTT assays of HeLa cells treated with ZnO-FA, DOX-ZnO-FA and free DOX. The incubation time is 48 h. Reproduced with permission.<sup>[345]</sup> Copyright 2011, Royal Society of Chemistry.

valuable addition in the targeted and stimuli responsive anticancer drug delivery inventory to improve the therapeutic outcome of chemotherapy. Furthermore, it was not satisfying that the maximum loading of DOX onto ZnO-NH<sub>2</sub> QDs was about 20%, but the releasing efficiency of DOX was as high as 96% at pH 5.0. Hence, the ZnO QDs and DOX could be complete dissolution. Additionally, a simple route for the synthesis of porous ZnO nanorods for targeted of DOX has been developed by Mitra et al.<sup>[348]</sup> In their studies, the drug loading efficiency could reach up to 88%, which was mainly due to the high surface area and well-distributed pores on the ZnO surface. It was found that about 71% of DOX was released from ZnO-FA at pH 5 and only 40% of DOX was released at pH 7.4 after 3 days. The biocompatibility of ZnO-FA was verified through oral and intravenous injection routes with *in vivo* evaluations concluding no significant toxicity on the blood stream.

Because conventional ZnO QDs are unstable in aqueous solutions, Zhang et al. developed a new core-shell-structured ZnO@polymer-DOX nanocomposite with stable luminescence in an aqueous solution.<sup>[347]</sup> The release profile of DOX shows that about 15 wt.% of DOX were released after 10 h at pH 7.0 and no more DOX was released over 30 h, whereas nearly 90 wt.% of DOX molecules were released within 10 h at pH 5.0 (Figure 21a). Both free DOX and ZnO@polymer-DOX exhibit dose-dependent cytotoxicity toward cancer cells.

With the continuous increase of the DOX concentration outside cells, the DOX cytotoxicity toward U251 reached a platform (about 40% of cell viability in Figure 21b). However, the cytotoxicity of ZnO@polymer-DOX is exhibited much more strongly when its DOX concentration was over 2 µg mL<sup>-1</sup>. Compared with DOX itself, DOX-loaded ZnO NPs should theoretically have lower toxicity. The situation changed when ZnO nanocarriers were employed. ZnO-DOX composites were engulfed by the endosomes and lysosomes after they were taken up by cells, with the result that DOX saturation in the cellular fluid was not reached, so more and more ZnO-DOX was taken up continuously. Finally, the ZnO-DOX composites decomposed in the lysosomes to release high concentrations of DOX molecules, thus exhibiting higher cytotoxicity. As a result, ZnO@polymer-DOX is able to kill cancer cells effectively at appropriate concentrations (Figure 21b), which has been proven by confocal laser scanning microscopy (CLSM) images for the cell-entering process of ZnO-DOX, the decomposition at lysosomes, and the release of DOX into the nucleus (Figure 21c–e). After 3 h incubation, red fluorescence from DOX was found throughout the cytoplasm, especially localized in the lysosomes labeled by the green lysotracker (see the yellow points in Figure 21e). In comparison with previously reported nanocomposite-based DOX-release systems, the system from Zhang et al. has some advantages.<sup>[347]</sup>

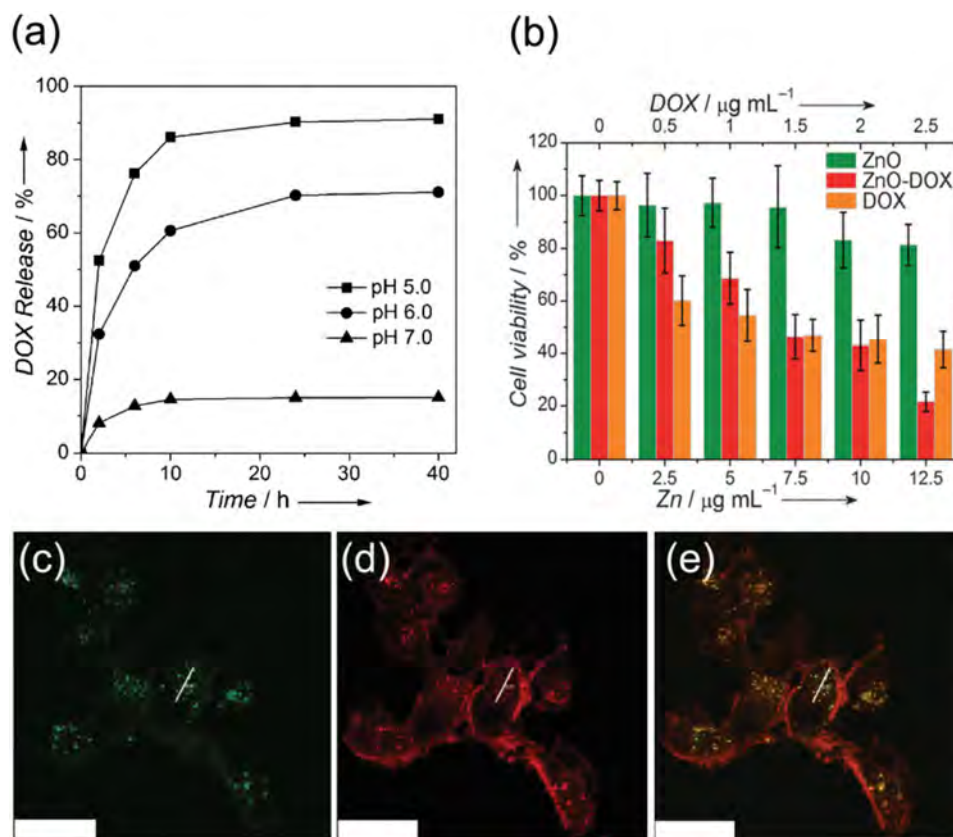


**Figure 21.** a) DOX release profile of ZnO@polymer-DOX at different pH values. b) Viability of U251 cells after treatment with ZnO@polymer QDs, ZnO@polymer-DOX composites, and free DOX for 48 h. The cytotoxicity of DOX and ZnO@polymer-DOX were evaluated with regard to their DOX content (see the upper scale mark). CLSM images of U251 cells after incubation with ZnO@polymer-DOX in the presence of LysoTracker for 3 h. c) LysoTracker stained U251 cells (green). d) ZnO@polymer-DOX (red). e) A merged image of the above two channels. Scale bars represent 25  $\mu\text{m}$ . Reproduced with permission.<sup>[347]</sup> Copyright 2013, Wiley-VCH.

Firstly, if ZnO NPs are coated tightly with protective shells, they will be very stable in aqueous solution at pH 7.4, but rapidly decompose at pH 6.0, thus ensuring the safety of healthy tissues. Secondly, not only ZnO but also the polymer shell is biodegradable and thus safe for cells, and the ZnO@polymer is nontoxic at low concentrations. Therefore, ZnO@polymer-DOX is a pH-responsive, degradable system for DOX delivery and suitable for specific targeting at solid tumors.<sup>[350]</sup>

In summary, ZnO nanostructured materials can effectively control the drug release as a type of pH-responsive drug carrier. Meanwhile, they can also reduce side effects because ZnO NPs are quite safe for living cells and consequently suitable for in vivo monitoring. Nanostructured ZnO is of great significance for improving the level of clinical pharmacy. Presently, the main challenge is obtaining ZnO-based nanocarriers that are stable in vivo. Since the ZnO NPs are unstable in water and they can be disintegrated in mildly acidic intracellular environments (pH < 6), surface modification using certain ligands is crucial for protecting ZnO NPs in biological systems. And the stability should be the combination of ZnO nanocarriers with the drugs to be loaded. Therefore, there is still a large scope for the development of novel morphology ZnO nanomaterials in drug delivery systems.

## 6. Conclusions and Outlook

A comprehensive analysis of the available literature concerning the biomedical applications of nanostructured ZnO in biosensing, tissue regeneration, bioimaging and drug delivery has been presented. Due to their unique crystalline and surface structures as well as their high level of conductivity, sensitivity to gases, biocompatibility and antibacterial activity, nanostructured ZnO materials have a promising future in biomedicine. As stated in recent reports concerning ZnO nanomaterials, it is vital to obtain a comprehensive understanding of the mechanisms of ZnO nanomaterials. Nevertheless, the good biocompatibility and rapid electron-transfer ability of ZnO nanostructures allow these materials to function as biomimetic membrane materials for the immobilization and modification of proteins. To date, nano-ZnO has been utilized to develop several hydrogen peroxide biosensors and glucose biosensors due to its high sensitivity to glucose and hydrogen peroxide. Regarding its use in tissue regeneration, nanostructured ZnO exhibited excellent antibacterial activity via the generation of ROS and the release of zinc ions from ZnO. Furthermore, the Zn ions released from ZnO nanostructures stimulated bone formation in vitro by activating protein synthesis in osteoblasts

and increasing the ATPase activity in bone, and promoted wound healing by enhancing keratinocyte migration toward the wound site. The tunable photoluminescent ZnO QD is a promising candidate for a bioimaging probe. As a of pH-responsive drug carrier, ZnO nanostructured materials have been rapidly developed. Taken together, the unique electrical and photocatalytic properties as well as the biocompatibility of ZnO nanostructures make them promising materials for use in biosensing, tissue regeneration, bioimaging and drug delivery. However, the debates concerning their nanotoxicity and biological mechanisms indicate that further investigations of these ZnO nanostructures are required.

## Acknowledgements

This study was jointly supported by the Special Prophase Program for Key Basic Research of the Ministry of Science and Technology of China (973 Program), grant no. 2014CB660809; the National Natural Science Foundation of China, grant nos. 51422102 and 81271715; the Hong Kong Research Grants Council (RGC) General Research Funds (GRF), grant nos. 112510 and 112212, City University of Hong Kong Applied Research Grant (ARG) nos. 9667066 and 9667069; and the Excellent Youth Foundation of the Hubei Scientific Committee, grant no. 2013CFA018. The sources of the table of contents image are as follows: images in center, reproduced with permission.<sup>[5]</sup> Copyright 2004, Elsevier. Images around from left to right, reproduced with permission.<sup>[166,41,225,280]</sup> Copyright 2009, Wiley-VCH; Copyright 2014, American Chemical Society; Copyright 2010 and 2011, Wiley-VCH.

Received: September 8, 2015

Revised: September 15, 2015

Published online: October 29, 2015

- [1] S. K. Arya, S. Saha, J. E. Ramirez-Vick, V. Gupta, S. Bhansali, S. P. Singh, *Anal. Chim. Acta.* **2012**, *737*, 1.
- [2] P. Yang, H. Yan, S. Mao, R. Russo, J. Johnson, R. Saykally, N. Morris, J. Pham, R. He, H. J. Choi, *Adv. Funct. Mater.* **2002**, *12*, 323.
- [3] L. Vayssieres, K. Keis, S. E. Lindquist, A. Hagfeldt, *J. Phys. Chem. B* **2001**, *105*, 3350.
- [4] Z. W. Pan, Z. R. Dai, Z. L. Wang, *Science* **2001**, *291*, 1947.
- [5] Z. L. Wang, *Mater. Today* **2004**, *7*, 26.
- [6] L. Guo, Y. L. Ji, H. Xu, P. Simon, Z. Wu, *J. Am. Chem. Soc.* **2002**, *124*, 14864.
- [7] H. Zhang, D. Yang, Y. Ji, X. Ma, J. Xu, D. Que, *J. Phys. Chem. B* **2004**, *108*, 3955.
- [8] X. H. Lu, D. Wang, G. R. Li, C. Y. Su, D. B. Kuang, Y. X. Tong, *J. Phys. Chem. C* **2009**, *113*, 13574.
- [9] C. Y. Kuo, R. M. Ko, Y. C. Tu, Y. R. Lin, T. H. Lin, S. J. Wan, *Cryst. Growth Des.* **2012**, *12*, 3849.
- [10] L. Schmidt-Mende, J. L. MacManus-Driscoll, *Mater. Today* **2007**, *10*, 40.
- [11] B. Q. Cao, M. Lorenz, A. Rahm, H. Wenckstern, C. Czekalla, J. Lenzner, G. Benndorf, M. Grundmann, *Nanotechnology* **2007**, *18*, 455707.
- [12] M. H. Huang, Y. Wu, H. Feick, N. Tran, E. Weber, P. Yang, *Adv. Mater.* **2001**, *13*, 113.
- [13] T.-J. Kuo, C. N. Lin, C. L. Kuo, M. H. Huang, *Chem. Mater.* **2007**, *19*, 5143.
- [14] H. Kind, H. Yan, B. Messer, M. Law, P. Yang, *Adv. Mater.* **2002**, *14*, 158.
- [15] Q. P. Luo, B. X. Lei, X. Y. Yu, D. B. Kuang, C. Y. Su, *J. Mater. Chem.* **2011**, *21*, 8709.
- [16] Y. H. Chen, Y. M. Shen, S. C. Wang, J. L. Huang, *Thin Solid Films* **2014**, *570*, 303.
- [17] M. Yamaguchi, *J. Trace Elem. Exp. Med.* **1998**, *11*, 119.
- [18] P. T. S. Kumar, S. Abhilash, K. Manzoor, S. V. Nair, H. Tamura, R. Jayakumar, *Carbohydr. Polym.* **2010**, *80*, 761.
- [19] L. Zhang, Y. Jiang, Y. Ding, N. Daskalakis, L. Jeuken, M. Povey, A. J. O'Neill, D. W. York, *J. Nanopart. Res.* **2010**, *12*, 1625.
- [20] M. Li, L. Zhu, D. Lin, *Environ. Sci. Technol.* **2011**, *45*, 1977.
- [21] K. R. Raghupathi, R. T. Koodali, A. C. Manna, *Langmuir* **2011**, *27*, 4020.
- [22] W. Song, J. Zhang, J. Guo, J. Zhang, F. Ding, L. Li, Z. Sun, *Toxicol. Lett.* **2010**, *199*, 389.
- [23] B. D. Berardis, G. Civitelli, M. Condello, P. Lista, R. Pozzi, G. Arancia, S. Meschini, *Toxicol. Appl. Pharm.* **2010**, *246*, 116.
- [24] M. V. Deshpande, D. P. Amalnerkar, *Prog. Polym. Sci.* **1993**, *18*, 623.
- [25] T. Ahuja, I. A. Mir, D. K. Rajesh, *Biomaterials* **2007**, *28*, 791.
- [26] N. J. Ronkainen, H. B. Halsall, W. R. Heineman, *Chem. Soc. Rev.* **2010**, *39*, 1747.
- [27] W. W. Zhao, J. J. Xu, H. Y. Chen, *Chem. Soc. Rev.* **2015**, *44*, 729.
- [28] J. Wang, *Chem. Rev.* **2008**, *108*, 814.
- [29] G. Zhao, J. J. Feng, J. J. Xu, H. Y. Chen, *Electrochem. Commun.* **2005**, *7*, 724.
- [30] M. I. Kim, Y. Ye, B. Y. Won, S. Shin, J. Lee, H. G. Park, *Adv. Funct. Mater.* **2011**, *21*, 2868.
- [31] Z. Wang, J. Yi, S. Yang, *Sens. Actuators, B* **2013**, *176*, 211.
- [32] S. Yang, Z. Lu, S. Luo, C. Liu, Y. Tang, *Microchim. Acta* **2013**, *180*, 127.
- [33] R. Ahmad, N. Tripathy, Y. B. Hahn, *Sens. Actuators, B* **2012**, *169*, 382.
- [34] Y. Lei, N. Luo, X. Yan, Y. Zhao, G. Zhang, Y. Zhang, *Nanoscale* **2012**, *4*, 3438.
- [35] Y. B. Hahn, R. Ahmad, N. Tripathy, *Chem. Commun.* **2012**, *48*, 10369.
- [36] P. K. Vabbina, A. Kaushik, N. Pokhrel, S. Bhansali, N. Pala, *Biosens. Bioelectron.* **2015**, *63*, 124.
- [37] M. M. Rahman, A. J. S. Ahammad, J. H. Jin, S. J. Ahn, J. J. Lee, *Sensors* **2010**, *10*, 4855.
- [38] E. Topoglidis, C. J. Campbell, A. E. G. Cass, J. R. Durrant, *Langmuir* **2001**, *17*, 7899.
- [39] R. Ahmad, N. Tripathy, N. K. Jang, G. Khang, Y. B. Hahn, *Sens. Actuators, B* **2015**, *206*, 146.
- [40] K. Jindal, M. Tomar, V. Gupta, *Biosens. Bioelectron.* **2014**, *55*, 57.
- [41] H. Y. Yue, S. Huang, J. Chang, C. Heo, F. Yao, S. Adhikari, F. Gunes, L. C. Liu, T. H. Lee, E. S. Oh, B. Li, J. J. Zhang, T. Q. Huy, N. V. Luan, Y. H. Lee, *ACS Nano* **2014**, *8*, 1639.
- [42] I. Y. Huang, M. C. Lee, *Sens. Actuators, B* **2008**, *132*, 340.
- [43] R. Yu, C. Pan, Z. L. Wang, *Energy Environ. Sci.* **2013**, *6*, 494.
- [44] R. Yu, C. Pan, J. Chen, G. Zhu, Z. L. Wang, *Adv. Funct. Mater.* **2013**, *23*, 5868.
- [45] J. Y. Kim, S. Y. Jo, G. J. Sun, A. Katoch, S. W. Choi, S. S. Kim, *Sens. Actuators, B* **2014**, *192*, 216.
- [46] K. E. Kim, T. G. Kim, Y. M. Sung, *CrystEngComm* **2012**, *14*, 2859.
- [47] Z. Dai, K. Liu, Y. Tang, X. Yang, J. Bao, J. Shen, *J. Mater. Chem.* **2008**, *18*, 1919.
- [48] M. B. Wayu, R. T. Spidle, T. Devkota, A. K. Deb, R. K. DeLong, K. C. Ghosh, A. K. Wanekaya, C. C. Chusuei, *Electrochim. Acta* **2013**, *97*, 99.
- [49] L. Y. Chen, B. X. Gu, G. P. Zhu, Y. F. Wu, S. Q. Liu, C. X. Xu, *Nano* **2007**, *2*, 281.
- [50] S. Guo, D. Wen, Y. Zhai, S. Dong, E. Wang, *ACS Nano* **2010**, *4*, 3959.

- [51] Y. Zhang, X. Bai, X. Wang, K. K. Shiu, Y. Zhu, H. Jiang, *Anal. Chem.* **2014**, *86*, 9459.
- [52] F. Jiang, R. Yue, Y. Du, J. Xu, P. Yang, *Biosens. Bioelectron.* **2013**, *44*, 127.
- [53] T. W. Miller, J. S. Isenberg, D. D. Roberts, *Chem. Rev.* **2009**, *109*, 3099.
- [54] X. He, L. Zhou, E. P. Nesterenko, P. N. Nesterenko, B. Paull, J. O. Omamogho, J. D. Glennon, J. H. T. Luong, *Anal. Chem.* **2012**, *84*, 2351.
- [55] K. J. Huang, D. J. Niu, X. Liu, Z. W. Wu, Y. Fan, Y. F. Chang, Y. Y. Wu, *Electrochim. Acta* **2011**, *56*, 2947.
- [56] H. Heli, J. Pishahang, *Electrochim. Acta* **2014**, *123*, 518.
- [57] Z. Zhang, J. Gao, L. M. Wong, J. G. Tao, L. Liao, Z. Zheng, G. Z. Xing, H. Y. Peng, T. Yu, Z. X. Shen, C. H. A. Huan, S. J. Wang, T. Wu, *Nanotechnology* **2009**, *20*, 135605.
- [58] C. Cheng, B. Liu, H. Yang, W. Zhou, L. Sun, R. Chen, S. F. Yu, J. Zhang, H. Gong, H. Sun, H. J. Fan, *ACS Nano* **2009**, *3*, 3069.
- [59] J. Jiang, J. P. Liu, X. T. Huang, Y. Y. Li, R. M. Ding, X. X. Ji, Y. Y. Hu, Q. B. Chi, Z. H. Zhu, *Cryst. Growth Des.* **2010**, *10*, 70.
- [60] Z. Liu, B. Zhao, Y. Shi, C. Guo, H. Yang, Z. Li, *Talanta* **2010**, *81*, 1650.
- [61] C. Xiang, Y. Zou, L. X. Sun, F. Xu, *Sens. Actuators, B* **2009**, *136*, 158.
- [62] J. Liu, C. Guo, C. M. Li, Y. Li, Q. Chi, X. Huang, L. Liao, T. Yu, *Electrochim. Commun.* **2009**, *11*, 202.
- [63] X. Zhu, I. Yuri, X. Gan, I. Suzuki, G. Li, *Biosens. Bioelectron.* **2007**, *22*, 1600.
- [64] Z. Yang, X. L. Zong, Z. Ye, B. Zhao, Q. L. Wang, P. Wang, *Biomaterials* **2010**, *31*, 7534.
- [65] X. Lu, H. Zhang, Y. Ni, Q. Zhang, J. Chen, *Biosens. Bioelectron.* **2008**, *24*, 93.
- [66] S. Palanisamy, S. Cheemalapati, S. M. Chen, *Anal. Biochem.* **2012**, *429*, 108.
- [67] C. Y. Lin, Y. H. Lai, A. Balamurugan, R. Vittal, C. W. Lin, K. C. Ho, *Talanta* **2010**, *82*, 340.
- [68] J. Wang, M. Xu, R. Zhao, G. Chen, *Analyst* **2010**, *135*, 1992.
- [69] Q. Wang, J. Zheng, *Microchim. Acta* **2010**, *169*, 361.
- [70] S. Palanisamy, S. M. Chen, R. Sarawathi, *Sens. Actuators, B* **2012**, *166–167*, 372.
- [71] C. P. Lu, C. T. Lin, C. M. Chang, S. H. Wu, L. C. Lo, *J. Agric. Food Chem.* **2011**, *59*, 11403.
- [72] V. Serafin, P. Hernández, L. Agüí, P. Yáñez-Sedeño, J. M. Pingarrón, *Electrochim. Acta* **2013**, *97*, 175.
- [73] A. I. Gopalan, S. Komathi, G. S. Anand, K. P. Lee, *Biosens. Bioelectron.* **2013**, *46*, 136.
- [74] B. Zhang, J. Zhou, S. Li, X. Zhang, D. Huang, Y. He, M. Wang, G. Yang, Y. Shen, *Talanta* **2015**, *131*, 243.
- [75] Y. Zhang, X. Sun, N. Jia, *Sens. Actuators, B* **2011**, *157*, 527.
- [76] S. Saadati, A. Salimi, R. Hallaj, A. Rostami, *Sens. Actuators, B* **2014**, *191*, 625.
- [77] C. Xia, N. Wang, L. Lidong, G. Lin, *Sens. Actuators, B* **2008**, *129*, 268.
- [78] Y. F. Li, Z. M. Liu, Y. L. Liu, Y. H. Yang, G. L. Shen, R. Q. Yu, *Anal. Biochem.* **2006**, *349*, 33.
- [79] Y. H. Yang, M. H. Yang, J. H. Jiang, *Chin. Chem. Lett.* **2005**, *16*, 951.
- [80] Y. L. Liu, Y. H. Yang, H. F. Yang, Z. M. Liu, G. L. Shen, R. Q. Yu, *J. Inorg. Biochem.* **2005**, *99*, 2046.
- [81] J. Huang, Y. Zhu, H. Zhong, X. Yang, C. Li, *ACS Appl. Mater. Interfaces* **2014**, *6*, 7055.
- [82] H. Wu, S. Fan, X. Jin, H. Zhang, H. Chen, Z. Dai, X. Zou, *Anal. Chem.* **2014**, *86*, 6285.
- [83] Y. Han, J. Zheng, S. Dong, *Electrochim. Acta* **2013**, *90*, 35.
- [84] G. Flätgen, S. Wasle, M. Lübke, C. Eickes, G. Radhakrishnan, K. Doblhofer, G. Ertl, *Electrochim. Acta* **1999**, *44*, 4499.
- [85] World Health Organisation: Diabetes Programme, <http://www.who.int/diabetes/en/> (accessed: March 2015).
- [86] American Diabetes Association: National Diabetes Statistics Report, <http://www.diabetes.org/diabetes-basics/statistics/?loc=db-slabnav> (accessed: March 2015).
- [87] T. B. Goriushkina, A. P. Soldatkin, S. V. Dzyadevych, *J. Agric. Food Chem.* **2009**, *57*, 6528.
- [88] K. Ma, J. M. Yuen, N. C. Shah, J. T. W. Jr, M. R. Glucksberg, R. P. V. Duyne, *Anal. Chem.* **2011**, *83*, 9146.
- [89] J. C. Pickup, F. Hussain, N. D. Evans, O. J. Rolinski, D. J. S. Birch, *Biosens. Bioelectron.* **2005**, *20*, 2555.
- [90] J. Wang, *Electroanalysis* **2001**, *13*, 983.
- [91] L. C. Clark Jr, C. Lyons, *Ann. N. Y. Acad. Sci.* **1962**, *102*, 29.
- [92] S. J. Bao, C. M. Li, J. F. Zang, X. Q. Cui, Y. Qiao, J. Guo, *Adv. Funct. Mater.* **2008**, *18*, 591.
- [93] C. X. Guo, Z. M. Sheng, Y. Q. Shen, Z. L. Dong, C. M. Li, *ACS Appl. Mater. Interfaces* **2010**, *2*, 2481.
- [94] P. K. Samanta, P. Kanti, *Sci. Adv. Mater.* **2012**, *4*, 219.
- [95] Z. Dai, G. Shao, J. Hong, J. Bao, J. Shen, *Biosens. Bioelectron.* **2009**, *24*, 1286.
- [96] A. Wei, X. Sun, J. X. Wang, Y. Lei, X. P. Cai, C. M. Li, Z. Dong, W. Huang, *Appl. Phys. Lett.* **2006**, *89*, 123902.
- [97] J. X. Wang, X. Sun, A. Wei, Y. Lei, X. P. Cai, C. M. Li, Z. Dong, *Appl. Phys. Lett.* **2006**, *88*, 233106.
- [98] K. Yang, G. W. She, H. Wang, X. M. Ou, X. H. Zhang, C. S. Lee, S. T. Lee, *J. Phys. Chem. C* **2009**, *113*, 20169.
- [99] M. Ahmad, C. Pan, Z. Luo, J. Zhu, *J. Phys. Chem. C* **2010**, *114*, 9308.
- [100] B. Fang, C. Zhang, G. Wang, M. Wang, Y. Ji, *Sens. Actuators, B* **2011**, *155*, 304.
- [101] Z. W. Zhao, X. J. Chen, B. K. Tay, J. S. Chen, Z. J. Han, K. A. Khor, *Biosens. Bioelectron.* **2007**, *23*, 135.
- [102] Y. Wei, Y. Li, X. Liu, Y. Xian, G. Shi, L. Jin, *Biosens. Bioelectron.* **2010**, *26*, 275.
- [103] Y. T. Wang, L. Yu, Z. Q. Zhu, J. Zhang, J. Z. Zhu, C. Fan, *Sens. Actuators, B* **2009**, *136*, 332.
- [104] D. Pradhan, F. Niroui, K. T. Leung, *ACS Appl. Mater. Interfaces* **2010**, *2*, 2409.
- [105] C. Yang, C. Xu, X. Wang, *Langmuir* **2012**, *28*, 4580.
- [106] J. Luo, P. Luo, M. Xie, K. Du, B. Zhao, F. Pan, P. Fan, F. Zeng, D. Zhang, Z. Zheng, G. Liang, *Biosens. Bioelectron.* **2013**, *49*, 512.
- [107] S. Yabuki, H. Shinohara, M. Aizawa, *J. Chem. Soc., Chem. Commun.* **1989**, *14*, 945.
- [108] C. G. J. Koopal, B. de Ruyter, R. J. M. Nolte, *J. Chem. Soc., Chem. Commun.* **1991**, *23*, 1691.
- [109] Z. Nasri, E. Shams, *Electrochim. Acta* **2013**, *112*, 640.
- [110] B. C. Janegitz, R. Pauliukaite, M. E. Ghica, C. M. A. Brett, O. Fatibello-Filho, *Sens. Actuators, B* **2011**, *158*, 411.
- [111] Z. Wang, X. Zhou, J. Zhang, F. Boey, H. Zhang, *J. Phys. Chem. C* **2009**, *113*, 14071.
- [112] A. Amine, J. M. Kauffmann, G. G. Guilbault, S. Bacha, *Anal. Lett.* **1993**, *26*, 1281.
- [113] J. C. Vidal, E. Garcia, J. R. Castillo, *Biosens. Bioelectron.* **1998**, *13*, 371.
- [114] R. Ahmad, N. Tripathy, J. H. Kim, Y. B. Hahn, *Sens. Actuators, B* **2012**, *174*, 195.
- [115] J. D. Newman, A. P. F. Turner, *Biosens. Bioelectron.* **2005**, *20*, 2435.
- [116] B. Li, T. Yoshii, A. E. Hafeman, J. S. Nyman, J. C. Wenke, S. A. Guelcher, *Biomaterials* **2009**, *30*, 6768.
- [117] L. Zhang, T. J. Webster, *Nano Today* **2009**, *4*, 66.
- [118] D. Campoccia, L. Montanaro, C. R. Arciola, *Biomaterials* **2013**, *34*, 8018.
- [119] M. L. Cohen, *Science* **1992**, *257*, 1050.
- [120] K. Anagnostakos, P. Hitzler, D. Pape, D. Kohn, J. Kelm, *Acta Orthop.* **2008**, *79*, 302.
- [121] H. Cao, X. Liu, F. Meng, P. K. Chu, *Biomaterials* **2011**, *32*, 693.

- [122] M. Lv, S. Su, Y. He, Q. Huang, W. Hu, D. Li, C. Fan, S. T. Lee, *Adv. Mater.* **2010**, *22*, 5463.
- [123] S. K. Bhargava, V. Bansal, *Nanoscale* **2014**, *6*, 758.
- [124] X. Xu, D. Chen, Z. Yi, M. Jiang, L. Wang, Z. Zhou, X. Fan, Y. Wang, D. Hui, *Langmuir* **2013**, *29*, 5573.
- [125] G. Applerot, A. Lipovsky, R. Dror, N. Perkas, Y. Nitzan, R. Lubart, A. Gedanken, *Adv. Funct. Mater.* **2009**, *19*, 842.
- [126] J. Panigrahi, D. Behera, I. Mohanty, U. Subudhi, B. B. Nayak, B. S. Acharya, *Appl. Surf. Sci.* **2011**, *258*, 304.
- [127] N. Tripathy, R. Ahmad, S. H. Bang, J. Min, Y. B. Hahn, *Chem. Commun.* **2014**, *50*, 9298.
- [128] H. Ma, P. L. Williams, S. A. Diamond, *Environ. Pollut.* **2013**, *172*, 76.
- [129] H. Ma, L. K. Wallis, S. Diamond, S. Li, J. Canas-Carrell, A. Parra, *Environ. Pollut.* **2014**, *193*, 165.
- [130] M. Heinlaan, A. Ivask, I. Blinova, H. C. Dubourguier, A. Kahru, *Chemosphere* **2008**, *71*, 1308.
- [131] T. Kavitha, A. I. Gopalan, K. P. Lee, S. Y. Park, *Carbon* **2012**, *50*, 2994.
- [132] C. C. Lin, Y. J. Chiang, *J. Ind. Eng. Chem.* **2012**, *18*, 1233.
- [133] H. Yin, P. S. Casey, M. J. McCall, M. Fenech, *Langmuir* **2010**, *26*, 15399.
- [134] A. A. Ramos, A. Azqueta, C. Pereira-Wilson, A. R. Collins, *J. Agric. Food Chem.* **2010**, *58*, 7465.
- [135] R. J. Youle, A. M. Blik, *Science* **2012**, *337*, 1062.
- [136] Y. Li, J. Niu, W. Zhang, L. Zhang, E. Shang, *Langmuir* **2014**, *30*, 2852.
- [137] W. He, H. Wu, W. G. Wamer, H. K. Kim, J. Zheng, H. Jia, Z. Zheng, J. J. Yin, *ACS Appl. Mater. Interfaces* **2014**, *6*, 15527.
- [138] P. J. P. Espitia, N. F. F. Soares, J. S. R. Coimbra, N. J. Andrade, R. S. Cruz, E. A. A. Medeiros, *Food Bioprocess Technol.* **2012**, *5*, 1447.
- [139] Z. Q. Guo, S. Park, J. Y. Yoon, I. Shin, *Chem. Soc. Rev.* **2014**, *43*, 16.
- [140] H. F. Lin, S. C. Liao, S. W. Hung, *J. Photochem. Photobiol., A* **2005**, *174*, 82.
- [141] J. Du, J. M. Gebicki, *Int. J. Biochem. Cell Biol.* **2004**, *36*, 2334.
- [142] O. Yamamoto, M. Komatsu, J. Sawai, Z. E. Nakagawa, *J. Mater. Sci.: Mater. Med.* **2004**, *15*, 847.
- [143] J. Sawai, E. Kawada, F. Kanou, H. Igarashi, A. Hashimoto, T. Kokugan, M. Shimizu, *J. Chem. Eng. Jpn.* **1996**, *29*, 627.
- [144] S. Wang, R. Gao, F. Zhou, M. Selke, *J. Mater. Chem.* **2004**, *14*, 487.
- [145] R. Bakalova, H. Ohba, Z. Zhelev, M. Ishikawa, Y. Baba, *Nat. Biotechnol.* **2004**, *22*, 1360.
- [146] I. Fridovich, *Arch. Biochem. Biophys.* **1986**, *247*, 1.
- [147] K. H. Tam, A. B. Djurišić, C. M. N. Chan, Y. Y. Xi, C. W. Tse, Y. H. Leung, W. K. Chan, F. C. C. Leung, D. W. T. Au, *Thin Solid Films* **2008**, *516*, 6167.
- [148] S. George, S. Pokhrel, T. Xia, B. Gilbert, Z. Ji, M. Schowalter, A. Rosenauer, R. Damoiseaux, K. A. Bradley, L. Mädler, A. E. Nel, *ACS Nano* **2010**, *4*, 15.
- [149] Y. W. Wang, A. Cao, Y. Jiang, X. Zhang, J. H. Liu, Y. Liu, H. Wang, *ACS Appl. Mater. Interfaces* **2014**, *6*, 2791.
- [150] G. Droval, I. Aranberri, L. Germán, E. Ivanov, E. Dimitrova, R. Kotsilkova, M. Verelst, J. Dexpert-Ghys, *J. Thermoplast. Compos. Mater.* **2012**, *5*, 1.
- [151] Y. Li, W. Zhang, J. Niu, Y. Chen, *ACS Nano* **2012**, *6*, 5164.
- [152] T. N. Phan, T. Buckner, J. Sheng, J. D. Baldeck, R. E. Marquis, *Oral Microbiol. Immunol.* **2004**, *19*, 31.
- [153] M. Merialdi, L. E. Caulfield, N. Zavaleta, A. Figueroa, K. A. Costigan, F. Dominici, J. A. Dipietro, *Am. J. Clin. Nutr.* **2004**, *79*, 826.
- [154] P. K. Stoimenov, R. L. Klinger, G. L. Marchin, K. J. Klabunde, *Langmuir* **2002**, *18*, 6679.
- [155] P. Chen, B. A. Powell, M. Mortimer, P. C. Ke, *Environ. Sci. Technol.* **2012**, *46*, 12178.
- [156] Z. Huang, X. Zheng, D. Yan, G. Yin, X. Liao, Y. Kang, Y. Yao, D. Huang, B. Hao, *Langmuir* **2008**, *24*, 4140.
- [157] L. Zhang, Y. Jiang, Y. Ding, M. Povey, D. York, *J. Nanopart. Res.* **2007**, *9*, 479.
- [158] R. Brayner, R. Ferrari-Iliou, N. Brivois, S. Djediat, M. F. Benedetti, F. Fiévet, *Nano Lett.* **2006**, *6*, 866.
- [159] N. Padmavathy, R. Vijayaraghavan, *Sci. Technol. Adv. Mater.* **2008**, *9*, 035004.
- [160] J. Pasquet, Y. Chevalier, E. Couval, D. Bouvier, G. Noizet, C. Morlière, M. A. Bolzinger, *Int. J. Pharm.* **2014**, *460*, 92.
- [161] E. Elizabeth, G. Baranwal, A. G. Krishnan, D. Menon, M. Nair, *Nanotechnology* **2014**, *25*, 115101.
- [162] H. Zeng, W. Cai, P. Liu, X. Xu, H. Zhou, C. Klingshirn, H. Kalt, *ACS Nano* **2008**, *2*, 1661.
- [163] A. Roguska, A. Belcarz, T. Piersiak, M. Pisarek, G. Ginalska, M. Lewandowska, *Eur. J. Inorg. Chem.* **2012**, *32*, 5199.
- [164] W. He, H. K. Kim, W. G. Wamer, D. Melka, J. H. Callahan, J. J. Yin, *J. Am. Chem. Soc.* **2014**, *136*, 750.
- [165] N. M. Jacob, G. Madras, N. Kottam, T. Thomas, *Ind. Eng. Chem. Res.* **2014**, *53*, 5895.
- [166] X. Wang, H. Zhu, F. Yang, X. Yang, *Adv. Mater.* **2009**, *21*, 2815.
- [167] C. Ren, B. Yang, M. Wu, J. Xu, Z. Fu, Y. Lv, T. Guo, Y. Zhao, C. Zhu, *J. Hazard. Mater.* **2010**, *182*, 123.
- [168] H. R. Pant, B. Pant, R. K. Sharma, A. Amarjargal, H. J. Kim, C. H. Park, L. D. Tijing, C. S. Kim, *Ceram. Int.* **2013**, *39*, 1503.
- [169] H. Koga, T. Kitaoka, H. Wariishi, *J. Mater. Chem.* **2009**, *19*, 2135.
- [170] D. Lin, H. Wu, R. Zhang, W. Pan, *Chem. Mater.* **2009**, *21*, 3479.
- [171] C. Gu, C. Cheng, H. Huang, T. Wong, N. Wang, T. Y. Zhang, *Cryst. Growth Des.* **2009**, *9*, 3278.
- [172] H. R. Liu, G. X. Shao, J. F. Zhao, Z. X. Zhang, Y. Zhang, J. Liang, X. G. Liu, H. S. Jia, B. S. Xu, *J. Phys. Chem. C* **2012**, *116*, 16182.
- [173] W. Lu, S. Gao, J. Wang, *J. Phys. Chem. C* **2008**, *112*, 16792.
- [174] B. Sadeghi, *Spectrochim. Acta, Part A* **2014**, *118*, 787.
- [175] X. Wang, C. J. Summers, Z. L. Wang, *Appl. Phys. Lett.* **2005**, *86*, 1.
- [176] P. Li, Z. Wei, T. Wu, Q. Peng, Y. Li, *J. Am. Chem. Soc.* **2011**, *133*, 5660.
- [177] M. D. L. R. Peralta, U. Pal, R. S. Zeferino, *ACS Appl. Mater. Interfaces* **2012**, *4*, 4807.
- [178] N. Udawatte, M. Lee, J. Kim, D. Lee, *ACS Appl. Mater. Interfaces* **2011**, *3*, 4531.
- [179] M. Misra, P. Kapur, M. L. Singla, *Appl. Catal., B* **2014**, *150–151*, 605.
- [180] Z. Zhang, J. B. Yi, J. Ding, L. M. Wong, H. L. Seng, S. J. Wang, J. G. Tao, G. P. Li, G. Z. Xing, T. C. Sum, C. H. A. Huan, T. Wu, *J. Phys. Chem. C* **2008**, *112*, 9579.
- [181] Z. B. Bahşi, A. Y. Oral, *Opt. Mater.* **2007**, *29*, 672.
- [182] H. Bai, Z. Liu, D. D. Sun, *Phys. Chem. Chem. Phys.* **2011**, *13*, 6205.
- [183] H. Oveis, S. Rahighi, X. Jiang, Y. Nemoto, A. Beitollahi, S. Wakatsuki, Y. Yamauchi, *Chem. Asian J.* **2010**, *5*, 1978.
- [184] H. Kong, J. Song, J. Jang, *Environ. Sci. Technol.* **2010**, *44*, 5672.
- [185] X. Liang, M. Sun, L. Li, R. Qiao, K. Chen, Q. Xiao, F. Xu, *Dalton Trans.* **2012**, *41*, 2804.
- [186] K. Rekha, M. Nirmala, M. G. Nair, A. Anukaliani, *Phys. B* **2010**, *405*, 3180.
- [187] K. Tomihata, Y. Ikada, *Biomaterials* **1997**, *18*, 567.
- [188] G. H. Wang, *J. Food Prot.* **1992**, *55*, 916.
- [189] Y. Wang, Q. Zhang, C. Zhang, P. Li, *Food Chem.* **2012**, *132*, 419.
- [190] L. H. Li, J. C. Deng, H. R. Deng, Z. L. Liu, X. L. Li, *Chem. Eng. J.* **2010**, *160*, 378.
- [191] P. Petkova, A. Francesco, M. M. Fernandes, E. Mendoza, I. Perelshtein, A. Gedanken, T. Tzanov, *ACS Appl. Mater. Interfaces* **2014**, *6*, 1164.
- [192] V. B. Schwartz, F. Thétiot, S. Ritz, S. Pütz, L. Choritz, A. Lappas, R. Förch, K. Landfester, U. Jonas, *Adv. Funct. Mater.* **2012**, *22*, 2376.

- [193] T. Yamashita, Y. Tanaka, N. Idota, K. Sato, K. Mawatari, T. Kitamori, *Biomaterials* **2011**, *32*, 2459.
- [194] A. R. C. Duarte, J. F. Mano, R. L. Reis, *Acta Biomater.* **2011**, *7*, 526.
- [195] M. E. Nash, W. M. Carroll, N. Nikoloskya, R. Yang, C. O. Connell, A. V. Gorelov, P. Dockery, C. Liptrot, F. M. Lyng, A. Garcia, Y. A. Rochev, *ACS Appl. Mater. Interfaces* **2011**, *3*, 1980.
- [196] X. Liu, Y. Mou, S. Wu, H. C. Man, *Appl. Surf. Sci.* **2013**, *273*, 748.
- [197] C. S. Chen, W. Y. Liao, G. J. Tsai, *J. Food Prot.* **1998**, *61*, 1124.
- [198] B. O. Jung, C. H. Kim, K. S. Choi, Y. M. Lee, J. J. Kim, *J. Appl. Polym. Sci.* **1999**, *72*, 1713.
- [199] E. I. Rabea, M. E. T. Badawy, C. V. Stevens, G. Smagghe, W. Steurbaut, *Biomacromolecules* **2003**, *4*, 1458.
- [200] N. R. Sudarshan, D. G. Hoover, D. Knorr, *Food Biotechnol.* **1992**, *6*, 257.
- [201] L. Zhang, C. Ning, T. Zhou, X. Liu, K. W. K. Yeung, T. Zhang, Z. Xu, X. Wang, S. Wu, P. K. Chu, *ACS Appl. Mater. Interfaces* **2014**, *6*, 17323.
- [202] D. Yan, G. Yin, Z. Huang, L. Li, X. Liao, X. Chen, Y. Yao, B. Hao, *Langmuir* **2011**, *27*, 13206.
- [203] M. H. Li, S. M. Pokhrel, X. Jin, L. Madler, R. Damoiseaux, E. M. V. Hoek, *Environ. Sci. Technol.* **2011**, *45*, 755.
- [204] M. Li, D. Lin, L. Zhu, *Environ. Pollut.* **2013**, *173*, 97.
- [205] M. Roselli, A. Finamore, I. Garaguso, M. S. Britti, E. Mengheri, *J. Nutr.* **2003**, *133*, 4077.
- [206] S. Nair, A. Sasidharan, V. V. D. Rani, D. Menon, S. Nair, K. Manzoor, S. Raina, *J. Mater. Sci.: Mater. Med.* **2009**, *20*, 235.
- [207] O. Yamamoto, *Int. J. Inorg. Mater.* **2001**, *3*, 643.
- [208] D. Campoccia, L. Montanaro, C. R. Arciola, *Biomaterials* **2006**, *27*, 2331.
- [209] S. L. Wu, Z. Y. Weng, X. M. Liu, K. W. K. Yeung, P. K. Chu, *Adv. Funct. Mater.* **2014**, *24*, 5464.
- [210] H. Tapiero, K. D. Tew, *Biomed. Pharmacother.* **2003**, *57*, 399.
- [211] J. Ovesen, B. Møller-Madsen, J. S. Thomsen, G. Danscher, L. Mosekilde, *Bone* **2001**, *29*, 565.
- [212] M. Yamaguchi, M. Fukagawa, *Calif. Tissue Int.* **2005**, *76*, 32.
- [213] M. Yamaguchi, H. Oishi, Y. Suketa, *Biochem. Pharmacol.* **1987**, *36*, 4007.
- [214] M. Yamaguchi, R. Yamaguchi, *Biochem. Pharmacol.* **1986**, *35*, 773.
- [215] A. Hoppe, N. S. Güldal, A. R. Boccaccini, *Biomaterials* **2011**, *32*, 2757.
- [216] A. Ito, H. Kawamura, M. Otsuka, M. Ikeuchi, H. Ohgushi, K. Ishikawa, K. Onuma, N. Kanzaki, Y. Sogo, N. Ichinose, *Mater. Sci. Eng., C* **2002**, *22*, 21.
- [217] R. L. Du, J. Chang, S. Y. Ni, W. Y. Zhai, J. Y. Wang, *J. Biomater. Appl.* **2006**, *20*, 341.
- [218] H. Zreiqat, Y. Ramaswamy, C. Wu, A. Paschalidis, Z. F. Lu, B. James, O. Birke, M. McDonald, D. Little, C. R. Dunstan, *Biomaterials* **2010**, *31*, 3175.
- [219] I. S. Kwun, Y. E. Cho, R. A. R. Lomeda, H. I. Shin, J. Y. Choi, Y. H. Kang, J. H. Beattie, *Bone* **2010**, *46*, 732.
- [220] M. Yamaguchi, H. Oishi, Y. Suketa, *Biochem. Pharmacol.* **1988**, *37*, 4075.
- [221] M. Yamaguchi, K. Ozaki, *Res. Exp. Med.* **1990**, *190*, 295.
- [222] F. M. Ghorbani, B. Kaffashi, P. Shokrollahi, E. Seyedjafari, A. Ardeshirylajimi, *Carbohydr. Polym.* **2015**, *118*, 133.
- [223] T. Amna, M. S. Hassan, M. S. Khil, H. K. Lee, I. H. Hwang, *Surf. Interface Anal.* **2014**, *46*, 72.
- [224] T. Amna, M. S. Hassan, F. A. Sheikh, H. K. Lee, K. S. Seo, D. Yoon, I. H. Hwang, *Appl. Microbiol. Biotechnol.* **2013**, *97*, 1725.
- [225] J. K. Park, Y. J. Kim, J. Yeom, J. H. Jeon, G. C. Yi, J. H. Je, S. K. Hahn, *Adv. Mater.* **2010**, *22*, 4857.
- [226] G. D. Winter, *Nature* **1962**, *193*, 293.
- [227] M. Ishihara, K. Nakanishi, K. Ono, M. Sato, M. Kikuchi, Y. Saito, H. Yura, T. Matsui, H. Hattori, M. Uenoyama, A. Kurita, *Biomaterials* **2002**, *23*, 833.
- [228] R. Jayakumar, M. Prabaharan, S. V. Nair, H. Tamura, *Biotechnol. Adv.* **2010**, *28*, 142.
- [229] T. Wang, X. K. Zhu, X. T. Xue, D. Y. Wu, *Carbohydr. Polym.* **2012**, *88*, 75.
- [230] R. Jayakumar, D. Menon, K. Manzoor, S. V. Nair, H. Tamura, *Carbohydr. Polym.* **2010**, *82*, 227.
- [231] R. Jayakumar, M. Prabaharan, P. T. S. Kumar, S. V. Nair, H. Tamura, *Biotechnol. Adv.* **2011**, *29*, 322.
- [232] H. Ueno, T. Mori, T. Fujinaga, *Adv. Drug Delivery Rev.* **2001**, *52*, 105.
- [233] G. L. Archer, *Clin. Infect. Dis.* **1998**, *26*, 1179.
- [234] C. Alemdaroglu, Z. Degim, N. Celebi, F. Zor, S. Ozturk, D. Erdogan, *Burns* **2006**, *32*, 319.
- [235] Y. Song, X. Du, T. Li, Y. Zhu, M. Li, *J. Med. Microbiol.* **2013**, *62*, 274.
- [236] T. Kim, T. Hyeon, *Nanotechnology* **2014**, *25*, 012001.
- [237] A. A. Tayel, W. F. El-Tras, S. Moussa, A. F. El-Baz, H. Mahrous, M. F. Salem, L. Brimer, *J. Food Saf.* **2011**, *31*, 211.
- [238] W. Zhang, Y. Li, J. Niu, Y. Chen, *Langmuir* **2013**, *29*, 4647.
- [239] B. Jia, Y. Mei, L. Cheng, J. Zhou, L. Zhang, *ACS Appl. Mater. Interfaces* **2012**, *4*, 2897.
- [240] D. M. Tobaldi, C. Piccirillo, R. C. Pullar, A. F. Gualtieri, M. P. Seabra, P. M. L. Castro, J. A. Labrincha, *J. Phys. Chem. C* **2014**, *118*, 4751.
- [241] C. Gunawan, W. Y. Teoh, C. P. Marquis, R. Amal, *ACS Nano* **2011**, *5*, 7214.
- [242] A. Mukhopadhyay, S. Basak, J. K. Das, S. K. Medda, K. Chattopadhyay, G. De, *ACS Appl. Mater. Interfaces* **2010**, *2*, 2540.
- [243] N. Gao, Y. Chen, J. Jiang, *ACS Appl. Mater. Interfaces* **2013**, *5*, 11307.
- [244] R. Kumar, S. Anandan, K. Hembram, T. N. Rao, *ACS Appl. Mater. Interfaces* **2014**, *6*, 13138.
- [245] S. Aoyagi, H. Onishi, Y. Machida, *Int. J. Pharm.* **2007**, *330*, 138.
- [246] P. T. S. Kumar, V. K. Lakshmanan, T. V. Anilkumar, C. Ramya, P. Reshmi, A. G. Unnikrishnan, S. V. Nair, R. Jayakumar, *ACS Appl. Mater. Interfaces* **2012**, *4*, 2618.
- [247] D. S. Vicentini, A. S. Jr, M. C. M. Laranjeira, *Mater. Sci. Eng., C* **2010**, *30*, 503.
- [248] J. Apelqvist, J. Larsson, A. Lstenström, *Br. J. Dermatol.* **1990**, *123*, 787.
- [249] M. Iwata, T. Takebayashi, H. Ohta, R. E. Alcalde, Y. Itano, T. Matsumura, *Histochem. Cell Biol.* **1999**, *112*, 283.
- [250] D. D. Cataldo, M. M. Gueders, N. Rocks, N. E. Sounni, B. Evrard, P. Bartsch, R. Louis, A. Noel, J. M. Foidart, *Cell. Mol. Biol.* **2003**, *49*, 875.
- [251] D. P. Cuthbertson, G. S. Fell, Catherine M. Smith, W. J. Tilstone, *Br. J. Surg.* **1972**, *59*, 925.
- [252] R. D. Lindeman, R. G. Bottomley, R. L. J. Cornelison, L. A. Jacobs, *J. Lab. Clin. Med.* **1972**, *79*, 452.
- [253] G. S. Fell, D. P. Cuthbertson, C. Morrison, A. Fleck, K. Queen, R. G. Bessent, S. L. Husain, *Lancet* **1973**, *301*, 280.
- [254] T. Hallböök, H. Hedelin, *Br. J. Surg.* **1977**, *64*, 271.
- [255] J. K. Chesters, R. Boyne, *Exp. Cell Res.* **1991**, *192*, 631.
- [256] B. Gonul, T. Soylemezoglu, A. Babul, N. Celebi, *J. Pharm. Pharmacol.* **1998**, *50*, 641.
- [257] X. Michalet, F. F. Pinaud, L. A. Bentolila, J. M. Tsay, S. Doose, J. J. Li, G. Sundaresan, A. M. Wu, S. S. Gambhir, S. Weiss, *Science* **2005**, *307*, 538.
- [258] D. R. Larson, W. R. Zipfel, R. M. Williams, S. W. Clark, M. P. Bruchez, F. W. Wise, W. W. Webb, *Science* **2003**, *300*, 1434.
- [259] X. Gao, Y. Cui, R. M. Levenson, L. W. K. Chung, S. Nie, *Nat. Biotechnol.* **2004**, *22*, 969.
- [260] J. K. Jaiswal, S. M. Simon, *Trends Cell Biol.* **2004**, *14*, 497.

- [261] R. O. Moussodia, L. Balan, C. Merlin, C. Mustin, R. Schneider, *J. Mater. Chem.* **2010**, *20*, 1147.
- [262] J. Zhou, N.-S. Xu, Z.-L. Wang, *Adv. Mater.* **2006**, *18*, 2432.
- [263] Q. Yuan, S. Hein, R. D. K. Misra, *Acta Biomater.* **2010**, *6*, 2732.
- [264] N. Pradhan, D. M. Battaglia, Y. Liu, X. Peng, *Nano Lett.* **2007**, *7*, 312.
- [265] N. Chen, Y. He, Y. Su, X. Li, Q. Huang, H. Wang, X. Zhang, R. Tai, C. Fan, *Biomaterials* **2012**, *33*, 1238.
- [266] S. T. Yang, L. Cao, P. G. Luo, F. Lu, X. Wang, H. Wang, M. J. Meziari, Y. Liu, G. Qi, Y. P. Sun, *J. Am. Chem. Soc.* **2009**, *131*, 11308.
- [267] J. Gao, K. Chen, R. Xie, J. Xie, S. Lee, Z. Cheng, X. Peng, X. Chen, *Small* **2010**, *6*, 256.
- [268] Q. Liu, Y. Sun, T. Yang, W. Feng, C. Li, F. Li, *J. Am. Chem. Soc.* **2011**, *133*, 17122.
- [269] A. van Dijken, E. A. Meulenkaamp, D. Vanmaekelbergh, A. Meijerink, *J. Phys. Chem. B* **2000**, *104*, 1715.
- [270] L. Spanhel, *J. Sol-Gel Sci. Technol.* **2006**, *39*, 7.
- [271] N. R. Jana, H. Yu, E. M. Ali, Y. Zheng, J. Y. Ying, *Chem. Commun.* **2007**, *14*, 1406.
- [272] H. M. Xiong, Z. D. Wang, D. P. Liu, J. S. Chen, Y. G. Wang, Y. Y. Xia, *Adv. Funct. Mater.* **2005**, *15*, 1751.
- [273] B. K. Woo, W. Chen, A. G. Joly, R. Sammynaiken, *J. Phys. Chem. C* **2008**, *112*, 14292.
- [274] L. Guo, S. Yang, C. Yang, P. Yu, J. Wang, W. Ge, G. K. L. Wong, *Chem. Mater.* **2000**, *12*, 2268.
- [275] Y. S. Fu, X. W. Du, S. A. Kulinich, J. S. Qiu, W. J. Qin, R. Li, J. Sun, J. Liu, *J. Am. Chem. Soc.* **2007**, *129*, 16029.
- [276] S. Saliba, C. V. Serrano, J. Keilitz, M. L. Kahn, C. Mingotaud, R. Haag, J. D. Marty, *Chem. Mater.* **2010**, *22*, 6301.
- [277] H. M. Xiong, D. P. Xie, X. Y. Guan, Y. J. Tan, Y. Y. Xia, *J. Mater. Chem.* **2007**, *17*, 2490.
- [278] J. Han, H. Su, J. Xu, W. Song, Y. Gu, Y. Chen, W. J. Moon, D. Zhang, *J. Nanopart. Res.* **2012**, *14*, 1.
- [279] H. M. Xiong, Y. Xu, Q. G. Ren, Y. Y. Xia, *J. Am. Chem. Soc.* **2008**, *130*, 7522.
- [280] Z. Y. Pan, J. Liang, Z. Z. Zheng, H. H. Wang, H. M. Xiong, *Contrast Media Mol. Imaging* **2011**, *6*, 328.
- [281] X. Tang, E. S. G. Choo, L. Li, J. Ding, J. Xue, *Chem. Mater.* **2010**, *22*, 3383.
- [282] H. Q. Shi, W. N. Li, L. W. Sun, Y. Liu, H. M. Xiao, S. Y. Fu, *Chem. Commun.* **2011**, *47*, 11921.
- [283] Y. Q. Li, Y. Yang, S. Y. Fu, X. Y. Yi, L. C. Wang, H. D. Chen, *J. Phys. Chem. C* **2008**, *112*, 18616.
- [284] Y. Lu, Y. Yin, B. T. Mayers, Y. Xia, *Nano Lett.* **2002**, *2*, 183.
- [285] L. Li, E. S. G. Choo, J. Yi, J. Ding, X. Tang, J. Xue, *Chem. Mater.* **2008**, *20*, 6292.
- [286] H. J. Zhang, H. M. Xiong, Q. G. Ren, Y. Y. Xia, J. L. Kong, *J. Mater. Chem.* **2012**, *22*, 13159.
- [287] H. M. Xiong, D. P. Liu, Y. Y. Xia, J. S. Chen, *Chem. Mater.* **2005**, *17*, 3062.
- [288] P. Felbier, J. Yang, J. Theis, R. W. Liptak, A. Wagner, A. Lorke, G. Bacher, U. Kortshagen, *Adv. Funct. Mater.* **2014**, *24*, 1988.
- [289] A. Aboulaich, L. Balan, J. Ghanbaja, G. Medjahdi, C. Merlin, R. Schneider, *Chem. Mater.* **2011**, *23*, 3706.
- [290] C. Wang, X. Gao, Q. Ma, X. Su, *J. Mater. Chem.* **2009**, *19*, 7016.
- [291] Z. Fang, P. Wu, X. Zhong, Y. J. Yang, *Nanotechnology* **2010**, *21*, 305604.
- [292] A. Aboulaich, M. Geszke, L. Balan, J. Ghanbaja, G. Medjahdi, R. Schneider, *Inorg. Chem.* **2010**, *49*, 10940.
- [293] Y. Yang, T. Zhao, T. Cheng, J. Shen, X. Liu, B. Yu, S. Lv, H. Zhang, *RSC Adv.* **2014**, *4*, 5642.
- [294] H. M. Xiong, R. Z. Ma, S. F. Wang, Y. Y. Xia, *J. Mater. Chem.* **2011**, *21*, 3178.
- [295] W. J. M. Mulder, G. J. Strijkers, G. A. F. van Tilborg, A. W. Griffioen, K. Nicolay, *NMR Biomed.* **2006**, *19*, 142.
- [296] P. Caravan, J. J. Ellison, T. J. McMurry, R. B. Lauffer, *Chem. Rev.* **1999**, *99*, 2293.
- [297] E. A. Anderson, S. Isaacman, D. S. Peabody, E. Y. Wang, J. W. Canary, K. Kirshenbaum, *Nano Lett.* **2006**, *6*, 1160.
- [298] S. S. Banerjee, D. H. Chen, *Nanotechnology* **2009**, *20*, 185103.
- [299] W. Wang, M. Zou, K. Chen, *Chem. Commun.* **2010**, *46*, 5100.
- [300] I. F. Lia, C. S. Yeh, *J. Mater. Chem.* **2010**, *20*, 2079.
- [301] S. Zeng, J. Xiao, Q. Yang, J. Hao, *J. Mater. Chem.* **2012**, *22*, 9870.
- [302] E. A. Schellenberger, D. Sosnovik, R. Weissleder, L. Josephson, *Bioconjugate Chem.* **2004**, *15*, 1062.
- [303] H. M. Xiong, D. G. Shchukin, H. Möhwald, Y. Xu, Y. Y. Xia, *Angew. Chem. Int. Ed.* **2009**, *48*, 2727.
- [304] Y. P. Du, Y. W. Zhang, L. D. Sun, C. H. Yan, *J. Phys. Chem. C* **2008**, *112*, 12234.
- [305] L. W. Sun, H. Q. Shi, W. N. Li, H. M. Xiao, S. Y. Fu, X. Z. Cao, Z. X. Li, *J. Mater. Chem.* **2012**, *22*, 8221.
- [306] N. H. Cho, T. C. Cheong, J. H. Min, J. H. Wu, S. J. Lee, D. Kim, J. S. Yang, S. Kim, Y. K. Kim, S. Y. Seong, *Nat. Nanotechnol.* **2011**, *6*, 675.
- [307] X. Wei, W. Wang, K. Chen, *J. Phys. Chem. C* **2013**, *117*, 23716.
- [308] Y. Liu, K. Ai, Q. Yuan, L. Lu, *Biomaterials* **2011**, *32*, 1185.
- [309] Q. Yin, X. Jin, G. Yang, C. Jiang, Z. Song, G. Sun, *RSC Adv.* **2014**, *4*, 53561.
- [310] D. M. McDonald, P. L. Choyke, *Nat. Med.* **2003**, *9*, 713.
- [311] M. L. Schipper, G. Iyer, A. L. Koh, Z. Cheng, Y. Ebenstein, A. Aharoni, S. Keren, L. A. Bentolila, J. Li, J. Rao, X. Chen, U. Banin, A. M. Wu, R. Sinclair, S. Weiss, S. S. Gambhir, *Small* **2009**, *5*, 126.
- [312] P. Ray, A. M. Wu, S. S. Gambhir, *Cancer Res.* **2003**, *63*, 1160.
- [313] K. R. Bhushan, P. Misra, F. Liu, S. Mathur, R. E. Lenkinski, J. V. Frangioni, *J. Am. Chem. Soc.* **2008**, *130*, 17648.
- [314] L. Sampath, S. Kwon, S. Ke, W. Wang, R. Schiff, M. E. Mawad, E. M. Sevcik-Muraca, *J. Nucl. Med.* **2007**, *48*, 1501.
- [315] C. M. Lee, H. J. Jeong, D. W. Kim, M. H. Sohn, *Nanotechnology* **2012**, *23*, 205102.
- [316] G. Sonavane, K. Tomada, A. Sano, H. Ohshima, H. Terada, K. Makino, *Colloids Surf., B* **2008**, *65*, 1.
- [317] Y. Zhang, T. R. Nayak, H. Hong, W. Cai, *Curr. Mol. Med.* **2013**, *13*, 1633.
- [318] H. Hong, J. Shi, Y. Yang, Y. Zhang, J. W. Engle, R. J. Nickles, X. Wang, W. Cai, *Nano Lett.* **2011**, *11*, 3744.
- [319] H. Hong, F. Wang, Y. Zhang, S. A. Graves, S. B. Z. Eddine, Y. Yang, C. P. Theuer, R. J. Nickles, X. Wang, W. Cai, *ACS Appl. Mater. Interfaces* **2015**, *7*, 3373.
- [320] S. S. Gambhir, *Nat. Rev. Cancer* **2002**, *2*, 683.
- [321] M. M. Alauddin, *Am. J. Nucl. Med. Mol. Imaging* **2012**, *2*, 55.
- [322] D. D. Nolting, M. L. Nickels, N. Guo, W. Pham, *Am. J. Nucl. Med. Mol. Imaging* **2012**, *2*, 273.
- [323] V. P. Torchilin, *Nat. Rev. Drug Discovery* **2005**, *4*, 145.
- [324] R. Duncan, *Nat. Rev. Cancer* **2006**, *6*, 688.
- [325] I. I. Slowing, J. L. Vivero-Escoto, C. W. Wu, V. S. Y. Lin, *Adv. Drug Delivery Rev.* **2008**, *60*, 1278.
- [326] J. J. Moon, B. Huang, D. J. Irvine, *Adv. Mater.* **2012**, *24*, 3724.
- [327] M. J. Sailor, J. H. Park, *Adv. Mater.* **2012**, *24*, 3779.
- [328] W. Fang, J. Yang, J. Gong, N. Zheng, *Adv. Funct. Mater.* **2012**, *22*, 842.
- [329] X. J. Kang, Y. L. Dai, P. A. Ma, D. M. Yang, C. X. Li, Z. Y. Hou, Z. Y. Cheng, J. Lin, *Chem. Eur. J.* **2012**, *18*, 15676.
- [330] J. Zhu, L. Liao, X. Bian, J. Kong, P. Yang, B. Liu, *Small* **2012**, *8*, 2715.
- [331] J. Z. Du, X. J. Du, C. Q. Mao, J. Wang, *J. Am. Chem. Soc.* **2011**, *133*, 17560.

- [332] J. Croissant, J. I. Zink, *J. Am. Chem. Soc.* **2012**, *134*, 7628.
- [333] H. J. Kim, H. Matsuda, H. Zhou, I. Honma, *Adv. Mater.* **2006**, *18*, 3083.
- [334] P. Pradhan, J. Giri, F. Rieken, C. Koch, O. Mykhaylyk, M. Döblinger, R. Banerjee, D. Bahadur, C. Plank, *J. Controlled Release* **2010**, *142*, 108.
- [335] J. Z. Du, T. M. Sun, W. J. Song, J. Wu, J. Wang, *Angew. Chem.* **2010**, *122*, 3703.
- [336] Y. Li, W. Xiao, K. Xiao, L. Berti, J. Luo, H. P. Tseng, G. Fung, K. S. Lam, *Angew. Chem.* **2012**, *124*, 2918.
- [337] D. Li, J. Tang, C. Wei, J. Guo, S. Wang, D. Chaudhary, C. Wang, *Small* **2012**, *8*, 2690.
- [338] R. Liu, Y. Zhang, X. Zhao, A. Agarwal, L. J. Mueller, P. Feng, *J. Am. Chem. Soc.* **2010**, *132*, 1500.
- [339] X. B. Xiong, A. Lavasanifar, *ACS Nano* **2011**, *5*, 5202.
- [340] Y. L. Zhao, Z. Li, S. Kabehie, Y. Y. Botros, J. F. Stoddart, J. I. Zink, *J. Am. Chem. Soc.* **2010**, *132*, 13016.
- [341] A. Goux, T. Pauporté, J. Chivot, D. Lincot, *Electrochim. Acta* **2005**, *50*, 2239.
- [342] K. C. Barick, S. Nigam, D. Bahadur, *J. Mater. Chem.* **2010**, *20*, 6446.
- [343] Q. Yuan, S. Hein, R. D. K. Misra, *Acta Biomater.* **2010**, *6*, 2732.
- [344] F. Muhammad, M. Guo, W. Qi, F. Sun, A. Wang, Y. Guo, G. Zhu, *J. Am. Chem. Soc.* **2011**, *133*, 8778.
- [345] F. Muhammad, M. Guo, Y. Guo, W. Qi, F. Qu, F. Sun, H. Zhao, G. Zhu, *J. Mater. Chem.* **2011**, *21*, 13406.
- [346] Y. Liu, J. Yang, P. Zhang, C. Liu, W. Wang, W. Liu, *J. Mater. Chem.* **2012**, *22*, 512.
- [347] Z. Y. Zhang, Y. D. Xu, Y. Y. Ma, L. L. Qiu, Y. Wang, J. L. Kong, H. M. Xiong, *Angew. Chem., Int. Ed.* **2013**, *52*, 4127.
- [348] S. Mitra, B. Subia, P. Patra, S. Chandra, N. Debnath, S. Das, R. Banerjee, S. C. Kundu, P. Pramanik, A. Goswami, *J. Mater. Chem.* **2012**, *22*, 24145.
- [349] H. Qiu, B. Cui, G. Li, J. Yang, H. Peng, Y. Wang, N. Li, R. Gao, Z. Chang, Y. Wang, *J. Phys. Chem. C* **2014**, *118*, 14929.
- [350] Y. Dai, P. Ma, Z. Cheng, X. Kang, X. Zhang, Z. Hou, C. Li, D. Yang, X. Zhai, J. Lin, *ACS Nano* **2012**, *6*, 3327.